Chemie der Erde 78 (2018) 269–298

Contents lists available at ScienceDirect

Chemie der Erde

journal homepage: www.elsevier.de/chemer

Invited review

Physical properties of the stone meteorites: Implications for the properties of their parent bodies

George J. Flynn[a,*], Guy J. Consolmagno[b], Peter Brown[c], Robert J. Macke[b]

[a] Department of Physics, SUNY-Plattsburgh,101 Broad St., Plattsburgh, NY 12901, USA
[b] Vatican Observatory, V-00120, Vatican City State
[c] Department of Physics and Astronomy and Centre for Planetary Science and Exploration, University of Western Ontario, London, N6A 3K7, ON, Canada

ARTICLE INFO

Article history:
Received 16 December 2016
Received in revised form 16 March 2017
Accepted 10 April 2017
Handling Editor: Klaus Keil

Keywords:
Chondritic meteorites
Porosity
Magnetic susceptibility
Compressive strength
Speed of sound
Hypervelocity impact

ABSTRACT

The physical properties of the stone meteorites provide important clues to understanding the formation and physical evolution of material in the Solar protoplanetary disk as well providing indications of the properties of their asteroidal parent bodies. Knowledge of these properties is essential for modeling a number of Solar System processes, such as bolides in planetary atmospheres, the thermal inertia of atmosphereless solid body surfaces, and the internal physical and thermal evolution of asteroids and rock-rich icy bodies. In addition, insight into the physical properties of the asteroids is important for the design of robotic and crewed reconnaissance, lander, and sample return spacecraft missions to the asteroids. One key property is meteorite porosity, which ranges from 0% to more than 40%, similar to the range of porosities seen in asteroids. Porosity affects many of the other physical properties including thermal conductivity, speed of sound, deformation under stress, strength, and response to impact. As a result of the porosity, the properties of most stone meteorites differ significantly from those of compact terrestrial rocks, whose physical properties have been used in many models of asteroid behavior. A few physical properties, such as grain density, magnetic susceptibility, and heat capacity are not functions of porosity. Taken together, the grain density and the magnetic susceptibility can be used to classify unweathered or minimally weathered ordinary chondrites. This provides a rapid screening technique to identify heterogeneous samples, classify new samples, and identify misclassified meteorites or interlopers in strewn fields.

Contents

1. Introduction 270
2. Density and porosity 272
   2.1. Grain density 273
   2.2. Bulk density 274
   2.3. Bulk density from meteor observations 275
   2.4. Porosity 276
   2.5. Variability 277
   2.6. Variations with weathering 277
   2.7. Variations with petrographic grade 278
   2.8. Shock state 279
   2.9. Types of porosity 279
3. Magnetic susceptibility 280
4. Thermal properties of meteorites 280
   4.1. Thermal conductivity 280
   4.2. Heat capacity 282

* Corresponding author at: SUNY- Plattsburgh, Plattsburgh, NY 12901, USA.
E-mail address: george.flynn@plattsburgh.edu (G.J. Flynn).

https://doi.org/10.1016/j.chemer.2017.04.002

5. Elastic properties of meteorites 282
5.1. Speed of sound 283
5.2. Elastic response to deformation 284
5.3. Bulk modulus 284
5.4. Shear modulus 285
5.5. Young's modulus 285
6. Material strength of meteorites 286
6.1. Compressive and tensile strengths 286
6.2. Compressive strength from meteor observations 289
6.2.1. Fireballs 289
6.2.2. Fainter optical meteor population (mm – cm –sizes) 291
7. Impact cratering and resistance to disruption 292
7.1. Hypervelocity disruption results 292
7.2. Hypervelocity cratering results 293
7.3. Attenuation of shock 293
8. Summary 293
Acknowledgements 294
References 294

1. Introduction

The identification of the stone meteorites as samples of extraterrestrial material more than 200 years ago (e.g., Biot, 1803) made possible the direct laboratory measurement of the properties of these meteorites and the inference of properties of their parent bodies. A summary of the mineralogy and chemistry of meteorites is given by Krot et al. (2014). The chondritic meteorites are classified according to their degree of thermal or aqueous alteration (Van Schmus and Wood, 1967), with the aqueously altered meteorites being assigned petrographic type 1 or 2 while predominantly thermally altered meteorites are assigned petrographic type values from 4 to 7. The degree of shock experienced by each meteorite, from unshocked (S1), shock pressures <5 GPa, to very strongly shocked (S6), shock pressures from 75 to 90 GPa (Stöffler et al., 1991), and the degree of terrestrial alteration, or the weathering state, characterized on a scale from unweathered (W0) to highly weathered (W6) (Wlotzka, 1993).

Complementing the chemical and mineralogical measurements, physical property measurements include bulk and grain densities, porosity, electric, magnetic, thermal and elastic properties, structural strength, and response to hypervelocity impact. While work in the mineralogical and chemical analysis of meteorites first began in the 19th century, systematic measurements of the physical properties of meteorites are much more recent. These data provide important constraints on the meteorites themselves, the interaction of their parent meteoroids with the Earth's atmosphere, and an indication of the physical properties of their parent bodies.

Laboratory physical properties measurements on meteorite samples can be divided into three categories: *non-destructive measurements*, such as density and porosity; *altering measurements*, such as thermal conductivity, speed of sound, and elastic properties, where samples must be cut into regular shapes such as rectangular blocks or rods; and *destructive measurements*, such as strength and response to impacts, where the sample is tested to failure. In recent years samples for non-destructive measurements have become widely available, with density and porosity measurements having been made on more than 1100 meteorite samples. However, the availability of samples for measurements requiring alteration or destruction have been more restricted, and these measurements are especially difficult to obtain for rare or valuable meteorites.

There is another way of estimating some of these physical properties. As noted above, the physical properties of infalling bodies, particularly their strength, bulk density, and thermal conductivity, are critical parameters governing the interaction of their parent meteoroids with the Earth's atmosphere. These properties control the survival, breakup, and ablation. Thus, the study of meteoroid flight through the atmosphere can provide constraints on the strength and bulk density of the bolides that give rise to some of the meteorites. Unlike the meteorites, which may be measured directly in the laboratory, the flight of meteoroids in the atmosphere permit only indirect inference of physical properties based on the observed ablation behavior (e.g., Ceplecha et al., 1998; Kikwaya et al., 2009; Kikwaya et al., 2011).

This drawback is counterbalanced by the wider range of material probed using the atmosphere as the "detector," since many weak or fast meteoroids do not survive to reach the ground. These weak or friable meteoroids, which are unlikely to be found in our collections as meteorites, are represented in the meteor population. In many cases, the orbit for each meteoroid is also measured, providing a linkage to either the asteroid or the comet parent population. Meteoroid bulk density and compressive strength are inferred from comparisons with models that describe, to varying degrees of complexity, the kinematic and dynamic response of meteoroids to hypervelocity encounter with the upper atmosphere and subsequent production of light, ablation products and electrons/ions, reviewed in detail by Borovička (2006).

The physical properties of meteoroids, inferred from atmospheric flight measurements, are generally divided into two size regimes – fireballs (cm to meter sizes), some of which produce meteorites, and optically measured meteors (mm to cm sizes), in the size range of the cosmic dust collected from polar ices (Maurette et al., 1987; Taylor et al., 1998), with the cosmic dust representing the fraction of incident material entering the atmosphere at velocities too low to vaporize. The division between fireballs and the smaller meteors is chosen because there is evidence that the parent population of meteoroids changes with size from meter- sizes to mm-sizes (Ceplecha et al., 1998), because fundamentally different methods or instruments are used to measure these populations, and because the orbits of these populations are increasingly affected by non-gravitational forces as size decreases, making associations with parent populations less clear for the smaller meteoroids (Nesvorný et al., 2011).

The increasing availability of video cameras, which record optical signatures of fireballs, and weather radar, which record meteorites deposited by fireballs, has resulted in several well observed fireballs that produced recovered meteorites. For these fireballs the orbital elements of the body can be determined from the atmospheric path, giving an indication of the source. Table 1 lists the twenty-six meteorite falls from observed fireballs that have

Table 1
Properties of Meteoroids that Produced Recovered Meteorites.

#	Meteorite Name	Date of Fall (UT)	Technique*	Meteorite Type	Recovered Mass (kg)	V_∞ (km/s))	a (AU)	e	i (deg.)	ω	Ω	T_J	PE	PE Type	CRE Age (Ma)	Meteorite Bulk Density (kg/m^3)	Fireball Comp. Strength (MPa)	Meteorite Comp. Strength (MPa)	References
1	Pribam	4/7/1959	P	H5	5.8	20.89	2.4	0.67	10.5	241.8	17.8	3.16	−4.4	I		3570	0.9		1, 1a, 1b, 1c
2	Lost City	1/4/70	P	H5	17	14.2	1.66	0.42	12	161.1	283.8	4.14	−4.4	I			0.7		2, 2a, 2b
3	Innisfree	2/6/77	P	L4/5	4.58	14.54	1.87	0.47	12.2	177.9	317.6	3.82	−4.3	I			0.1		3, 3a
4	Benesov	5/7/1991	P	H5/LL3.5	0.011	21.1	2.483	0.627	23.98	218.4	47	3.08	−4.6	I			1		4, 4a
5	Peekskill	10/9/1992	CV	H6	12.4	14.72	1.49	0.41	4.9	307.6	17	4.46				3300	0.7		5, 5a, 1a
6	Tagish Lake	1/18/2000	CV, I, S, Sa	C2	~10	15.8	1.98	0.55	2	224.4	297.9	3.66	−5.4	IIIA	7.8	1670	0.3		6, 6a, 6b
7	Moravka	5/6/2000	CV, I, S, Sa	H5	1.4	22.5	1.85	0.47	32.2	203.5	46.3	3.7	−4.1	I		3590	1		7, 1a
8	Neuschwanstein	4/6/2002	P, S, I	EL6	6.19	20.95	2.4	0.67	11.4	241.2	16.8	3.16	−4.6	I		3500	3.6		8, 8a
9	Park Forest	3/27/2003	CV, I, S, Sa	L5	18	19.5	2.53	0.68	3.2	237.5	6.1	3.08	−4.6	I/II		3900	0.3		9, 9a
10	Villalbeto de la Pena	1/4/2004	CV, I, S	L6	3.5	16.9	2.3	0.63	0	132.3	283.7	3.29	−4.4	I		3420			10, 10a
11	Bunburra Rockhole	7/20/2007	P	Euc.	0.324	13.31	0.85	0.25	9.1	209.9	297.6	6.89	−4.5	I			0.1		11
12	Almahata Sitta (2008 TC3)	10/7/2008	CV, I, Sa	Ure. Anom.	3.95	12.42	1.31	0.31	2.5	234.5	194.1	4.92	−5.7	IIIa		2800, 3100	0.25	56 ± 26	12, 12a, 12b
13	Buzzard Coulee	11/21/2008	CV, I	H4	> 50	18	1.23	0.22	25.5	212	238.9	5.08	−4.5	I		3460			13, 13a, 13b
14	Maribo	1/17/2009	P, CV, V, R	CM2	0.025	28.3	2.48	0.807	0.11	279.2	297.12	2.91	−4.9	II	0.8–1.4		0.03		14, 14a, 14b, 14c
15	Jesenice	4/9/2009	P, V, I, S	L6	3.6	13.8	1.75	0.43	9.6	190.5	19.2	4	−4.3	I			0.3		15
16	Grimsby	9/25/2009	V, I, R	H4-6	0.215	20.91	2.04	0.518	28.07	159.9	182.96	3.49	−4.1	I		3370	0.3		16, 16a
17	Kosice	2/28/2010	P,V, I, S	H5	4.3	15	2.71	0.647	2	204.2	340.07	3.02	−4.9	II		3430	0.1		17, 17a
18	Mason Gully	4/13/2010	P	H5	0.025	14.53	2.47	0.602	0.832	18.95	203.21	3.21	−4.4	I		3320			18, 18a
19	Krizevci	2/4/2011	P, V	H6	0.291	18.21	1.544	0.521	0.64	254.4	315.55	4.3	−4.2	I			0.9		19
20	Sutter's Mill	4/22/2012	CV, I, S, Sa	CM2	0.8	28.6	2.45	0.817	2.63	76.5	32.71	2.91	−5.3	II	0.082	2310		82 ± 6	20, 20a
21	Novato	10/18/2012	CV, V	L6	0.36	13.67	2.09	0.526	5.5	347.4	24.941	3.56				3400	0.7	1100 ± 250	21
22	Chelyabinsk	2/15/2013	CV, I, S, Sa	LL5	>100	19.03	1.72	0.571	4.98	107.7	326.46	3.96	−4.8	II		3320		64	22, 22a, 22b, 22c
23	Annama	4/18/2014	CV, V	H5	0.168	24.2	1.99	0.69	14.7	264.8	28.611	3.48	−4.2	I	30	3500			23, 23a
24	Zdar nad Sazavou	12/9/2014	P, C, I, S	L3.9	0.087	21.94	2.101	0.681	2.803	257.8	257.26	3.41	−4.5	I		3050			24
25	Murrili	11/27/2015	C	H5	1.68	13.7	2.62	0.62	3.58	356.3	64.63	3.1				3470			25, 25a
26	Stubenberg	3/6/2016	C, P	LL6	1.473	14	1.525	0.395	2.07	221	346.52	4.4	−4.6	I					26

*Observation Technique: P – Dedicated photographic network, CV – Casual video, V – Dedicated video network, I – infrasound, S-Seismic, Sa – Satellite, R – radar, C—CCD detector (non-video-frame-rate)

References:

1. Ceplecha (1961); 1a. Borovička and Kalenda (2003); 1b. Ceplecha (1977); 1c. Britt and Consolmagno (2003)
2. McCrosky et al. (1971); 2a. Ceplecha (1996); 2b. Ceplecha and ReVelle (2005)
3. Halliday et al. (1978); 3a. Halliday et al. (1981)
4. Spurný (1994); 4a. Borovička et al. (1998)
5. Brown et al. (1994); 5a. Ceplecha et al. (1996)
6. Brown et al. (2001); 6a. Hildebrand et al. (2006); 6b. Brown et al. (2002); 6c. Nakamura et al. (2001)
7. Borovička et al. (2003)
8. Spurný et al. (2003), 8a. Spurný et al. (2002)
9. Brown et al. (2004); 9a. Simon et al. (2004)
10. Trigo-Rodriguez et al. (2006); 10a. Llorca et al. (2005)
11. Spurný et al. (2012a)
12. Jenniskens et al. (2009) ; 12a. Welten et al. (2010); Kohout et al. (2011)
13. Milley et al. (2010); 13a. Milley, (2010) ; 13b. Fry et al. (2013)
14. Keuer et al. (2009); 14a. Haak et al. (2010); 14b. Haak et al. (2011); 14c. Spurný et al. (2013) 14d. Haak et al. (2012)
15. Spurný et al. (2010)
16. Brown et al. (2011); 16a. Cartwright et al. (2010)
17. Borovička et al. (2013a); 17a. Kohout et al. (2014b)
18. Spurný et al. (2012b); 18a. Dyl et al. (2016)
19. Borovička et al. (2015)
20. Jenniskens et al. (2012); 20a. Nishiizumi et al. (2014)
21. Jenniskens et al. (2014)
22. Borovička et al. (2013b); 22a. Brown et al. (2013b); 22b. Kohout et al. (2014a); 22c. Grokhovsky et al. (2013)
23. Trigo-Rodriguez et al. (2015); 23a. Kohout et al. (2015); Kohout et al. (2017)
24. Spurný (2015)
25. Bland et al. (2016); 25a. Macke et al. (2016)
26. Spurný et al. (2016)

been published through late 2016. The table includes the orbital elements, a (the semi-major axis), e (the eccentricity), i (the inclination relative to the ecliptic plane), ω (the argument of the perigee), and Ω (the right ascension of the ascending node), as well as T_J (the Tisserand parameter with respect to Jupiter), which provides an indicator of the source (as discussed in Section 2.3), and PE, a parameter developed to classify meteoroid strength (discussed in Section 6.2.1). Table 1 also includes the bulk density of the recovered meteorite, and the compressive strength of the recovered meteorite for the few cases where these properties have been reported.

Of these twenty six meteorites, twenty-four have orbital characteristics consistent with an asteroidal origin, while two, the Sutter's Mill and Maribo CM2 carbonaceous chondrites, have orbital characteristics borderline between asteroidal and Jupiter Family Comet (JFC) origins. In these twenty-six cases it is possible to directly compare the results from laboratory measurements of the recovered samples with inferences from the fireball, although few comparisons have, thus far, been reported.

The vast majority of physical properties measurements on stones found in the literature were performed on terrestrial materials. Since there are few measurements or inferences of the physical properties of asteroids, these terrestrial rock data have frequently been used as a starting point to model the behavior of asteroids. But measurements on meteorite samples, observations of meteoroid ablation dynamics in the atmosphere, inferences of asteroid densities, and some observations of crater morphologies, indicate that the actual properties of the meteorites, and likely their parent bodies, are significantly different from those of compact terrestrial rocks. These meteorite measurements provide a starting point for the understanding of the properties of asteroids from which they are derived.

The available asteroid density measurements have been reviewed by Britt et al. (2002). However, most other physical properties measurements have only been inferred from remote sensing, which generally provides values for the regolith, rather than the underlying rock. For example, the thermal inertia measurements reported for asteroid 21 Lutetia are interpreted as indicating the presence of a well-developed regolith layer with a low thermal conductivity (O'Rourke et al., 2012), but they provide no data on the interior properties of this asteroid. As noted by McSween et al. (2002) improvement of thermal evolution models of asteroids requires "improved constraints from meteorites. . . [including] additional measurements of specific heat capacities and diffusivity." Until spacecraft missions that probe asteroid interiors become common, the meteorite measurements are likely to provide the best constraints on the physical properties of the bedrock underlying asteroid regoliths.

2. Density and porosity

The most striking difference between the stone meteorites, and likely their parent asteroids, and most terrestrial rocks is the higher porosity of the meteorites. (Flynn, 2004; Consolmagno et al., 2008c). Porosity is a particularly important characteristic of rocks since many other physical properties, including strength, thermal conductivity, speed and attenuation of sound, and response to impacts vary with the porosity, or more directly with the connectivity of the rock.

Although porosities have only been inferred for a few dozen asteroids, most of these range from 20% to more than 50%, with a mean of ~30% (Britt et al., 2002). This porosity reflects both the macroporosity of potentially fractured or rubble-pile asteroids, and the microporosity within the rocky ingredients of the asteroids themselves, which is the porosity recorded in the meteorite samples. Since sample porosity controls many other physical properties, it follows that asteroids, and the meteorites derived from them, are likely to have physical properties significantly different from those of compact terrestrial rocks.

The porosity of the parent bodies of the meteorites is particularly important in determining the response to impact cratering and disruption, since highly porous meteorites require significantly more impactor kinetic energy per unit target mass to produce a disruption, than do non- porous targets (Flynn and Durda, 2004). Thus, the highly porous asteroids are likely to be more resistant to collisional disruption than non-porous asteroids, since the porous asteroids can withstand collisions over a wider range of impactor mass-velocity space than non-porous asteroids of the same mass, which has significant implications for the collisional evolution of the asteroid belt (Flynn, 2014).

The small bodies of our Solar System, the asteroids, comets, and some moons, formed and evolved under conditions quite unlike those of planetary formation. Their small sizes and lower gravity resulted in less gravitational compaction, which might be expected to allow many of these bodies to preserve some of the structure, e.g., intergrain and intragrain porosity that characterized the original dust of the Solar System (Sasso et al., 2009). In addition many asteroids and comets were not as severely heated during accretion and decay of radioactive elements as were the rocky planets, and many of these parent bodies did not experience aqueous processing. Thus, the degree to which meteorites are in fact *not* highly porous indicates that there was a pervasive, efficient, and not completely understood process of lithification from dust to rock in the early solar system.

Presumably the impact history of materials in the early solar system played a role in meteorite lithification (e.g., Bischoff et al., 1983). The asteroids were subjected to significant impact cratering and disruption over their history, which could have the power both to lithify and destroy. Cratering or disruption events are the likely processes that remove meteorites from their parent bodies and, thus, most meteorites should have experienced some degree of impact shock and heating. In addition, some meteorites sample parent bodies that experienced significant thermal and/or aqueous processing, though a few meteorites and many interplanetary dust particles (Brownlee, 1985; Flynn et al., 2016a) escaped the most severe effects of these processes.

In recent years, the densities of more than a thousand different meteorite samples have been measured in several laboratories. These measurements differentiate between *grain density* (ρ_g), the mass divided only by the volume of the solid component, excluding the volume of the pores, and *bulk density* (ρ_b), the mass divided by the total enclosed volume of the meteorite including pore spaces. The grain density is a measure of the intrinsic mineralogy of the meteorite, since it varies only with composition and proportions of the different minerals present, and can be considered a weighted average density of the mineral components making up the rock. The bulk density is a measure of the physical state of the meteorite, since it varies with the porosity, P, the fraction of the sample's volume that is empty space.

Measurements of the bulk density, grain density, and porosity of stone meteorites are reported in the literature (e.g., Britt and Consolmagno, 2003; Consolmagno et al., 2006; Consolmagno, 2008c; Kohout et al., 2008; Macke et al., 2016, 2010b, 2011a, 2011b). This work, which provides a comprehensive understanding of the typical density for most meteorite types and the range of variation among members of the same type, will not be repeated here. Rather, this review will focus on describing the other physical properties of the meteorites and assessing their correlations with meteorite porosity.

Systematic differences between measurements from different laboratories can result from slight variations in the measurement procedure. For example, Ibrahim (2012) notes that beads of ~1 mm

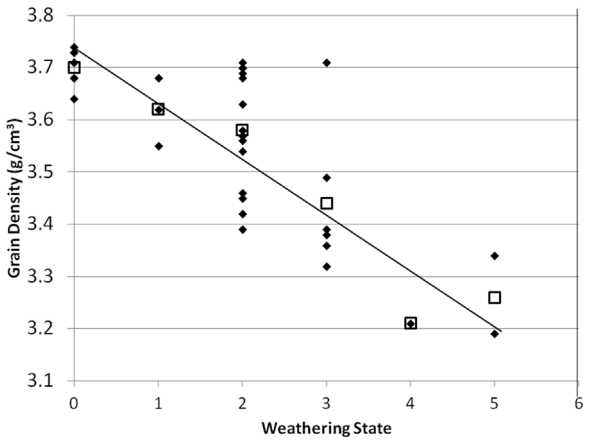

Fig 1. Mean grain density (from Macke, 2010) vs weathering state for 30 H-chondrite falls and finds for which the weathering state has been reported in the Meteoritical Bulletin Database or Grady (2000) (diamonds). The best fit linear regression line to the mean grain density for each weathering state (squares) shows a clear trend of decreasing grain density with increasing weathering state, with the correlation coefficient r = −0.95 (Macke, 2010). The mean grain density was not measured on the same sample as the weathering state.

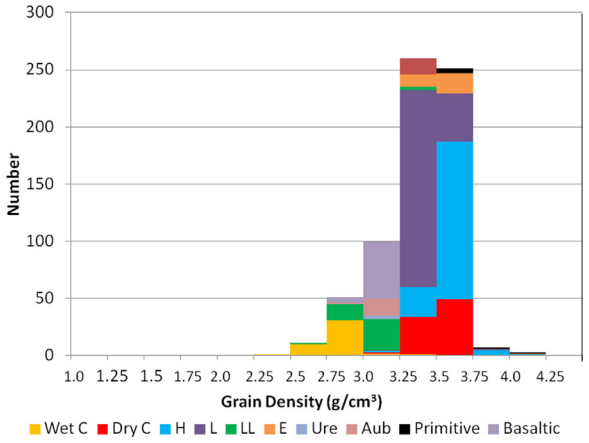

Fig. 2. Grain densities measured on 642 stone meteorite falls including 45 individual samples of 14 wet carbonaceous chondrites, 82 individual samples of 11 dry carbonaceous chondrites, 171 individual samples of 115 H (including 3 H/L) ordinary chondrites, 216 individual samples of 115 L (including 7 L/LL) ordinary chondrites, 45 individual samples of 31 LL ordinary chondrites, 30 samples of 11 enstatite chondrites, 3 samples of 1 ureilite, 16 individual samples of 8 aubrites, 6 individual samples of 3 primitive achondrites, and 69 individual samples of 32 basaltic (HED) achondrites. (Data from Macke, 2010).

diameter, one or two orders of magnitude larger than the conventional size used by some other studies (e.g., the 40–80 μm diameter beads used by Macke et al., 2010a) were used in her study. These larger beads are less likely to penetrate pre-existing cracks, and can result in larger vacancies between the beads and the container walls. To avoid systematic differences between measurements from different laboratories we have focused the density and porosity sections on the largest study of density and porosity of stone meteorites, the 642 stone meteorites measured by Macke (2010), and used this data to investigate correlations of porosity with weathering state, petrographic grade, and shock state.

2.1. Grain density

The grain density of rocks is generally measured by ideal-gas pycnometry, a non-destructive technique in which the grain volume is determined by placing the sample in a gas-tight chamber of known volume and pressurizing it with an inert gas, generally He but N_2 is also commonly used. The gas is allowed to expand into a secondary chamber of known volume, causing the pressure to drop. From the initial and final pressures, the volume displaced by the meteorite can be calculated by applying the ideal-gas law. The ratio of the sample mass to this grain volume gives the grain density (ρ_g).

Terrestrial alteration is a significant concern, especially for finds (e.g., Bland et al., 1998), which may have a long residence time on Earth. The metal-rich H-chondrites are expected to be particularly susceptible to terrestrial modification since high-density Fe-metal easily reacts to produce lower density Fe-oxide. Macke (2010) reported a mean grain density for 207 samples from 116 different H-chondrite falls of 3.71 g/cm^3, while he reported a significantly lower mean grain density of 3.51 g/cm^3 for 79 samples from 63 different H-chondrite finds. Whereas the degree of weathering has been reported for fewer meteorites, this trend of decreasing grain density with increasing weathering is even more apparent in a plot of the mean grain density versus weathering state (Fig. 1) measured on 30 H-chondrite falls and finds.

To consider only those meteorite samples minimally affected by terrestrial modification, the discussion of meteorite grain densities will be restricted to meteorite falls. However, it is important to recognize that even some samples of meteorites that are classified as falls may have experienced significant terrestrial weathering, since some samples from an observed fall may be collected long after the fall. For example, many samples of the Tatahouine meteorite were recovered shortly after it was observed to fall in Algeria in 1931, but more weathered fragments were collected in 1994, by sifting the first few centimeters of the soil in the strewnfield (Gillett et al., 2000). Furthermore, recent searches of the strewnfield recovered weathered samples of the Allende carbonaceous chondrite decades after its 1969 fall. Even samples of meteorites collected promptly after the fall can be altered by exposure to the atmosphere while in collections. Corrigan et al. (1997) noted that old thin sections of the Orgueil CI meteorite frequently exhibit cracking and exfoliation due to remobilization and precipation of hydrous magnesium sulfates in cracks as a result of exposure to the terrestrial atmosphere, and Gounelle and Zolensky (2001) further documented the formation of sulfate veins in CI meteorites.

Because of the possibility of variation resulting from different experimental techniques, Fig. 2 shows only grain densities of 642 stone meteorites that were measured by the same technique and equipment (Macke, 2010). The mean grain densities are given for each meteorite group in Table 2. It is particularly interesting to note that, independent of group, most anhydrous stony meteorites have grain densities within about 10% of 3.5 g/cm^3. This similarity reflects the fact that most stone meteorites have a relatively simple chemistry and mineralogy. Most undifferentiated meteorites are derived from "cosmic" abundances of the major rock forming elements, varying primarily in the oxidation state of the iron. While this oxidation does lead to measurable differences in meteorite grain densities from group to group, those differences are relatively minor. The most notable exceptions are basaltic achondrites and volatile-rich meteorites, which are 10% to 30% less dense than this average. Basaltic meteorites are less dense because they are depleted in metallic iron, while the volatile-rich CM and CI meteorites are less dense because they contain abundant OH-bearing minerals, which are lower in density than the anhydrous silicate minerals.

Meteorites are generally classified by their chemical and mineralogical composition, the same traits that determine their grain densities. Thus it is not surprising that within a particular class of meteorite, the variation in grain density is generally less than 5%. The small increase in grain density between the L, LL, and H ordinary chondrites is attributable to the progressive increase in

Table 2
Mean Grain and Bulk Densities, Porosities and Magnetic Susceptibilities of Stone Meteorites (Data from Macke, 2010).

Type	Grain Density (g/cm^3)	Bulk Density (g/cm^3)	Porosity (%)	Magnetic Susceptibility log $\chi*$ (log 10^{-9} m^3/kg)
Ordinary Chondrites				
H falls	3.71 ± 0.01	3.35 ± 0.01	9.5 ± 0.4	5.30 ± 0.01
L falls	3.58 ± 0.01	3.30 ± 0.01	8.0 ± 0.3	4.87 ± 0.01
LL falls	3.52 ± 0.01	3.18 ± 0.02	9.5 ± 0.6	4.13 ± 0.05
Carbonaceous Chondrites				
CI	2.42	1.57	34.9	4.49 ± 0.38
CM	2.96 ± 0.04	2.27 ± 0.02	22.2 ± 0.7	3.80 ± 0.05
CR	3.42 ± 0.08	3.11 ± 0.14	9.5 ± 2.7	5.02 ± 0.07
CB	5.65 ± 0.01	5.25 ± 0.19	3.9 ± 1.9	5.57 ± 0.10
CH	3.65 ± 0.00	3.79 ± 0.05	−3.7 ± 1.4	5.30 ± 0.08
CV	3.61 ± 0.01	2.97 ± 0.03	17.7 ± 1.0	3.91 ± 0.06
CO falls	3.36 ± 0.02	3.10 ± 0.07	7.6 ± 2.3	4.41 ± 0.05
CK	3.58 ± 0.02	2.90 ± 0.05	17.7 ± 1.7	4.67 ± 0.01
Enstatite Chondrites				
EL falls	3.61 ± 0.03	3.48 ± 0.05	3.7 ± 0.9	5.36 ± 0.08
EH falls	3.66 ± 0.04	3.58 ± 0.05	2.1 ± 1.0	5.50 ± 0.03
Achondrites				
Howardites	3.26 ± 0.02	2.85 ± 0.03	12.5 ± 0.9	3.34 ± 0.06
Eucrites	3.19 ± 0.01	2.84 ± 0.02	10.9 ± 0.6	3.07 ± 0.06
Diogenites	3.43 ± 0.01	3.10 ± 0.03	9.2 ± 1.0	3.04 ± 0.07
Ureilites	3.36 ± 0.02	3.22 ± 0.02	4.0 ± 0.9	4.60 ± 0.08

Where separate measurements were reported in Macke (2010) for falls and for finds, the fall data is listed and the meteorite type is noted with the word falls.

Fe-metal content from the LL to L to H types (Table 2). The exceptionally high grain density of the CB carbonaceous chondrites is due to the presence of a substantial amount of metal.

2.2. Bulk density

There are several techniques available for measuring the bulk density of a meteorite. The most common techniques used for terrestrial samples are inappropriate for many meteorites, since they require altering or potentially contaminating the sample. For example, Archimedean volume measurement using liquids have been performed on a limited number of samples (Keil, 1962; Pesonen et al., 1993), but submersing meteorites in contaminating liquids such as water or carbon tetrachloride is extremely undesirable for preservation of these important samples, making this method inapplicable for statistically significant surveys of large collections or for measurement of rare meteorites. In addition, such fluids may enter pore spaces to an unknown extent, producing a measurement that is neither a grain nor a bulk density but something between the two.

Sample altering measurement techniques have also been attempted; for example, the sample can be cut into a uniform shape, such as a cube or a slab, allowing easy and precise determination of the volume. This has been employed on a limited number of samples (e.g., Yomogida and Matsui, 1981, 1983), but it is impractical for valuable or rare meteorites, and for surveying large collections where altering the meteorite would not be permitted.

Consolmagno and Britt (1998) developed a non-destructive and non-contaminating variation on the Archimedes method, replacing the fluid by chemically inert spherical beads. This has made it practical to non-destructively determine the bulk densities of many meteorites. The method involves submersing the sample in small, spherical glass beads that collectively behave as a fluid, but do not penetrate the sample's pore space. The mass of beads displaced by the meteorite yields the volume of the sample through simple calculations. The Archimedean glass bead method has enabled a survey of meteorite bulk density over a wide variety of meteorite types including multiple samples from the same meteorite (Consolmagno and Britt, 1998; Flynn et al., 1999; Britt and Consolmagno, 2003; Consolmagno et al., 2006, 2007, 2008c; Macke, 2007; Jones, 2009; Macke, 2010; Ibrahim, 2012). Because it is non-destructive and non-contaminating this method is not limited to meteorites; its application includes any irregularly shaped samples such as terrestrial geological specimens and museum artifacts.

This method assumes that the beads flow like an incompressible fluid of constant density. However, in practice bead density depends on such factors as packing efficiency and ambient environmental conditions such as humidity. In addition, due to the irregular shape of the meteorite itself, the beads may not settle homogeneously. All of these effects are further complicated by the various methods that can be used to settle the beads in the container. Together, these may introduce systematic error into measurements of bulk volume. Macke et al. (2010a) assessed the systematic error in bead method measurements of meteorite bulk volume and density and to generally be less than 2% for samples larger than 5 cm^3.

More recently, the use of laser scanners for bulk volume determination has also been employed as a standard technique (Smith et al., 2006a), who noted that the densities determined using 3-D laser imaging compare well with previously published values, based on a variety of other measurement techniques. However, nine out of the eleven samples they studied had higher bulk densities determined using 3-D laser imaging than previously published results, which they attributed to friction between fluid and container, and bead compaction that might have led to an overestimation of the volume measured using Archimedean bead methods (Smith et al., 2006a). This method involves creating three- dimensional shape models, allowing computer calculation of the volume. Laser scanning systems capable of high- resolution scans on a range of albedos and surface textures have the advantages of being entirely contact- free and more accurate than the beads. The trade-off is that acquiring and processing the data takes much longer per sample than the bead method.

Fig. 3 shows the bulk densities measured on the same 642 stone meteorite falls shown in Fig. 2. The vast majority of these samples were measured via glass bead immersion. The mean bulk densities are given for each meteorite group in Table 2.

The bulk densities of the stone meteorites show a much wider range than is seen for the grain densities. Some meteorites have the same bulk and grain density, indicating they contain no void spaces, while others have much lower bulk than grain densities, indicating

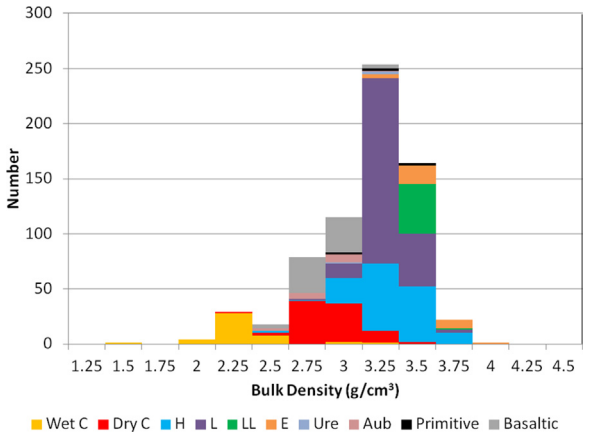

Fig. 3. Bulk densities measured on 642 stone meteorite falls as listed in Fig. 2. (Data from Macke, 2010).

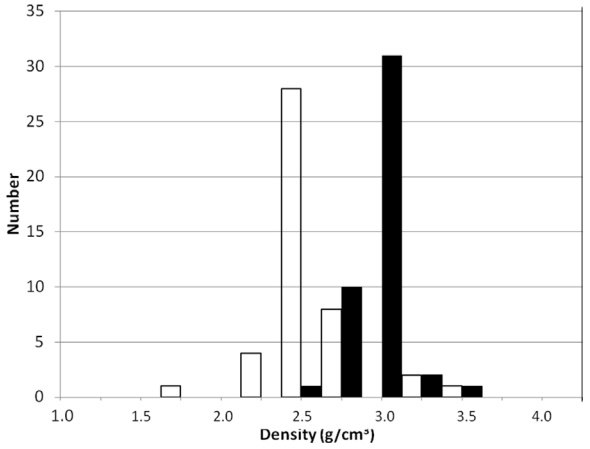

Fig. 4. Bulk density (open) and the grain density (solid) for 45 wet carbonaceous chondrite meteorite samples (petrographic grade <3.0) from 14 different meteorites. The low bulk densities compared to the grain densities indicates these wet carbonaceous chondrites have significant porosities. (Data from Macke, 2010).

a significant fraction of their volume consists of void spaces. Large porosities are seen most dramatically for the wet (i.e., petrographic grades less than 3.0) carbonaceous chondrites (Fig. 4).

2.3. Bulk density from meteor observations

Bulk densities of the meteoroids, which are the immediate parent objects of the meteorites, can be roughly inferred from their observed atmospheric dynamics, luminosity and electron density production by making some assumptions about various model parameters. The estimated bulk densities depend on assumptions about shape and luminous efficiency. Thus there may be systematic effects though relative densities are probably reasonably represented in these datasets.

When a meteoroid enters the atmosphere, collisions with air molecules decelerate the meteoroid. The measured deceleration, together with estimates of the shape and mass of the meteoroid, can be used to estimate the meteoroid bulk density, assuming the body does not fragment. At any point along the visible trajectory momentum conservation requires that:

$$m dv/dt = -\Gamma A \rho v^2 \quad (1)$$

where m is the instantaneous mass of the meteoroid, v is its speed, Γ is the drag coefficient, which is often assumed to be 1 for small meteoroids at high altitude, A is the cross sectional area and ρ is the mass density of atmosphere (e.g., Ceplecha et al., 1998). Rewriting Eq. (1) in terms of a shape factor $S = A m^{-2/3} \delta^{2/3}$ and the meteoroid bulk density δ gives:

$$dv/dt = -\Gamma S \delta^{-2/3} \rho m^{-1/3} v^2 \quad (2)$$

Thus, the deceleration (dv/dt) is directly related to the product $\Gamma S \delta^{-2/3}$ which is collectively termed the shape-density coefficient. From observations it is only possible to estimate the shape- density coefficient and not uniquely separate the bulk density from the product of the drag coefficient and the shape factor, which is the ratio of the surface area to volume of the meteoroid. The shape factor is 1.21 for a sphere and may vary from 1 (for a cube) to almost 2 for a hemispherical body. Most investigators assume the shape-density coefficient is a constant, make assumptions for the shape factor (usually a sphere) and take $\Gamma \sim 1$. The inferred values for bulk densities for meteoroids follow from these assumptions.

While most or all meteorites sample asteroidal parent bodies, the association of some meteor streams with active comets demonstrates that many meteors are from cometary parent bodies. The Tisserand parameter, a dynamical quantity that is approximately conserved during an encounter between a planet and a small interplanetary body, provides a way to connect the post-encounter dynamical properties with the pre-encounter properties, distinguishing most asteroidal from most cometary meteors (Murray and Dermot, 2000). The Tisserand parameter relative to Jupiter (T_J) derived as a restricted circular three-body approximation including the effects of the Sun, Jupiter, and the interplanetary body is given by:

$$T_J = \frac{a_J}{a} + 2\left[\left(1 - e^2\right)\frac{a}{a_J}\right]^{1/2} \cos(i) \quad (3)$$

where:

a_J = semimajor axis Jupiter

a,e,i = semimajor axis, eccentricity and inclination of object

In general, a $T_J < 2$ is characteristic of Halley type or nearly-isotropic comets (NICs) which have a wide range of orbital inclinations, $2 \le T_J \le 3$ is characteristic of Jupiter Family Comets (JFCs), which have inclinations close to the ecliptic plane, and a TJ > 3 is typical of asteroidal orbits (Levison, 1996). However, modeling and spectral observations suggest that up to 50% of kilometer-sized objects with $2 \le TJ \le 3$ may be derived from the main-belt (e.g., DeMeo and Binzel, 2008). Particularly near the boundary at TJ ~ 3 substantial mixing between source populations is expected (Tancredi, 2014), so a TJ > 3 value does not automatically exclude a cometary origin. As an example of this overlap, the Tisserand parameter, TJ, of comet 2P/Encke is 3.027, while Encke is clearly an active comet.

Kikwaya et al. (2011) and Kikwaya Eluo (2011) estimated bulk densities for 92 optical meteors with pre-atmospheric masses larger than 5×10^{-4} g (Fig. 5). Of these, 51 meteoroids (or 55%) had $T_J < 2$, 15 (or 16%) had $2 \le T_J \le 3$, and 26 (or 28%) had $TJ > 3$. They found that meteoroids with TJ < 2 consistently had the lowest densities. In all but one case, meteoroids with TJ < 2 had bulk densities falling between 0.36 and 1.51 g/cm3. Those with $T_J > 2$ generally had densities greater than 2.5 g/cm3. There was considerable overlap between the bulk densities of the meteors with $2 \le TJ \le 3$, mostly from the JFCs, and those with $TJ > 3$, mostly from the asteroids. High-density objects (> 4.5 g/cm3), likely indicating they were dominated by metal or sulfide, predominantly had TJ > 3, while objects of intermediate density, between 2.5 and 4.0 g/cm3, were found in similar proportions in both the JFC and asteroid categories. The unusually high bulk density (mean of 3.1 g/cm3) associated with meteoroids having JFC-like orbits is at strong variance with other measurements of some JFC meteoroid densities

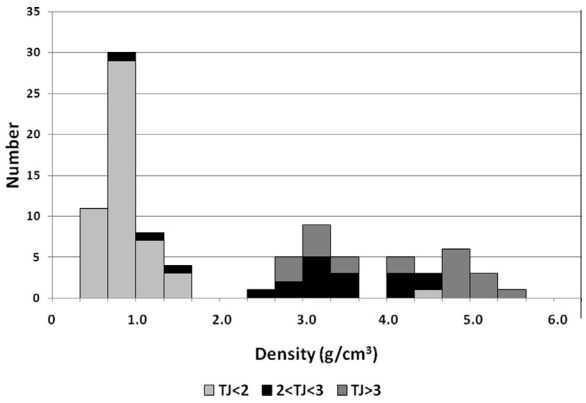

Fig. 5. Distribution of the best fit values for meteoroid bulk densities from a model fit to optical meteor data from Kikwaya Eluo (2011). The data are sorted by their Tisserand parameter relative to Jupiter (T_J), with these mm-sized meteoroids having $T_J < 2$ shown light gray, $2 \leq T_J \leq 3$ shown in black, and $T_J > 3$ shown in dark gray.

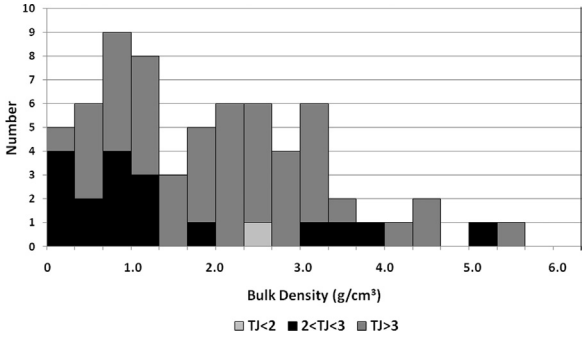

Fig. 6. Distribution of the best fit values for 66 fireball bulk densities, inferred from the deceleration measured near the end point for fireball, from Halliday et al. (1996). The data are sorted by their Tisserand parameter relative to Jupiter (T_J), with fireballs having $T_J < 2$ shown in light gray, $2 \leq T_J \leq 3$ shown in black, and $T_J > 3$ shown in dark gray. The binning size is not intended to indicate the error in the measurement.

(e.g., Borovička et al., 2007) and with expectations that JFC-related meteoroids should be of low density (e.g., Fernández, 2005).

Of the 642 stone meteorite falls measured by Macke (2010), only one, the CI carbonaceous chondrite Orgueil, has a bulk density less than 2.0 g/cm^3. However, the meteors measured by Kikwaya et al. (2011) are in the size range of the micrometeorites collected from the sea floor or the Polar ices rather than in the size range of meteorites. These micrometeorites sample the fraction of meteoroids in this size range that were not heated sufficiently to vaporize during atmospheric entry.

Halliday et al. (1996) analyzed data on 259 meteoric "fireballs" identified in the Meteorite Observation and Recovery Project (MORP), the largest systematic study of fireball fluxes, bulk densities and orbital distributions. The meteoroids producing fireballs in the Halliday et al. (1996) study are generally much larger in size than the optical meteors studied by Kikwaya et al. (2011), with estimated masses ranging from ~1 g, for the fastest ones, to hundreds of kilograms. Sixty-six of these fireballs did not significantly fragment, so Halliday et al. (1996) were able to determine their deceleration and infer their bulk densities. Since fragmentation depends on strength as well as entry speed, entry angle and shape, these 66 meteors are not necessarily the strongest of the 259 meteors in the data set. Of the 66 meteors, only one (or 1.5%) had $T_J < 2$, 18 (or 27%) had $2 \leq T_J \leq 3$, and 47 (or 71%) had $T_j > 3$. The inferred densities show broad distributions for both the $2 \leq T_J \leq 3$, likely JFC group, and the $T_J > 3$, likely asteroidal group (Fig. 6). However the mean bulk density of the $2 \leq T_J \leq 3$ group, 1.5 g/cm^3, is significantly lower than the mean bulk density of the $T_J > 3$ group, 2.2 g/cm^3. It is noteworthy that the mean bulk density for the meteors with $T_J > 3$ is significantly lower than the mean bulk density of the ordinary chondrite meteorites, which ranges from 3.18 to 3.35 g/cm^3 for the different types (Table 2), which are the most common meteorites among collected falls.

Applying a new data analysis technique that includes the effects of luminosity, fragmentation, ablation, and entry dynamics, Ceplecha and ReVelle (2005) confirmed the shape density coefficients found in earlier work. However, they noted that there are significant uncertainties in porosities derived from fireball data because the values of Γ and S in Eq. (2) are not known.

A major bias in the fireball data is with respect to mass. The MORP survey, like all fireball surveys, is brightness limited, not mass limited, so that for meteoroids with $T_J \sim 0$, which have a high atmospheric entry velocity, the limiting mass sensitivity is close to 50 times smaller than for those meteoroids with $T_J \sim 3$. Further bias is created by any fragmentation (even small scale), which will tend to artificially decrease the apparent mass and thus lower the apparent bulk density estimate.

A comparison between the bulk densities of meteorites and fireballs indicates that there is general agreement between these densities for many meteors. These data show that there is a class of extremely low-density objects that fail to reach Earth's surface as recognizable meteorites. Many of the low density objects in the fireball population, with densities <1.7 g/cm^3, have values of T_J indicating orbits consistent with meteors from JFCs, but some have $T_J > 3$, suggesting a main-belt asteroidal origin. This indicates that Earth's atmosphere acts as a filter, likely fragmenting and/or vaporizing weak or highly-porous objects before they reach the ground, resulting in the meteorites being a biased sample of the material from their parent bodies. Halliday et al. (1996) suggested that many of the low density fireballs in the $T_J > 3$ group might be cometary, because of the overlap between the JFC and asteroidal groups for T_J values near 3.

2.4. Porosity

For meteorite samples on which both the bulk density (ρ_{bulk}) and the grain density (ρ_{grain}) have been measured, the *porosity* (P) can be calculated directly:

$$P = [1 - \rho_{bulk}/\&\#961;_{grain}] \times 100\%. \quad (4)$$

If only the bulk density is measured on the sample, then a *model porosity* can be inferred by using the same formula, taking as the grain density the mean grain density for that type of meteorite, or using a calculated grain density if the mineralogy of the sample is well determined.

Fig. 7 shows the porosities measured using pycnometry on more than 600 stone meteorite falls, sorted by meteorite type. These porosities span the range from essentially 0% to >40% porosity, comparable to the wide range seen for asteroid porosities. However, the mean porosity measured for the meteorites is noticeable lower than for asteroids. Scott et al. (1992) suggested that highly porous, friable stones are unlikely to survive ejection from the parent asteroid while Baldwin and Sheaffer (1971) and Consolmagno et al. (2008a, 2008b) suggested they could not survive atmospheric entry and landing. Very high porosities are observed in smaller samples, including some interplanetary dust particles collected from the Earth's stratosphere by NASA (Flynn and Sutton, 1991) and, less frequently, micrometeorites collected from the Polar ice and snow (Flynn et al., 2016).

The highest porosities measured by Macke (2010; later work), those larger than 30%, are all on samples of carbonaceous chondrites: 34.9% for the CI meteorite Orgueil, four CM2 meteorites, Crescent (30.7%), Sutter's Mill (31.0%), Mighei (32.2%), and Santa Cruz (36.7%), and the highest value of 41.3% for the dry CO3 Ornans.

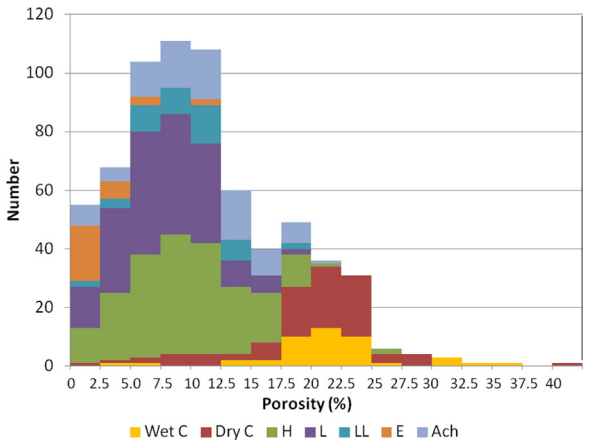

Fig. 7. Porosities measured on more than 600 stone meteorite falls, sorted by meteorite type. The wet and the dry carbonaceous chondrites generally have the highest porosities. Low porosity (<5%) meteorites are atypical among all types of meteorites except the enstatite chondrites (Data from Macke, 2010, and later unpublished work).

Corrigan et al. (1997) determined the porosity of the matrix of a different, much smaller, Orgueil sample using digital images of the surface of a potted butt that had been ultramicrotomed. They found a matrix porosity of only 4% and cautioned that terrestrial hydration can alter Orgueil, with recrystalization possibly causing cracks to expand dramatically. Despite their porosity, most ordinary chondrites have bulk densities from 2.7 to 3.7 g/cm^3 (Fig. 3), which is denser than most terrestrial rocks.

The porosities inferred for the few comets that have been measured are even higher than those of asteroids. Spacecraft flyby measurements allowed estimates of the bulk densities of 0.1–0.3 g/cm^3 for comet 26P/Borrelly (Davidsson and Gutiérrez, 2004), 0.6–0.8 g/cm^3 for comet 81P Wild 2 (Davidsson and Gutiérrez, 2006), 0.2–1.0 for comet 9P/Temple 1 (Richardson et al., 2007), and 0.18–0.88 g/cm3 for comet 103P/Hartley 2 (A'Hearn et al., 2011), each implying a high porosity for an ice/rock mixture. Comet 67P/Churyumov-Gerasimenko, a JFC studied in detail by the orbiting Rosetta spacecraft, has a bulk density of 0.470 ± 0.045 g/cm3 and a porosity of 70–80% (Sierks et al., 2015). Such low bulk densities are common among the optical NIC meteoroids, but relatively rare among optical JFC meteoroids (Fig. 5), but they are relatively common among the fireballs with either JFC or asteroidal orbital characteristics (Fig. 6).

2.5. Variability

The mean porosity and range of porosity values around this mean vary from class to class or, in some cases, among subgroups within a class. Most ordinary chondrites have porosities between 5 and 15%. Typically the enstatite chondrites have porosities less than 5%, while some carbonaceous chondrite classes have porosities in excess of 30%. The most striking difference among subgroups is that between two sub-groups of the CV carbonaceous chondrites, the CV_r, or reduced group, and CV_o, or oxidized group, whose average porosities are 3% and 21% respectively (Macke, 2010). The low porosity of the CV_r group likely reflects compression of the parent body after formation, evidenced by the observation of flattened chondrules in the CV_r group (McPherson and Krot, 2002).

Even individual samples of the same fall can exhibit considerable variability in their bulk densities and porosities. Macke (2010) reported the properties of 36 individual samples, ranging from 9.14 to 148.02 g, from the Holbrook L/LL6 ordinary chondrite shower. He found a narrow range of grain densities from 3.37 to 3.72 g/cm^3, with a mean of 3.55 g/cm^3. However the measured bulk densities of these samples show a wider range, from 3.00 to 3.54 g/cm^3, with a mean of 3.18 g/cm^3. The porosities of these Holbrook samples ranged from 1.5%, in an 18.2 g sample, to 14.6%, in a 23.9 g sample. While Holbrook is a fall known to have been collected over a long period of time, the similarities in grain densities for these samples argues that these differences are *not* due to different degrees of terrestrial weathering; such weathering, which introduces oxides into pore spaces, alters grain density much more strongly than bulk density. Macke (2010) reported similar variation on 23 samples from the Pultusk (H5) shower. The grain densities varied from 3.54 to 3.89 g/cm^3, while the bulk densities ranged from 3.22 to 3.77 g/cm^3. Porosities of these samples varied from 0.3% in a 13.4 g sample to 12.1% in a 5.8 g sample. Kohout et al. (2014a) examined 25 samples, 18 from the light lithology and 7 from the dark lithology, from the Chelyabinsk meteor shower. They found the bulk density ranged from 3.14 to 3.48 g/cm^3, the grain density ranged from 3.22 to 3.60 g/cm^3 and the porosity ranged from 1.5% to 11.4% with only small differences in the mean values between the two lithologies. Kohout et al. (2014b) examined 67 samples, most of them recovered within 4 weeks of the fall, from the Košice meteor shower. In samples ranging fromm 0.56 g to 2167.4 g they found grain densities ranging from 3.7 to 4.3 g/cm^3, bulk densities ranging from 3.0 to 3.6 g/cm^3, and porosities ranging from 4 to 20%.

The carbonaceous chondrites show a similar variability in their porosity. Macke (2010) reported measurements on 49 samples from the Allende (CV3) shower. The grain densities varied from 3.59 to 3.86 g/cm^3, while the bulk densities varied from 2.66 to 3.00 g/cm^3. The porosities ranged from 17.6% for a 43.9 g sample to 27.9% for a 25.1 g sample. These results indicate considerable local variability in the porosity of the bolide entering Earth's atmosphere at size scales of centimeters to meters.

The data set for meteorite porosity is now sufficiently large to allow examination of the data for correlations between weathering state, petrographic grade, and shock state with porosity. While the mass and the grain density can be determined with high precision and accuracy, measurement of the bulk volume is subject to larger errors. Macke et al. (2010a) showed that the accuracy of the glass bead method of determining bulk volume, which has been used by most investigators over the past two decades, depends on the procedure used to settle the beads into the container, the humidity of the room, and the size of the beads. To minimize these effects in investigating correlations we examined the data on the 642 stone meteorites all measured by Macke (2010) using the same procedure.

2.6. Variations with weathering

Terrestrial weathering of ordinary chondrites generally produces minerals having lower grain densities than those they replace, e.g., Fe-oxide from Fe-metal, sulfate from sulfide, or clays from anhydrous silicates. In addition, these replacement phases incorporate elements from the terrestrial air or fluid responsible for the alteration. Thus, these replacement phases are likely to partially fill void spaces, reducing the porosity of the sample, but these species expand into existing pore space without significantly altering the exterior dimensions of the stone, leaving bulk density largely unaltered. For weathered meteorites a model porosity can approximated using the measured volume and mean grain density of the appropriate meteorite type.

Fig. 8 shows the porosity versus weathering state for the 33 H-chondrite samples that have both measured porosities and published weathering states, and Fig. 9 shows the same data for 45 L-chondrite samples. The data for both the H- and L- chondrites show a higher mean porosity for unweathered samples (W0), with an essentially flat pattern for all of the higher weathering states.

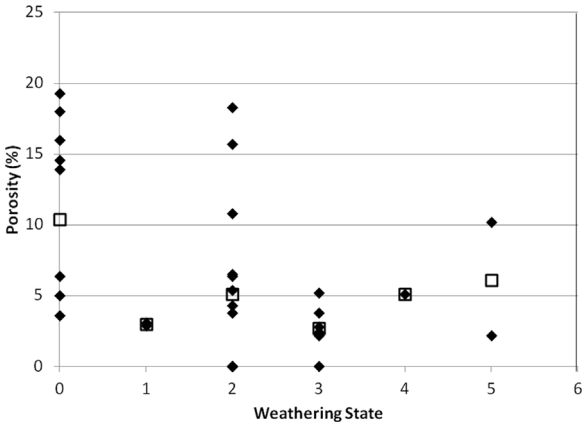

Fig. 8. Porosity (Macke, 2010) vs. weathering state, reported in the Meteoritical Bulletin Database or Grady (2000) , for 33H-chondrite samples (diamonds) from 14 falls and 19 finds. The mean value for each weathering state (squares) shows a relatively flat pattern from W1 through W5.

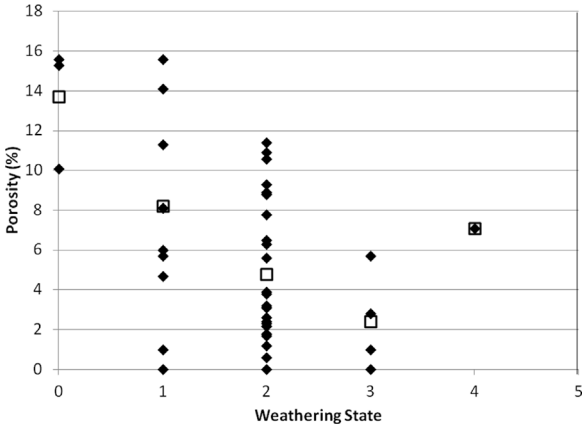

Fig. 9. Porosity (Macke, 2010) vs. weathering state, reported in the Meteoritical Bulletin Database or Grady (2000) , for 45 L-chondrite samples (diamonds) from 13 falls and 32 finds. The mean value for each weathering state (squares) shows a relatively flat pattern from W1 through W4.

This suggests that pore reduction in ordinary chondrites is a relatively rapid process, with an ~50% reduction in the porosity going from W0 to W1. However, even at the highest weathering state the porosity may not be completely removed from the ordinary chondrite samples. Fig. 10 shows the porosity vs weathering state for 22 dry carbonaceous chondrite samples, with no clear trend.

2.7. Variations with petrographic grade

Internal heating of the H-chondrite parent body, likely from the decay of ^{26}Al, has been suggested to result in an onion skin structure in which material from the greatest depths experienced a higher degree of thermal metamorphism than material from the near surface (e.g., Trieloff et al., 2003). In this model, petrologic type, increasing from 3 to 7, can serve as a proxy for increasing depth in the parent body.

Yomogida et al. (1983) noted that for H-chondrites, porosity decreases with increasing metamorphic temperature (petrologic type). Although there is considerable variation in porosity among individual samples from the same petrologic group, the much larger data set currently available supports their claim, with the mean porosity for samples in each petrographic grade showing a trend of declining porosity with increasing petrographic grade (Fig. 11) for the H- chondrites. Except for the very low porosity of the L3.7 Mezo-Madaras (1.9%), the mean porosity also shows a declining

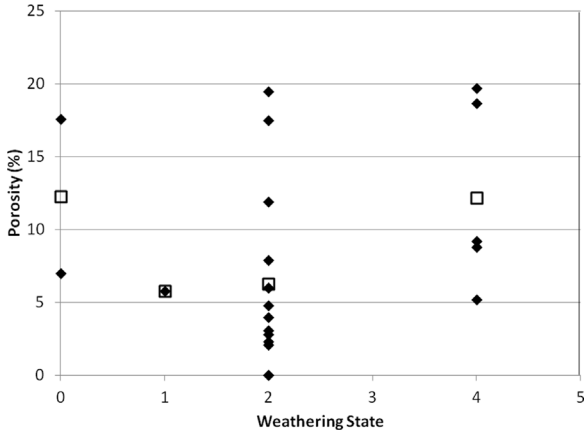

Fig. 10. Porosity (Macke, 2010) vs. weathering state, reported in the Meteoritical Bulletin Database or Grady (2000) , for 22 dry carbonaceous chondrite samples (diamonds). The mean value for each weathering state (squares) shows no clear trend.

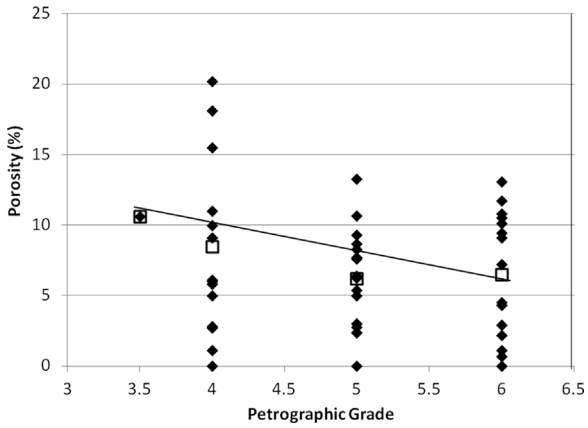

Fig. 11. Porosity (Macke, 2010) vs. petrographic grade, from the Meteoritical Bulletin Database, for H-chondrites (diamonds). The mean porosity for H-chondrites of each petrographic grade (squares) shows a slight decreasing trend with increasing petrographic grade.

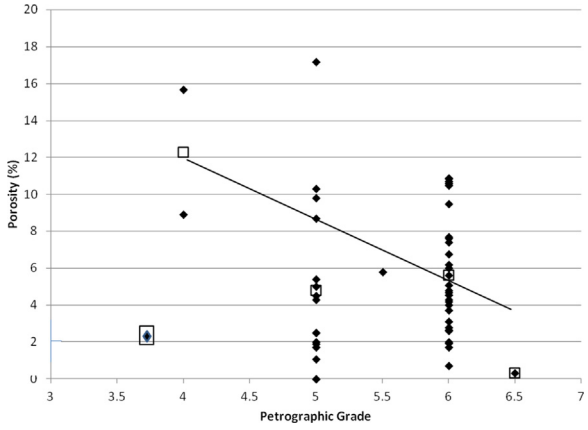

Fig. 12. Porosity (Macke, 2010) vs. petrographic grade, from the Meteoritical Bulletin Database, for L-chondrites (triangles). Except for the single L3.7 sample, the mean porosity for L-chondrites of each petrographic grade (squares) shows a decreasing trend with increasing petrographic grade.

trend with increasing petrologic grade for the L-chondrites (Fig. 12). More limited data on the scarcer LL- chondrites makes it difficult to test for any meaningful trend.

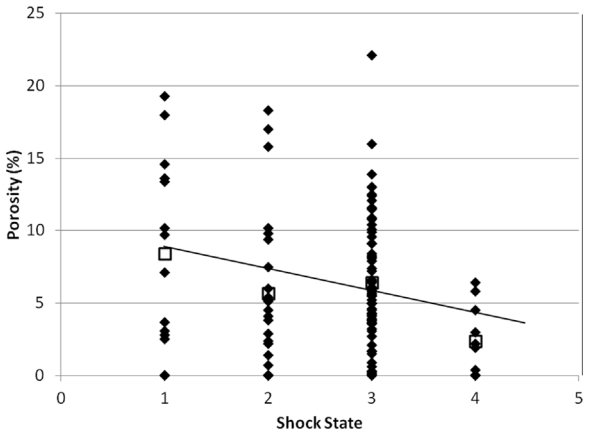

Fig. 13. Porosity (Macke, 2010) vs. shock state, from the Meteoritical bulletin Database or Grady (2000), for 119H- chondrite samples (diamonds). The mean porosity for each shock state (squares) shows a slight decrease with increasing shock state, as indicated by the least squares fit line to the mean values, which has r = −0.89.

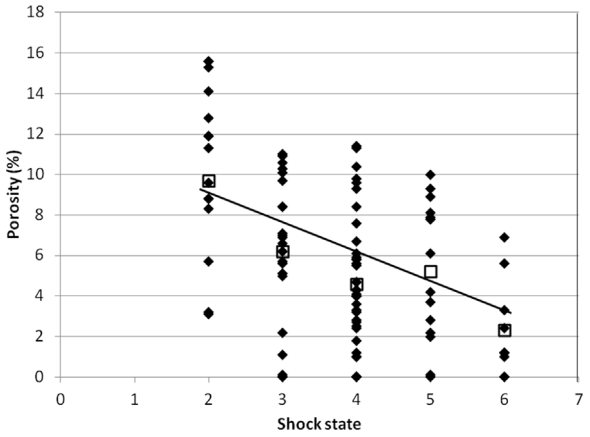

Fig. 14. Porosity (Macke, 2010) vs. shock state, from the Meteoritical Bulletin Database or Grady (2000), for 102 L-chondrite samples (diamonds). The mean porosity for each shock state (squares) shows a slight decrease with increasing shock state as indicated by the least squares fit line to the mean values, which has r = −0.92.

These results suggest that the parent bodies of the ordinary chondrites formed from planetesimals that had significant porosity. This porosity may have subsequently been reduced either by thermal metamorphism or gravitational pressure. However, these data suggest that even at the depths in the parent bodies sampled by the H6 and L6 ordinary chondrites, the effects of parent body heating and gravitational pressure were insufficient to completely remove the preaccretional porosity from these samples.

2.8. Shock state

The most common mechanism proposed for the ejection of meteorites from their parent bodies is impact cratering or disruption. This exposes the meteorites to heating and shock pressure, which might either compact the sample or induce new porosity by fracturing. Consolmagno et al. (1998c) reported a general dependence of porosity on shock state, an effect confirmed on a larger sample set by Macke (2010)

Fig. 13 shows the porosity versus shock state for 119 H-chondrite samples, while Fig. 14 shows it for 102 L- chondrite samples. Although there is considerable scatter in the individual measurements, there is a clear trend of decreasing porosity with increasing shock state for the mean porosity in each group. This suggests that impact shock and the accompanying heating reduces the porosity of the ejected meteorites, a factor that might at least partially explain the difference between the mean porosity of meteorites and the higher mean porosity for asteroids on which porosities have been measured.

Information on the effect of shock on porosity among the carbonaceous chondrites is more limited. An X-ray computed tomography study of a 44 g stone from the wet carbonaceous chondrite Murchison found evidence of deformation caused by impact in a sample recording a shock state S1 (Hanna et al., 2015). They suggested that Murchison suffered significant porosity loss, deformation, and compaction from impact on a parent body whose samples recorded only a low level of shock

2.9. Types of porosity

Two types of porosity are generally distinguished by their size-scale: microporosity and macroporosity. Microporosity consists of voids, pores, and fractures, typically at the size scale of tens of micrometers, present in samples the size of meteorites. Macroporosity is the additional large scale voids and fractures in the parent bodies of the meteorites.

While He-pycnometry (Consolmagno and Britt, 1998; Consolmagno et al., 2008c) provides accurate total porosity values, it gives no indication of the location or structure of the pores in the meteorites. Optical microscope or Scanning Electron Microscope (SEM) examination of thin sections images the microporosity present in the meteorites (Consolmagno et al., 1999; Strait and Consolmagno, 2002, 2005). The microporosity of most stone meteorites is dominated by an interconnected fabric of cracks, and most of the porosity found in ordinary chondrite hand samples can be accounted for by the microcracks seen in the thin sections (Strait and Consolmagno, 2002). However, the dominant type of porosity in a few stone meteorites consists of overlapping void spaces. The L5 chondrite Mount Tazerzait, having a porosity of 17 ± 1% (Flynn et al., 1999), consists of well-defined, spherical chondrules embedded in a porous matrix containing voids up to 1 mm across. The L5 chondrite Baszkówka is similar to Mount Tazerzait, but it exhibits even higher porosity (~20%) with voids up to 5 mm in diameter. In Baszkówka the pores are clearly interstitial to the chondrules and other large grains, i.e., leftover space in a very loosely compacted rock (Wlotzka et al., 1997). The Mason Gully H5 ordinary chondrite, having a porosity of 10.7%, also exhibits intergranular void spaces rather than the microscopic cracks found in most ordinary chondrites (Dyl et al., 2016).

Computed x-ray microtomography (CMT) provides the opportunity to image samples in 3-dimensions, revealing the structure of the porosity as well as its connectivity. Flynn et al. (2000) performed CMT on ~1 cm size samples of 12 stone meteorites and identified both cracks and voids in images with an ~30 μm voxel size. In the case of a cm-size sample of the H5 ordinary chondrite Gao-Guenie, a crack cross-cuts the fusion crust, indicating that either the crack postdated the formation of the fusion crust or that a preexisting crack significantly widened after the formation of the fusion crust, possibly induced by impact with the ground (Flynn et al., 2008).

Combined CMT and He pycnometry examination of two samples of Baszkówka indicated that two-thirds of its ~19.0% porosity is in the form of inter- and intra-granular voids, with a power law size distribution, having volumes between $\sim 3 \times 10^{-5}$ and 3 mm^3 (Friedrich et al., 2008). Voids also dominate the porosity of the H5 chondrite Sahara 98034, and the CM2 carbonaceous chondrite Nogoya. Sasso et al. (2009) performed high-resolution CMT to investigate the pore structure of five highly-porous chondrites, NWA 2380 (LL5), Tjerebon (L5), Mount Tazerzait (L5), Sahara 98034 (H5), and Miller (Arkansas) (H5). They reported bulk porosities ranging from 10 to 20%, with ~64% of the void space as intergranular voids. They concluded that the parent bodies of these

meteorites accreted with incomplete compaction, preserving a significant amount of accretional porosity, and that this was a common occurrence in the asteroid belt.

3. Magnetic susceptibility

Since the metallic iron content of ordinary chondrites is a major factor in their classification as LL-, L- or H-type, Sugiura (1977) suggested that their magnetic properties could be used to provide an indication of type. Rochette et al. (2003) reviewed the literature of earlier measurements and reported magnetic susceptibility measurements on 971 meteorite samples. They showed a clear separation between the mean logχ, where χ is the ratio of the magnetization of the material to the strength of an applied magnetic field, of falls from the three types of ordinary chondrites, with the LL chondrites having logχ of 4.10 ± 0.30, the L chondrites logχ of 4.87 ± 0.10, and the H chondrites logχ of 5.32 ± 0.10.

Rochette et al. (2003, 2006, 2008, 2009) demonstrated the utility of magnetic susceptibility measurements for classification of ordinary chondrites, and suggested that at least 5% of meteorites surveyed in a number of different collections were mislabeled, misclassified, or otherwise misidentified. Earlier, Pesonen et al. (1993) had shown that combining measurements of magnetic susceptability with bulk density could be used to classify meteorites. However they noted some overlap between the groups. Smith et al. (2006b) determined four parameters of low-field magnetic susceptibility, the bulk value, the frequency dependence, the degree of anisotropy, and the ellipsoid shape for 321 stone meteorites from the National Collection of Canada, and demonstrated that chondrites show a clear trend of increasing bulk susceptibility from the LL to L to H to E types. Consolmagno et al. (2006) combined *grain* density with magnetic susceptibility, examining 132 ordinary chondrites. They demonstrated that taken together, grain density and magnetic susceptibility provide a reliable method of classifying unweathered ordinary chondrites or surveying meteorite collections to identify misclassified ordinary chondrites. Unlike traditional chemical tests, this method is fast, nondestructive, and characterizes the whole rock, making it especially appropriate for surveying large collections. In each case where the magnetic susceptibility of the meteorite fell outside the expected range for its type, the grain density was also discordant with the type, suggesting either the meteorite was highly weathered or misclassified (Consolmagno et al., 2006). The combination of grain density and magnetic susceptibility provides a useful screening technique to identify interlopers in large, recent ordinary chondrite strewn fields. This classification technique has the benefit of being inexpensive and non- destructive, and unlike other methods, does not depend on selecting a small and possibly uncharacteristic subsample, but instead characterize the whole stone.

This system is less viable for finds since extensive weathering of metallic iron in an H chondrite can cause it to plot among L chondrites, while heavily weathered L chondrites plot among the LL group. Classification by grain density and magnetic susceptibility is also likely to be problematic for inhomogeneous meteorites, including highly brecciated meteorites such as Almahatta Sitta.

The combined density and magnetic susceptibility study of 51 stones from the Allende fall found generally good agreement between the values for the individual samples, with a mean bulk density of 2.86 ± 0.08 g/cm^3, a mean grain density of 3.65 ± 0.06 g/cm^3, and a mean magnetic susceptibility of logχ of 3.65 ± 0.06 (Macke et al., 2011a). Nonetheless, they reported slight differences between 39 stones in the American Museum of Natural History (AMNH) collection and 12 stones in the Smithsonian Institution – National Museum of Natural History (NMNH) collection. The AMNH Allende stones had a lower mean bulk density (2.84 ± 0.01 g/cm^3 versus 2.93 ± 0.01 g/cm^3), while the NMNH Allende stones had a lower mean grain density (3.62 ± 0.02 g/cm^3 versus 3.66 ± 0.01 g/cm^3) and lower mean magnetic susceptibility (3.61 ± 0.02 versus 3.66 ± 0.01). They suggested the results could indicate differences in terrestrial alteration resulting from differences in the humidity in the sample storage areas of the two institutions over four decades.

4. Thermal properties of meteorites

The thermal properties of meteorites are critical to the accurate modeling of the physical state and evolution of asteroids and other small solar system bodies, but these properties are understudied. Knowledge of meteorite heat capacity and thermal conductivity are essential in modeling the cooling of asteroids after the era of heating by the decay of short lived radioactive elements (e.g., ^{26}Al). The thermal conductivity and heat capacity are also critical parameters in modeling the orbital evolution of asteroids since they effect the response to Solar radiation. But most models of asteroid thermal and orbital evolution assume the measured properties of pure terrestrial materials. In addition, from the densities of the larger, ice-rich bodies and the presence of dust in the tails of comets it is clear that icy bodies also contain significant amounts of rocky material, which might be best modeled using the physical characteristics of meteorites. Thus, these data are also needed for accurate models of ice-rich bodies, such as comet nuclei, the moons of the major planets, the Centaurs and trans-Neptunian Objects, and the dwarf planets, such as Pluto and Ceres.

The physical and orbital evolution of asteroids is strongly dependent on the way that the asteroidal material responds to heating, both from the insolation of sunlight and the internal production of heat via the decay of radioactive nuclei. The effectiveness of the various Yarkovsky effects described by Bottke et al. (2006), which perturb the orbits of asteroids, is controlled by the thermal inertia of an asteroid's surface, while its internal thermal evolution is controlled by the thermal diffusivity of the material that makes up the interior of the asteroid. Both the thermal inertia and the thermal diffusivity are functions of the material's density, heat capacity, and thermal conductivity.

Until recently, there had been no published, reliable, direct measurements of thermal properties of meteorites, especially over the temperature range experienced by asteroids in the main-belt. The standard reference for meteorite thermal properties has been Yomogida and Matsui (1983), who measured the thermal *diffusivity* of 20 ordinary chondrite meteorites and then used *calculated* heat capacities, estimated from the mineral make up of the meteorites, to compute the thermal conductivities.

4.1. Thermal conductivity

The first direct measurements of the thermal conductivity of meteorite samples at main-belt asteroidal temperatures were published by Opeil et al. (2010, 2012). These authors used a cryogenic refrigerator system that allows measurements of thermal conductivity, κ [W/m-K], over a temperature range from 2 K to 400 K. In this system, the sample puck, generally a few millimeters thick, is held in a cryostatic chamber whose temperature is automatically stepped from 300 K to below 5 K at a rate of 0.5 K/min, in a vacuum (pressure $<1.33 \times 10^{-4}$ Pa). The thermal conductivity is determined by applying a heat pulse via a heater attached to one end of the sample in order to create a user-specified temperature difference, which is measured via two calibrated Cernox thermometers located at the sample ends.

Fig. 15 shows that for temperatures above 100 K, the thermal conductivity of most meteoritic materials, except for enstatite

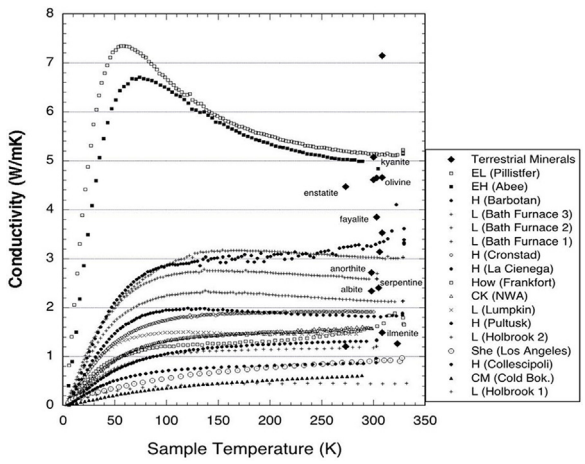

Fig. 15. The thermal conductivity of stony meteorites over the temperature range from near 0–340 K, measured with a Quantum Design system (Opeil et al., 2012;. Reproduced with permission from J. Wiley and Sons, Inc.)

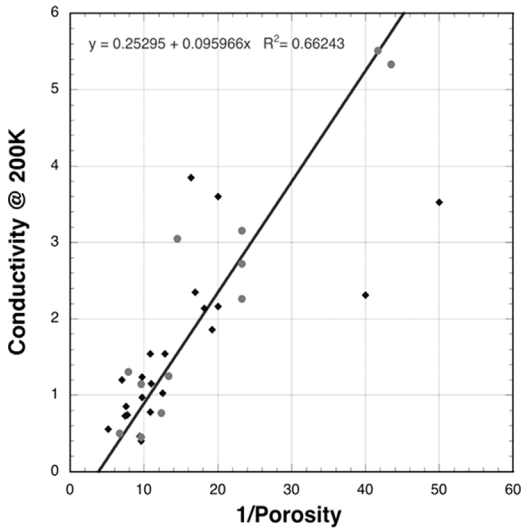

Fig. 16. Thermal conductivity k (at 200 K) vs 1/P yields a best fit line with an r^2 value of 0.66. The circular points are from Opeil et al. (2012), diamonds from Yomogida and Matsui (1983) .

chondrites, is only a weak function of temperature, typically changing by only a few percent over the range from 100 to 300 K. Except for the enstatite chondrites, which have very low porosities, the room temperature thermal conductivities of the chondritic meteorites are significantly lower than those of anhydrous crystalline minerals, e.g., olivine (Fig. 15).

Opeil et al. (2012) found that the thermal conductivity of one sample was significantly different when measured in different directions, across different faces of the same cut sample. They found a strong correlation between the thermal conductivity of a meteorite and its porosity (Fig. 16). From this they concluded that meteorite thermal conductivity is controlled by its physical state: the effect of porosity dominates over its changes in mineral composition, and the nature and orientation of internal cracks in the sample plays a dominant role. This pattern has been seen as well in numerical models of the heat flow in porous samples (Macke and Consolmagno, 2014), which showed that the thermal conductivity does not vary simply with porosity, but is strongly dependent on the geometric characterization of the pore space, with cracks perpendicular to the heat propagation direction more strongly affecting the thermal conductivity and than those parallel to it.

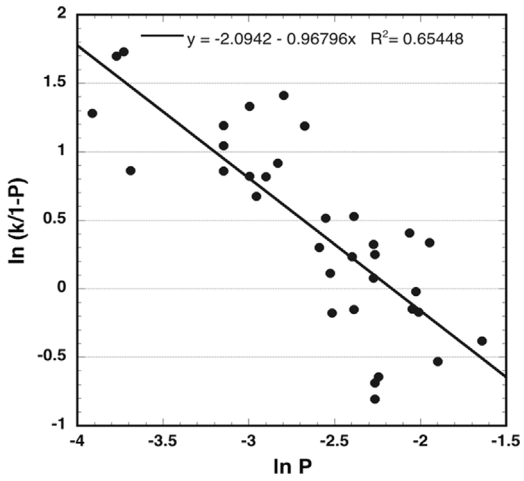

Fig. 17. Log of porosity vs. the log of thermal conductivity k (at 200 K) divided by 1-P yields a line of slope −0.968 or about −1, giving the value of −g in the equation $(1\text{-}P)\ P^{-g}$.

Studies of soils have long demonstrated the effect of porosity on the thermal conductivity. While most such studies concentrate on the effect of moisture in the pore spaces, which is not an important factor in most asteroids, several studies have attempted to extrapolate from conditions of dry soils. In some formulations, the conductivity is seen to be a function of the relative density of the soil compared to compacted material, which is the same as comparing a bulk density to a grain density. Studies of terrestrial soil indicate that conductivity should vary as (1-P). Other workers have empirically measured soils of varying porosity and fit the resulting change of conductivity with P as a function of P^{-g}, where g has been estimated to range anywhere from less than 1 to as much as 2.2 in a sample with a homogeneous distribution of porosity (e.g., Johanson, 1975), rather than oriented cracks.

The role of porosity in heat conduction can be understood by considering a unit cell where heat is transported across an area A along a path length r. The rate at which heat is transported will vary linearly with the available area A: twice the area provides twice the opportunity for heat transport. On the other hand, one would expect that the resistance to heat transport would increase linearly with r, the distance the heat must travel, and so the conductivity – the inverse of resistivity – should vary as 1/r; twice the path length results in half the conductivity.

Porosity affects both quantities. The presence of voids, where conduction of heat is no longer possible, decreases the available surface area A by a factor of (1-P). On the other hand, assuming that the pore spaces are small compared to the distance over which the heat must travel, each pore space also increases the effective path length that the heat must travel in order to go around, rather than through, the voids. In the limit of near-equilibrium heat flow and a uniform distribution of tiny voids of equal size, one could model this path length following a random walk from pore to pore, and conclude that the conductivity should increase as the square root of the number of such voids, i.e., $\gamma = 0.5$. However, given that the porosity in most meteorite samples tends to occur in cracks, not infinitesimal voids, it is not surprising that the actual distance of travel may increase more rapidly with porosity and be dependent on crack orientation. There is a need to study further the dependence of thermal conductivity on pore geometry.

Fig. 17 shows the published meteorite thermal conductivity data for samples where porosity has been measured, plotted as the log of the quantity k/(1-P) against the log of P. The linear trend is consistent with the assumption that the conductivity k should vary as a function of $(1\text{-}P)\ P^{-g}$, and the slope of the line is a good estimate for g. In these data, we find that g = 0.968, or approximately 1. Applying

this functional form to the data, a reasonably good estimate for the thermal conductivity as function of porosity P is given by:

$$k \approx 0.11(1-P)/P(W/m \bullet K) \quad (5)$$

This formula fails at porosities near zero, but it appears to give good results for porosities as low as 2%.

4.2. Heat capacity

Heat capacity is also an essential parameter in many aspects of asteroid modeling, from determining interior thermal evolution to calculating the changes in the orbit of the asteroid due to reradiating absorbed solar heat, known as the Yarkovsky and YORP effects (e.g., Bottke et al., 2006). These effects are important non-gravitational forces that perturb the orbits of some asteroids, resulting in the delivery of asteroids and meteoroids with diameters < 40 km from their source locations in the main belt to chaotic resonance zones capable of transporting this material to Earth-crossing orbits and also results in the dispersal of asteroid families. In addition, the heat capacity can provide a non-destructive way of inferring the bulk composition of a whole sample since it varies with the mineralogy.

Standard heat capacity measurements require heating small samples to relatively high temperatures. Only a few meteorite heat capacities measured in this way have been published, virtually all at temperatures at or above 300 K. Of these, some have been problematical. For example, Matsui and Osako (1979) measured values for meteorites from room temperature to 450 K but, in a later paper (Yomogida and Matsui, 1983), they rejected these data, citing the small sizes of the samples measured and the possibility that metallic iron may have been overrepresented in them. Instead, in their later work, they preferred to use values calculated from meteorite modal compositions.

Beech et al. (2009) reported the heat capacity of two chondrites and an iron meteorite; one chondrite sample was measured at room temperature and the others at 350 K. A plot in Szurgot (2011) shows room-temperature values of heat capacities for a dozen ordinary chondrites, but only in Szurgot et al. (2012) and Wach et al. (2013) do they report the actual values for a given meteorite, with a description of the procedure used. These measurements (Table 3) are, to date, the only hand samples of meteorites for which reliable specific heats have been published, most of them measured at temperatures at or above room temperature. The Wach et al. (2013) work is notable for including data at temperatures as low as 220 K for two meteorites, Sołtmany and NWA 4560.

The Quantum Design Physical Properties Measurement System, described in Opeil et al. (2010), can be adapted to measure heat capacities over a range from cryogenic temperatures up to 300 K. The heat capacity of the shergottite Los Angeles measured in this device was published in Opeil et al. (2012). Further measurements of meteorite heat capacities using this system are ongoing.

Thermodynamic theory indicates that heat capacity is a strong function of temperature, especially at the lower temperatures in the asteroid belt. In the absence of phase changes, the heat capacity for a crystalline substance as a function of temperature should follow a characteristic curve similar to that derived by Debye (1912) . To illustrate the observed shape of this curve, Fig. 18 shows the meteorite heat capacity data currently available, plus literature data for the minerals enstatite and wollastonite (Mg and Ca pyroxene end-members, which represent the extremes of the range of pyroxene heat capacity values reported by Krupka et al., 1985) and pure quartz (Hemingway et al., 1991).

All the data show a very similar dependency on temperature below 250 K. Between 75 and 250 K, these values are well fit by a linear equation Cp = −8.1 + 2.82 T (r^2 value of 0.98). Above 400 K, the heat capacity is no longer a strong function of temperature. Wach et al. (2013) suggest that the downturn in heat capacity for the LL sample NWA 4560 reflects a phase change at around 600 K.

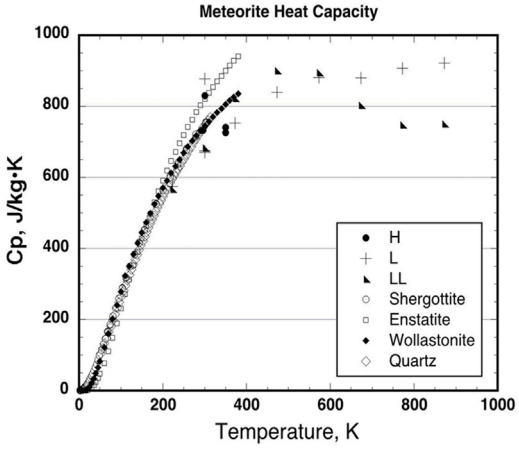

Fig. 18. Measured heat capacities of meteorites and representative minerals as a function of temperature. For temperatures of interest in the asteroid belt, the heat capacities for stony meteorites range from under 250 J/kgK at 100 K to over 600 J/kgK at 250 K.

Consolmagno et al. (2013) developed a procedure for measuring the heat capacity of meteorites at low temperatures that is inexpensive and non-destructive. The mass of a Dewar of liquid nitrogen is recorded at regular intervals; when a sample is dropped in the Dewar, the liquid nitrogen rapidly boils while the temperature of the sample drops from room temperature (about 300 K) to the boiling point of liquid nitrogen (77 K). The total mass of liquid nitrogen boiled away due to cooling the sample is determined, and from this one can directly compute the average value of the sample's heat capacity over that temperature range, i.e., temperatures typical of the asteroid belt (around 200 K). To correct for any systematic errors, these results were compared to samples of electronics-grade quartz. They found an average heat capacity value between 77 and 294 K for ordinary chondrites of 494 J/kg•K, the same as quartz at that temperature.

As seen in Fig. 18, the heat capacity varies significantly over the temperature range from 77 to 294 K. However, the average heat capacity over this temperature range closely approximates the heat capacity at 175 K.

The data currently available indicate that the average heat capacity of meteorites at temperatures appropriate to the asteroid belt and further out in the solar system is about half that of materials that were measured at room temperature. Consolmagno et al. (2013) found that, as expected, metal rich meteorites have significantly lower heat capacities than stony meteorites, while hydrated meteorites and hydrated asteroids may have a higher heat capacity than anhydrous samples.

5. Elastic properties of meteorites

The physical properties of rocks, including the elastic constants and the speed of elastic waves are affected significantly by the volume, shape and distribution of pore spaces (Walsh, 1965). Thus, these properties are expected to be significantly different for porous meteorites and their parent bodies than for compact terrestrial rocks.

The elastic properties of a solid measure the response of the solid to external forces, for example, by applying *stress* to a sample of the material and observing its effects: its *strain*. Stress measures the object's internal ability, due to intermolecular/atomic and lattice forces, to resist an external force. *Strain* is relative change in dimension (length) of shape of a body subjected to stress. A mate-

Table 3
Heat Capacity of Stone Meteorites.

Meteorite	Type	Mass (g)	T (K)	C_p	Source
Gao-Guenie	H5	3.01	296.15	732 ± 7.5	Beech et al. (2009)
Gao-Guenie	H5	61.37	350	740 ± 27.5	Beech et al. (2009)
Jilin	H5	62.35	350	726 ± 13.2	Beech et al. (2009)
Sikhote-Alin	Iron IIAB	51.37	350	458 ± 10.7	Beech et al. (2009)
Sołtmany	L6		223	575	Wach et al. (2013)
Sołtmany	L6		300	671	Wach et al. (2013)
Sołtmany	L6		373	753	Wach et al. (2013)
Sołtmany	L6		473	839	Wach et al. (2013)
Sołtmany	L6		573	881	Wach et al. (2013)
Sołtmany	L6		673	879	Wach et al. (2013)
Sołtmany	L6		773	907	Wach et al. (2013)
Sołtmany	L6		873	922	Wach et al. (2013)
NWA 4560	LL3.2		223	566	Wach et al. (2013)
NWA 4560	LL3.2		300	682	Wach et al. (2013)
NWA 4560	LL3.2		373	821	Wach et al. (2013)
NWA 4560	LL3.2		473	900	Wach et al. (2013)
NWA 4560	LL3.2		573	894	Wach et al. (2013)
NWA 4560	LL3.2		673	803	Wach et al. (2013)
NWA 4560	LL3.2		773	747	Wach et al. (2013)
NWA 4560	LL3.2		873	750	Wach et al. (2013)

rial is said to be elastic if it is able to return to its original shape or size immediately after being stretched (tensile stress) or squeezed (compressive stress). Almost all materials are elastic, and thus obey Hooke's law, to some degree as long as the applied load does not cause it to permanently deform or fail.

A series of elastic properties, called *moduli*, measure the amount of force per unit area needed to achieve a given amount of deformation of a solid. Solids are usually characterized by Young's Modulus, a proportionality constant between the uniaxial stress and strain, the Bulk Modulus, a measure of the change in volume of a solid as it is subjected to hydrostatic pressure, and the Shear Modulus, a measure of a substance's resistance to shear. The elastic properties of a solid are influenced by both the shape and volume of the pores. For isotropic materials, the Bulk Modulus and the Shear Modulus can be determined from the Young's Modulus and Poisson's Ratio, which describes the response of the solid in the directions orthogonal to the uniaxial stress applied to determine the Young's Modulus. These elastic properties are important in understanding the response of asteroids to impacts.

The propagation of sound waves in an elastic medium are comprised of compressional or P-waves, where the particle motion is in the direction of propagation, and shear or S-waves, where the particle motion is perpendicular to the direction of propagation. For most solids the shear wave velocity is approximately one-half that of compressional wave velocity.

5.1. Speed of sound

Alexayeva (1958, 1960) measured the compressional wave velocity (v_p), or speed of sound, in eight ordinary chondrites, reporting values ranging from 2050 to 4200 m/s, substantially lower than the 5400–5600 m/s measured in compact terrestrial rocks. Alexeyeva (1960) also measured shear wave velocities (v_s) on these samples, reporting values from 600 to 1220 m/s.

Gorshkov (1973) noted that the compressional wave velocity showed a linear dependence on the density among different meteorite classes. Yomogida and Matsui (1983) measured the compressional wave velocities on 21 ordinary chondrite samples and shear wave velocities on 19 ordinary chondrite samples on which porosity was also measured. They showed a relatively strong correlation between increasing porosity and decreasing compressional wave velocity as well as increasing porosity and decreasing s-wave velocity. However, much of the literature data on compressive and shear wave speeds is on samples on which the bulk density or porosity was not measured.

Hons (2004) measured compressional and shear wave velocities on 72 meteorite samples and only compressional wave velocities on 13 more samples. The compressional wave velocities spanned the range from 1500 to 7000 m/s. These measurements also showed the expected decrease in compressional wave velocity with increasing porosity. Flynn (2005) reported compressional wave velocities for samples of the CV3 meteorite Axtel, seven ordinary chondrites, and the iron meteorite Gibeon, eight of which also had porosities measured on the same sample, and reported shear wave velocities on Axtel and two of the ordinary chondrite samples. Slyuta et al. (2008) reported compressional wave velocities for the ordinary chondrites Sayh al Uhaymir 001 and Ghubara

The most comprehensive study, thus far, of sound propagation in ordinary chondrite meteorites, by Jones (2009), reported compressional and shear wave velocities on 79 meteorites: 2 carbonaceous chondrites, 26 H, 37 L, and 8 LL ordinary chondrites, and 6 enstatite chondrites. Ibrahim (2012) measured the compressional and shear wave velocities on 28 carbonaceous chondrites: 12 CM, 2 CR, 6 CO, 6 CV, and 2 CK meteorites.

The mean compressional wave velocities reported by Jones (2009) are 2114 ± 195 m/s for carbonaceous chondrites, 3330 ± 1324 m/s for LL, 3443 ± 1389 m/s for L, 3634 ± 1060 m/s for H, and 5153 ± 595 for enstatite chondrites. The mean compressional wave velocities for carbonaceous chondrites reported by Ibrahim (2012) are 2335 ± 574 m/s for the CM, 2770 ± 993 for the CR, 2401 ± 545 m/s for the CO, 2995 ± 1263 m/s for the CV, and 1566 ± 573 m/s for the CK chondrites. The distribution of compressional wave velocities reported for 145 stone meteorites is shown in Fig. 19.

The mean shear wave velocities reported by Jones (2009) are 1085 ± 497 m/s for carbonaceous chondrites, 2074 ± 920 m/s for LL, 2028 ± 787 m/s for L, 2109 ± 637 m/s for the H, and 3093 ± 219 for the enstatite chondrites. The mean shear wave velocities for carbonaceous chondrites reported by Ibrahim (2012) are 1472 ± 352 m/s for CM, 1751 ± 611 for CR, 1526 ± 374 m/s for CO, 1934 ± 778 m/s for CV, and 1049 ± 327 m/s for the CK chondrites (Ibrahim, 2012). The distribution of shear wave velocities reported for 133 stone meteorites is shown in Fig. 20.

For the very porous carbonaceous chondrites the mean velocities are quite low, compared to compact terrestrial rocks, but the mean velocities for the enstatite chondrites are comparable to compact terrestrial rocks, likely reflecting their very low porosity. There

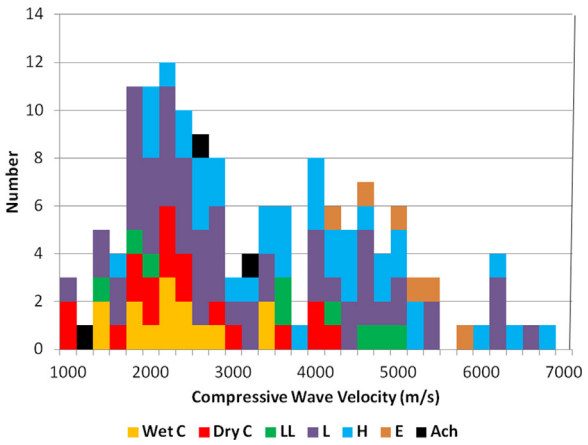

Fig. 19. Compressive wave velocity measurements on 145 stone meteorites, sorted by meteorite type. There is no obvious difference between the LL, L, and H ordinary chondrites, with all three types spanning essentially the entire range of measurements. Both the wet and the dry carbonaceous chondrites generally have lower compressive wave velocities, likely reflecting their higher porosities, while the enstatite chondrites all have higher compressive wave velocities, likely reflecting their low porosities. (Data from Yomogida and Matsui, 1983, Flynn, 2005, Jones, 2009, Ibrahim, 2012, and Cotto-Figueroa et al., 2016).

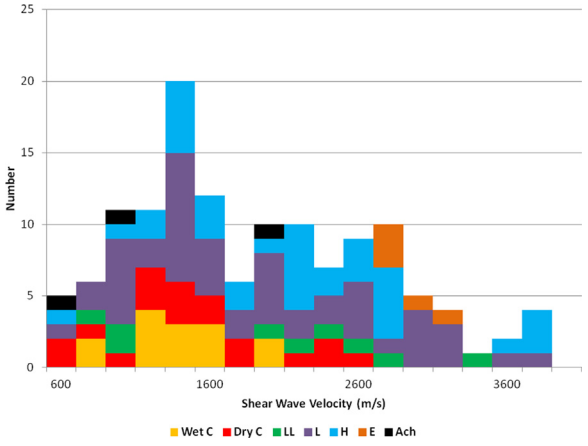

Fig. 20. Shear wave velocity measurements on 133 stone meteorites, sorted by meteorite type. There is no obvious difference between LL, L, and H ordinary chondrites, with all three types spanning essentially the entire range of measurements. Both the wet and the dry carbonaceous chondrites generally have lower shear wave velocities, likely reflecting their higher porosities, while the enstatite chondrites all have higher shear wave velocities, likely reflecting their low porosity. (Data from Yomogida and Matsui, 1983, Flynn, 2005, Jones, 2009, Ibrahim, 2012, and Cotto-Figueroa et al., 2016).

are no significant differences in the mean velocities among the LL, L, and H chondrites (Fig. 19). For comparison, the compressional and shear wave velocities in polycrystalline orthopyroxene at 1 atm pressure are 8030 and 4380 m/s respectively (Flesch et al., 1998), and measurements on single crystal olivine ($Fo_{93}Fa_7$) give 8420 and 4800 m/s respectively (Kumazawa and Anderson, 1969).

The wide diversity in sound velocities likely reflects the differing porosities or bulk densities of the meteorite samples. For any specific material, the compressional wave velocity is expected to be proportional to $\rho^{-1/2}$. However, in many cases the compressional wave velocity was measured on a different sample than was used to determine the porosity. Jones (2009) reported a good correlation between increasing porosity and decreasing compressional wave velocity in the H and the LL chondrites, but found an essentially horizontal relationship for the L chondrites. She also found good correlations between increasing porosity and decreasing shear wave velocity for the H and L chondrites, but the LL chondrite data were too limited to provide a convincing test.

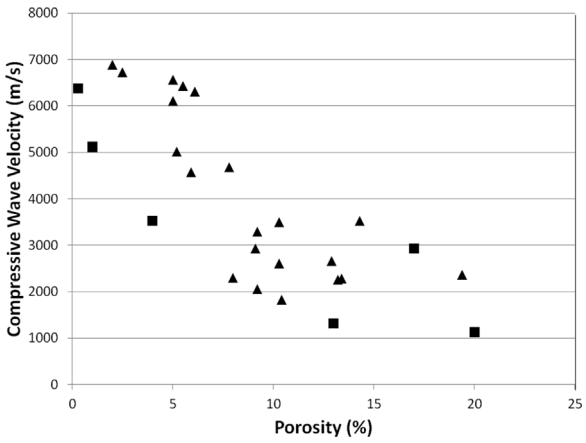

Fig. 21. Compressive wave velocity vs. porosity for 21 ordinary chondrites (triangles) (Yomogida and Matsui, 1983) and 7 ordinary chondrites (squares) (Flynn, 2004) for which porosities were determined on the same sample. A clear trend of decreasing compressive wave velocity with increasing porosity is apparent.

Since porosity varies from sample to sample of the same meteorite, only samples on which porosity and compressional wave velocity were both measured, can be used to test for this correlation. The plot of compressional wave velocity vs. porosity (ρ) (Fig. 21) for cases where both the compressional wave velocity and the porosity were reported on the same sample, is consistent with that variation.

As with the thermal conductivity, the speed of sound varies with the geometry of the porosity in the sample. Flynn (2005) measured two samples of the Saratov L4 ordinary chondrite, one with no visible cracks and a second with a visible crack running across and almost completely through the sample approximately perpendicular to the direction of sound propagation. The sample with no visible cracks had a compressional wave velocity approximately twice as high as the one with the crack running almost completely through the sample.

5.2. Elastic response to deformation

Most solids, described as "elastic," respond to the application of a load by extension or compression in direct proportion to the applied load until they reach their maximum tensile strength or maximum compressive strength, when they fail. The mechanical behavior of elastic solids is described by Young's modulus, the shear modulus, and the bulk modulus.

The elastic moduli can be calculated from other physical properties of the sample – the *p*-wave (v_p) and s-wave (v_s) velocities and the bulk density (ρ_{bulk}). For example, the bulk modulus is given by:

$$\text{Bulk Modulus} = \rho_{bulk[v_p{}^2 - 4\,v_s{}^{2/3}]} \quad (6)$$

This procedure was employed in the work reported by Flynn (2005), Jones (2009), and Ibrahim (2012). A technique for the direct measurement of Young's Modulus, employed by Consolmagno et al. (2011), is described in Section 5.5. The extent to which these two techniques yield the same results has not been evaluated for porous, inhomogeneous materials such as chondritic meteorites.

5.3. Bulk modulus

The bulk modulus is the ratio between a pressure that acts to change the volume of the substance and the fractional change in volume produced. Yamogida and Matsui (1983) measured the bulk modulus of 20 ordinary chondrites, including 11 collected

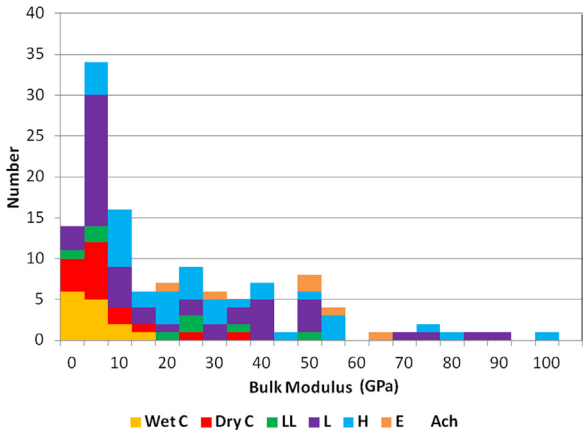

Fig. 22. Bulk moduli for 30 carbonaceous chondrite samples, 8 LL, 45 L, and 35 H ordinary chondrite samples, 6 eucrites and 3 achondrites. Data from Yomogida and Matsui (1983), Flynn (2005), Jones (2009) and Ibrahim (2012).

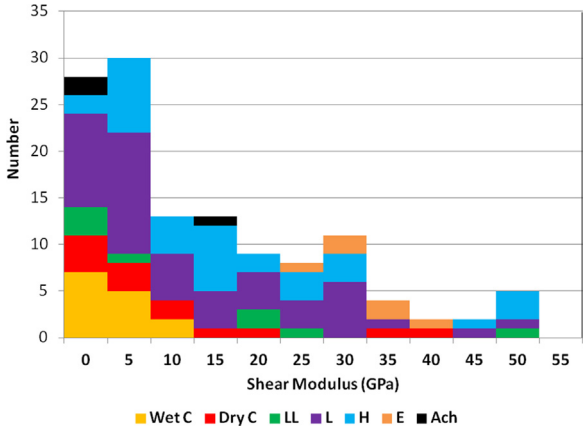

Fig. 23. Shear moduli for 27 carbonaceous chondrite samples, 8 LL, 48 L, and 33H ordinary chondrite samples, 6 eucrites and 3 achondrites. Data from Yomogida and Matsui (1983), Flynn (2005), Jones (2009) and Ibrahim (2012).

in Antarctica. Jones (2009) reported measurements on 2 carbonaceous chondrites, 7 LL, 36 L, and 25 H ordinary chondrites, and 6 eucrites. Ibrahim (2012) reported bulk modulus measurements on 27 carbonaceous chondrites. The results (Fig. 22) show a wide range of values as did the sound velocities. Jones (2009) noted a clear trend of decreasing bulk modulus with increasing porosity for H and L chondrites, with too limited data on LL chondrites to demonstrate a trend. Ibrahim (2012) found that the bulk modulus varied with meteorite type, reporting values of 6.1 ± 1.0 GPa for the wet carbonaceous chondrites, 8.9 ± 1.8 GPa for the dry carbonaceous chondrites, and 20.0 ± 1.8 GPa for the ordinary chondrites.

5.4. Shear modulus

The shear modulus is the ratio between the force per unit area, or shearing stress, that laterally deforms a substance, and the shear, or shearing strain, that is produced by this stress. Yamogida and Matsui (1983), Jones (2009) and Ibrahim (2012) measured the shear modulus of the same samples for which they determined the bulk modulus (see above). Flynn (2005) reported an additional 3 measurements of 1 carbonaceous chondrite and 2 ordinary chondrites. The shear moduli, (Fig. 23), vary from near zero to 55 GPa. Jones (2009) noted a clear trend of decreasing shear modulus with increasing porosity for H and L chondrites, with too limited data on the LL chondrites to demonstrate a clear trend. Ibrahim (2012) found that the shear modulus varied with meteorite

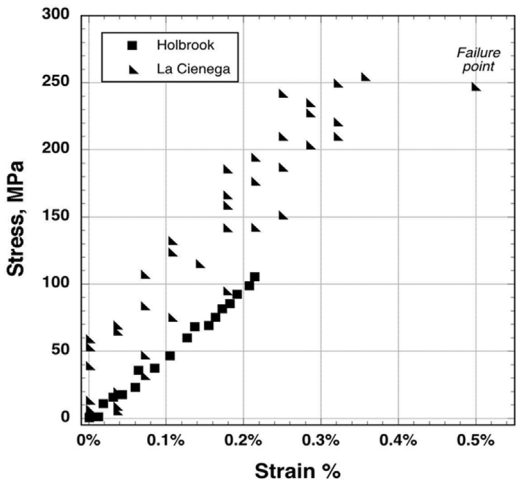

Fig. 24. Stress vs strain under compression for the Holbrook (L6) and La Cienega (H6) chondrites. (Data from Consolmagno et al., 2011).

type, reporting values of 5.1 ± 0.8 GPa for the wet carbonaceous chondrites, 8.3 ± 1.6 GPa for the dry carbonaceous chondrites, and 11.7 ± 1.0 GPa for the ordinary chondrites. These meteorite values are much lower than are reported in the literarture for common terrestrial crystalline materials, e.g., for enstatite at 75 GPa and forsterite at 82 GPa (Petrovic, 2001).

5.5. Young's modulus

Young's modulus, also known as the elastic modulus, is the ratio between a stress that acts to change the length of a body and fractional change in length caused by this force. Young's modulus is basically the slope of its stress/strain plot within the elastic range, where the stress applied does not lead to permanent deformation or failure. If the material is loaded to any value of stress in this part of the curve, it will return to its original shape. Stressing the sample beyond this point, the material eventually enters the plastic deformation region where applied stress permanently deforms the sample. Continued application of stress ultimately moves the material to its fracture point, where essentially the sample breaks or all its mechanical properties fail.

The measurement technique described by Consolmagno et al. (2011) is typical of those employed for the direct measurement. Uniform meteorite samples of known length and cross sectional area are held (at room temperature, in the measurements reported to date) in compressive or tensile stress, which might be created, for example, by a plate attached to a large screw which can be turned up or down at the top of the probe. The force developed in the screw can be measured with a force monitor gauge, which can be calibrated to within $\leq$ 1% error using known masses. As force is applied to the meteorite, the strain developed in the material can be monitored by a strain gauge attached to the side of the meteorite, as shown in Fig. 24.

Yamogida and Matsui (1983) measured the Young's modulus on 20 ordinary chondrites, including 11 collected in Antarctica. Jones (2009) reported measurements on 2 carbonaceous chondrites, 7 LL, 36 L, and 25 H ordinary chondrites, and 8 eucrites. Ibrahim (2012) reported measurements on 27 carbonaceous chondrites, and Hogan et al. (2015) on two Antarctic L chondrites. These measurements, (Fig. 25), range from near zero to 140 GPa. Ibrahim (2012) noted that the Young's moduli of 27 carbonaceous chondrites showed a range of values slightly lower than were measured by Jones (2009) on ordinary chondrites. Ibrahim (2012) found that Young's modulus varied with meteorite type, reporting values of 11.8 ± 1.8 GPa for the wet carbonaceous chondrites, 18.9 ± 3.7 GPa

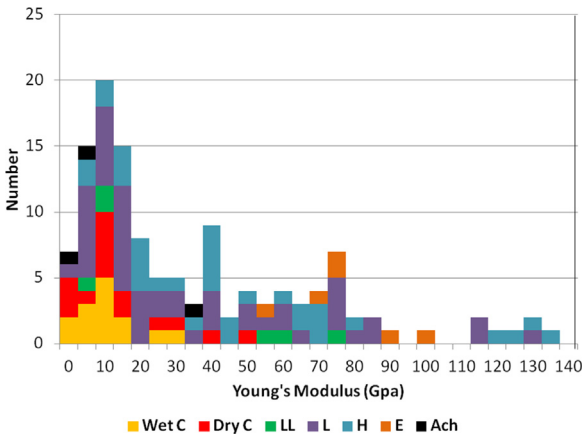

Fig. 25. Young's modulus for 29 carbonaceous chondrite samples, 6 LL, 50 L, and 33H ordinary chondrite samples, 6 eucrites and 3 achondrites. (Data from Yomogida and Matsui, 1983, Jones, 2009, Ibrahim, 2012 and Hogan et al., 2015).

for the dry carbonaceous chondrites, and 28.8 ± 2.4 GPa for the ordinary chondrites. Both carbonaceous and ordinary chondrites have mean Young's moduli significantly lower than literature values for 16 terrestrial basalt samples, which ranged from 34.9 GPa to 100.6 GPa with a mean of 62.6 GPa (Johnson and DeGraff, 1988) and terrestrial crystalline materials, e.g., fayalite at 140 GPa and forsterite at 204 GPa (Petrovic, 2001).

6. Material strength of meteorites

The mechanical strength of a meteorite determines if it will fragment when it hits the Earth's surface, and controls the response of the parent asteroid to impact cratering. However, there are many fewer measurements of the compressive and the tensile strengths of stone meteorites than there are of the elastic properties, most likely because strength measurements are destructive, requiring testing to failure.

The mechanical strength is even more important for a meteoroid, determining if it will break apart during atmospheric entry and, if so, at what altitude, or dynamic pressure, the fragmentation will begin. The compressive strength of the material is important in modeling and interpreting the light curves of meteors and the break- up of bolides.

Knowing how asteroidal material behaves under different conditions of stress is important in understanding both how asteroids accrete, and how they behave during cratering or disruptive collisions. Most models of asteroid collisions assume the measured mechanical properties of pure terrestrial materials. By contrast, Slyuta et al. (2008) reviewed the data for ordinary chondrites and concluded that "there are no analogues among terrestrial igneous and sedimentary rocks and ores [for the] physical and mechanical properties of the meteorites." What little data exist for ordinary chondrites are mostly in older Russian literature, difficult to access in the West, or reported only in unrefereed extended abstracts. Furthermore, these data cover only a very limited range of meteorite types. In spite of that, even with the limited set of measurements currently available, there are significant differences from measurement to measurement, which may provide clues as to the important variables relating strength to other physical properties of meteorites.

6.1. Compressive and tensile strengths

Buddhue (1942) measured the compressive strengths of 8 stone meteorites (Table 4), which varied from 6.2 MPa for the L6 ordinary chondrite Holbrook to 381 MPa for the L5 ordinary chondrite La Lande. Medvedev et al. (1985) reported both the compressive and tensile strengths of five ordinary chondrite meteorites, and Petrovic (1991) and Tsvetkov and Skripnik (1991) reviewed the meteorite strength data published through 1991. They found 14 compressive strength measurements, 12 on ordinary chondrites and two on iron meteorites, and 16 tensile strength measurements, two on carbonaceous chondrites, 12 on ordinary chondrites, one on a eucrite, and one on an iron meteorite. A summary of much of the available data is found in Popova et al. (2011). In addition to the data presented there, in Tables 4 and 5 we have added more data from the literature (references are given in Table 4). In some cases, important details concerning the specific samples tested, in particular their size or mass, the degree of weathering, etc., were not given in the reports. For example, Medvedev et al. (1985) provide measurements of a number of meteorites, but the only details of the size of one of them, the meteorite Tsarev (L5), are given in a later paper by Zotkin et al. (1987).

Of particular interest are the measurements reported on the L5 desert meteorite Sayh al Uhaymir 001 and the previously-studied meteorite Tsarev by Slyuta et al. (2009). They found significant anisotropy in the failure stress for the same samples measured along different axes, reminiscent of the anisotropy seen in thermal conductivity. One presumes the origin for these anisotropies are the same – cracks induced in the sample, likely by impact shock.

There are few measurements available, and a significant fraction of them are on the same meteorite, Tsarev, which was found in 1968 but is suspected to have fallen in 1922, so it may not be representative of unweathered ordinary chondrites. We list the data in terms of individual measurements (Table 4) and then list the average value for each of the individual meteorites (Table 5). The compilation of all the measurements shows the wide range that can be obtained from piece to piece of the same meteorite and even by varying the axis along which the sample is measured (Table 4)

Of the 22 ordinary chondrites listed in Table 5, the average stress producing compressional failure is 164 ± 102 MPa, while the stress producing tensional failure in the 14 ordinary chondrites in Table 5 is 24 ± 11 MPa. There is a small difference between values for H and L chondrites, but given the small number of samples and the large range among the samples (compressional failure at 200 ± 82 MPa for H chondrites vs 149 ± 116 MPa for L chondrites, tensional failure at 33 ± 8 MPa for H chondrites, 21 ± 12 MPa for L chondrites) that difference is not statistically significant.

So far only two H chondrite falls have been measured, but for the L chondrites, comparable numbers of falls and finds have been measured. In these data, the falls are significantly weaker than finds under compression, while under tension falls and finds are indistinguishable.

Based on modeling of flaw distribution, it is expected that larger samples of the same material would be weaker than smaller samples. Zotkin et al. (1987) suggested that larger samples break more easily (e.g., a 1 cm sample of Tsarev broke at 46 MPa while a 10 cm sample broke at 26 MPa). However, Cotto-Figueroa et al. (2016) noted that the smallest (~0.5 cm cubes) Allende samples they measured were weaker than the larger samples ones. He suggested that the 1 cm Allende cubes may have been too small to represent the bulk sample, with one weak volume element that provides little resistance to deformation resulting in an increase in stress concentrated in other regions of the cube.

Slyuta (2013) noted that the compressive strength of "ordinary chondrites and accordingly S-asteroids [is] 105–203 MPa [and] carbonaceous chondrites and accordingly C- asteroids [is] 35–70 MPa." The ordinary chondrite data they cite are essentially those reported in Table 4. The carbonaceous chondrite data are referenced to work not yet published.

Clearly more data on the compressive and tensile strengths of meteorites are needed. Only through a large data set on samples of

Table 4
Compressive and Tensile Strengths of Stone Meteorites.

Meteorite	Class	Compressive Strength	Tensile Strength	Shock	Reference
		(MPa)	(MPa)	State	
Murchison	CM2	50			Miura et al. (2008)
Sutter's Mill	CM2	82			Jenniskens et al. (2012)
Allende	CV3		28		Svetsov et al. (1995)
Allende	CV3	22.5, 24.7, 27.6, 31.7, 32.3, 36.5, 39.2, 39.6, 41.1, 58.4			Cotto-Figueroa et al. (2016)
Kainsaz	CO3		31		Svetsov et al. (1995)
Krymka	LL3	160	22	S3[c]	Medvedev et al. (1985)
Northwest Africa 869	L3/6	98.4		S3	Molesky et al. (2015)
Sayh al Uhaymir 001	L4/5	97.5	16.4	S2[e]	Slyuta et al. (2008)
Sayh al Uhaymir 001	L4/5	143, 94, 91[a]	18,17,18[a]	S2[e]	Slyuta et al. (2009)
Chelybinsk	LL5	64		S4	Grokhovsky et al. (2013)
Ghubara	L5	72.2	23.6		Slyuta et al. (2008)
Elenovka	L5	20	2	S2[c]	Medvedev et al. (1985)
Tsarev	L5	157, 222	16, 26		Medvedev et al. (1985)
Tsarev	L5	450, 420	55, 62		Tsvetkov and Skripnik (1991)
Tsarev	L5	260 to 465[b]	39 to 53[b]		Zotkin et al. (1987)
Tsarev	L5	262, 168, 160[a], 223, 182, 174	28, 34, 27[a], 31, 34, 29[a]		Slyuta et al. (2009)
Kunashak	L5	265	49		Medvedev et al. (1985)
Arapahoe	L5	358			Buddhue, J. D. (1942)
La Lande	L5	381		S4[c]	Buddhue, J. D. (1942)
Homestead	L5		34		Medvedev et al. (1985)
Macalpine Hills 88118	L5	161			Kimberley et al. (2010)
La Criolla	L6	98		S4[c]	Miura et al. (2008)
Holbrook	L6	63		S2[c]	Buddhue, J. D. (1942)
Ness County	L6	84			Buddhue, J. D. (1942)
Kyushu	L6	98		S5[c]	Medvedev et al. (1985)
Mocs	L6		26	S3/5[c]	Svetsov et al. (1995)
Bruderheim	L6		31	S4[c]	Svetsov et al. (1995)
Peace River	L6		6	S3[d]	Svetsov et al. (1995)
GRO 85209	L6	22.5			Hogan et al. (2015)
Novato	L6	1100			Jenniskens et al. (2014)
Dhajala	H3		26	S1[c]	Svetsov et al. (1995)
Seminole	H4	173	22.5	S3[c]	Baldwin and Sheaffer (1971)
Jilin (Kirin)	H5		42	S3	Svetsov et al. (1995)
Pultusk	H5	213	31	S3[c]	Medvedev et al. (1985)
Covert	H5	77			Buddhue, J. D. (1942)
Alamogordo	H5	274		S3[c]	Buddhue, J. D. (1942)
Tamdakht	H5	83.6 120.5, 130.7, 84.3, 186, 25.9, 247.4, 120.5, 160.2, 76, 99.6, 97.0, 183.0		S3	Cotto-Figueroa et al. (2016)
Morland	H6	163			Buddhue, J. D. (1942)
Kimble County	H6	327			Tsvetkov and Skripnik (1991)
Lowicz	Meso.		37		Svetsov et al. (1995)
Almahata Sitta	Ure.		56		Kohout et al. (2011)

[a] Measured along three orthogonal axes.
[b] Range for multiple samples.
[c] Shock stage from Grady (2000) .
[d] Shock stage from Chen et al. (1996).
[e] Shock stage from Slyuta et al. (2009).

various types, porosities, shock states, and weathering states can one finally determine how the strength of meteorites depends on these quantities, and how those values vary as a function of differences in the sizes of the fragments measured vs physical differences from meteorite to meteorite. The ultimate goal would be to find a relationship between strength values and the density, porosity, or other physical parameters of the meteorite. In addition, future work should address how these values vary with temperature, especially at the low temperatures applicable to the asteroid belt and the outer solar system.

The compressive strengths have been reported for 22 ordinary chondrites (Table 4). They span a wide range from 20 MPa to 450 MPa, with some stone meteorites being as strong or stronger than many terrestrial rocks, with compact terrestrial granites varying from ~100 to 250 MPa and compact terrestrial basalts from 100 to 300 MPa (Schultz, 1995). This very limited data set on 22 ordinary chondrites and three carbonaceous chondrites shows no correlation of compressive strength with meteorite group (Fig. 26). Tensile strengths of the 2 carbonaceous chondrites, 14 ordinary chondrites, and one mesosiderite also span a large range of values (Fig. 27). Again there is no obvious correlation of strength with group.

Based on his limited data set of eight measurements, Buddhue (1942) noted that the very weak Holbrook fall produced numerous small fragments and the comparatively weak Covert and Ness County falls produced multiple stones, while the stronger stone meteorites were generally recovered as a single mass. However, an individual stone from Pultusk, which produced one of the largest showers of small stone meteorites ever recorded, has a rather large compressive strength, 213 MPa (Medvedev et al., 1985).

Table 5
Mean Values of the Compressive Strengths, Tensile Strengths, and Young's Moduli (Data from sources in Table 4).

Meteorite	Type	Grade	Fall/Find	Young's Mod. (GPa)	Compressive Strength (Mpa)	Tensile Strength (MPa)
Murchison	CM	2	Fall		50	
Sutter's Mill	CM	2	Fall		82	
Allende	CV	3	Fall		35.4	28
Kainsaz	CO	3	Fall		&# 160;	31
Dhajala	H	3	Fall			26
Jilin	H	5	Fall			42
Pultusk	H	5	Fall	76	213	31
Alamogordo	H	5	Find		274	
Covert	H	5	Find		77	
Tamdakht &# 160; &#16 0;	H	5	Fall		124.2	
Kimble County	H	6	Find		327	
La Cienega	H	6	Find	67.5	250	
Morland	H	6	Find		163	
Seminole	H	4	Find		173	
Bruderheim	L	6	Fall			31
Elenovka	L	5	Fall	56	20	2
Holbrook	L	6	Fall	48	63	
Homestead	L	6	Fall			34
Kunahsak	L	5	Fall	69.5	181.5	30
Kyushu	L	6	Fall		98	11
Mocs	L	6	Fall			26
Peace River	L	6	Fall			6
Arapahoe	L	5	Find		358	
Ghubara	L	5	Find		72.2	23.6
La Lande	L	5	Find		381	
Ness County (1894)	L	6	Find		84	
SAUH 001	L	5	Find	17.1	109.3	17.67
Tsarev	L	5	Find	152.5	222	31.07
GRO 85209	L	6	Find	14		
MAC 88118	L	5	Find	3.2		
La Criolla	L	6	Fall		98	
NWA 869	L	03-Jun	Find		98.4	
Novato	L	6	Fall		1100	
Chelybinsk	LL	5	Fall		64	
Krymka	LL	3	Fall	78	160	22
Lowicz	Meso..		Fall		37	
Almahata Sitta	Ure.		Fall		56	

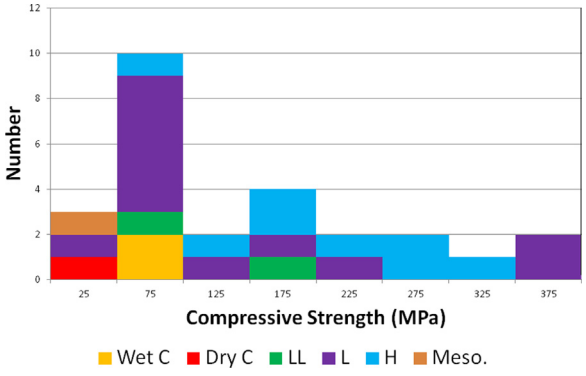

Fig. 26. Compressive strength measurements on 26 stone meteorites from Table 5, sorted by meteorite group. The compressive strength varies over a wide range, with no obvious difference between the LL, L, and H ordinary chondrites. (Data from sources in Table 4.).

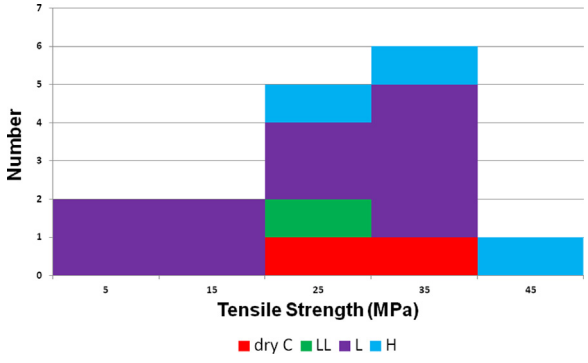

Fig. 27. Tensile strength measurements on 14 stone meteorites from Table 5, sorted by meteorite group, varies over a wide range, with no obvious difference between the LL, L, and H ordinary chondrites. (Data from sources in Table 4.).

More likely, fragmentation occurs along the weakest boundaries, so the recovered samples from shower meteorites are the strongest material in the meteoroid. The recent Almahata Sitta fall, which produced a strewn field of diverse individual stones, suggests the meteor consisted of relatively strong individual stones that were relatively weakly bound together.

Interpreting any of the compressive and tensile strengths data is complicated by the observation that these properties vary significantly from sample to sample of the same meteorite. Slyuta et al. (2007) performed strength measurements on multiple samples from the Sayh al Uhaymir 001 L4/5 shower, from which at least 2670 samples weighing more than 450 kg were collected. They reported a mean compressive strength of 101.6 Mpa, but measurements on 28 samples varied from 47.5 to 173.9 MPa. Similarly, the mean tensile strength was 16.12 Mpa, but the 27 samples varied from 6.46 to 27.38 Mpa. Cotto-Figueroa et al. (2016) reported compressive strengths on 13 samples of the Tamdakht H5 ordinary chondrite, measuring a mean compressive strength of 124.2 MPa, but a range from 25.9 to 247.4 MPa. For ten Allende samples, Cotto-Figueroa et al. (2016) reported a mean compressive strength of

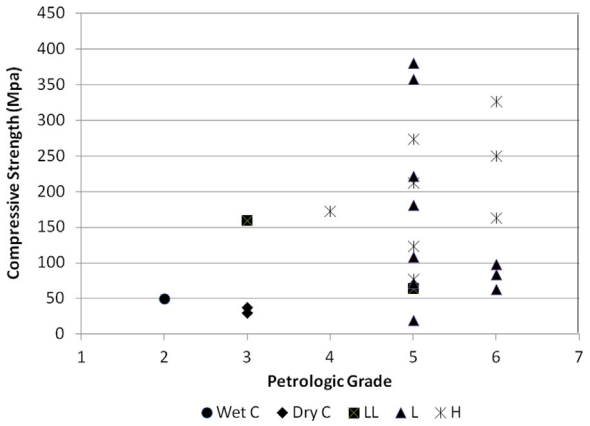

Fig. 28. Compressive strength vs. petrologic grade for 24 chondritic meteorites. (Strength data from sources in Table 4.).

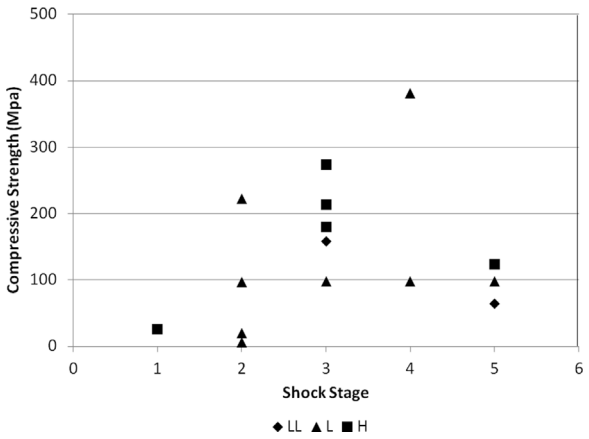

Fig. 29. Compressive strength vs. shock stage for 15 ordinary chondrite meteorites for which both measurements have been reported. (Data from sources in Table 4.).

35.4 MPa, but a range from 24.7 to 58.4 MPa. The strengths of different samples of the L5 ordinary chondrite Tsarev have been measured by several different groups (Table 4), who reported compressive strengths ranging from 157 to 465 MPa and tensile strengths ranging from 16 to 62 MPa. The wide variation in compressive and tensile strengths for stones from the same shower indicates that a single measurement on one stone may not provide a value representative of the entire body that entered the atmosphere, especially since the meteoroid is likely to have fragmented along its weakest boundaries.

In addition, Slyuta et al. (2009) measured the compressive and tensile strengths of one sample of Sayh al Uhaymir 001 and two different samples of Tsarev along three orthogonal directions. They found that the compressive strength along one of three directions was significantly larger than that along the other two directions, which have almost equal values (Table 4). The magnitude of this anisotropy ranges from 1.3 to 1.6 in the three samples. They suggested this anisotropy may reflect some preferential orientation in the parent asteroids, revealing conditions of formation of the ordinary chondrites.

It might be expected that highly thermally-metamorphosed chondrites would have larger compressive and tensile strengths. The upper range of the compressive strength data in Fig. 28 for ordinary chondrites suggests that increasing thermal evolution may have increased the mean compressive strength, but several meteorites of high petrologic grade have very low compressive strengths. This could reflect the effects of fracture from impacts onto their parent bodies, which can produce very large pressures, resulting in heating, melting, fragmenting, and deformation of rocks. So the magnitude of the peak shock pressure experienced by a meteorite might show a correlation with the compressive or tensile strength. However, only a few of the stone meteorites for which compressive strengths have been determined also have identified shock stages. Stöffler et al. (1991) tabulated the shock stages of 14 LL, 27 L, and 35 H chondrites. Similar data are available for 60 eucrites (Rubin et al., 1997), but no strength measurements have been reported for these eucrites. Fig. 29 plots the compressive strength vs. shock stage for the 1 LL, 7 L, and 4 H group chondrites for which both measurements have been reported, although not on the same samples. The current data are insufficient to demonstrate a clear correlation (Fig. 29). More data is desirable.

Dynamic compression experiments on the L5 ordinary chondrite MacAlpine Hills (MAC) 88118 by Kimberley and Ramesh (2011) indicated a significant increase in compressive strength with increasing strain rate. They noted that this increase is larger than the increases typically observed in terrestrial rock specimens compressed over a similar range of strain rates. In addition, they observed details of the failure process by recording ultra-high speed images of the samples in real time and found crack growth speeds in these dynamic compression experiments to be significantly lower than the speeds observed in terrestrial analogues, which are typically used in numerical investigations of large-scale impacts.

Tsuchiyama et al. (2009) measured the tensile strengths of very small meteorite fragments, ~50 to 200 μm in size, using a micro-testing instrument, allowing measurements on rare meteorites not made available for destructive testing in larger sizes. They reported values of samples of two CM2 meteorites, Murray (8.8 ± 4.8 MPa) and Murchison (2.0 ± 1.5 MPa), two CI meteorites, Ivuna (0.7 ± 0.2 MPa) and Orgueil (2.8 ± 1.9 MPa), and the carbonate-poor lithology of Tagish Lake (0.8 ± 0.3) MPa. However, it is not clear how to compare these small scale measurements to those made on much larger samples.

6.2. Compressive strength from meteor observations

The compressive strength of a meteoroid is not directly measureable, so a common approach (Ceplecha, 1958; Ceplecha and McCrosky, 1976; Jacchia, 1958) is to generate one-dimensional parameterizations from observations of meteors (e.g., using the beginning or end height, mass, speed, entry angle, etc.) as proxies for the "strength" of meteoroids.

6.2.1. Fireballs

The physical characteristics of meteoroids in the fireball regime are known from fireball survey observations (Halliday, 1973) and in particular from the twenty-six instrumentally recorded fireballs that have produced recovered meteorites (Table 1). The strength of these meteoroids in interplanetary space is best estimated based on the meteor fragmentation heights, where it is assumed that the dynamic atmospheric pressure (ρv^2), where ρ is the atmospheric density and v is the meteor speed at the height of fragmentation, is indicative of the compressive strength of the object. While the compressive strengths of meteorites generally range from tens to hundreds of MPa (Tables 4, 5), the data from fireball measurements show that typical strengths of cm-meter sized asteroidal precursors of meteorites are of order a few MPa or less (Popova et al., 2011), with no strong trend with size. This result has been interpreted to imply that the global strength for meteoroids in this size range is limited by pre-existing shock fractures (Halliday et al., 1989; Borovička, 2006).

Under the assumption that the penetration ability of fireballs is linked to their strength, Ceplecha and McCrosky (1976) proposed a strength classification system for fireballs based on the air density

Table 6
Meteor Strength Classification (from Ceplecha et al., 1998).

Type.	PE Range.	Meteorite Association.
type I:	PE > −4.60	Ordinary Chondrite-like
type II:	−5.25 < PE ≤ −4.6	Carbonaceous Chondrite (CI or CM)
type IIIa:	−5.7 < PE ≤ −5.25	Short period cometary
type IIIb:	PE ≤ −5.7	Weak cometary material

at their observed end height normalized to the mass, speed and entry angle of each fireball. This PE-criterion is given by:

$$PE = \log(\rho_E) - 0.42\log(m_\infty) + 1.49\log(V_\infty) - 1.29\log(\cos Z_R) \quad (7)$$

where ρ_E is the atmospheric mass density (in g/cm^3) at the height of the fireball end point; m_∞ is the entry mass in grams, computed from the total light production; V_∞ is the entry speed in km/s, and Z_R is the entry angle from the zenith. Larger (i.e., less negative) PE values correspond to stronger material displaying less ablation. Ceplecha and McCrosky (1976) further proposed that specific types of fireballs might be separated into four distinct taxonomic classes via the PE criteria (Table 6).

In this interpretation, only material from Type I and II fireballs have been recovered as meteorites, a result generally consistent with the observation in Table 1 that of the twenty-six recovered meteorites having well determined orbits, twenty-four have T_J values consistent with main-belt asteroidal material while the remaining two are very close the boundary between asteroidal and JFC orbits.

One approach to linking fireball PE values with material properties is to use recovered meteorites from fireballs with instrumental records as a form of ground-truth. A complication to this approach is that the mass scale used to derive the PE criterion is from the work of Ceplecha and McCrosky (1976), but many later fireball measurements were made with instruments other than photographic film and using differing values for luminous efficiency, the fraction of total energy which is detected in the sensor passband. Ceplecha (1988) developed mass scaling factors between the various photographic fireball networks and the estimated true mass, with the resulting differences producing systematic differences of 0.1–0.2 in PE values.

The PE values for instrumentally measured meteorite falls (Table 1), confirm the general trend predicted by Ceplecha and McCrosky (1976). While not adhering to the strict boundaries they propose, which they acknowledge are approximate, the ordinary chondrite-producing fireballs are generally associated with type I (or very strong type II material), while the three carbonaceous chondrite falls show lower values of PE (type II or IIIa). The major exception to this trend is the asteroid 2008TC3, the parent object of the Almahata Sitta anomalous ureilite, which showed fireball behavior more consistent with very weak carbonaceous or even cometary material having a PE = −5.7. In this unusual case, the pre-atmospheric object was likely to have been highly porous, explaining the weak structure (Kohout et al., 2011; Welten et al., 2010), and the recovered meteorites are breccias consisting of clasts of several different lithologies frequently separated by void spaces.

With this empirical calibration of the PE scale, the fireballs that did not produce meteorites, but which have known orbits, can be examined, linking the relative physical strength of the meteoroid, based on its ablation behavior, with its likely source region using the Tisserand parameter with respect to Jupiter. Fig. 30 shows all fireballs reported in the literature with sufficient data to generate PE values and T_J (see Fig. caption for details). This is a raw distribution and has various biases, but it demonstrates a few key qualitative points about the physical properties of meteoroids derived from observations of fireballs and their associated source regions:

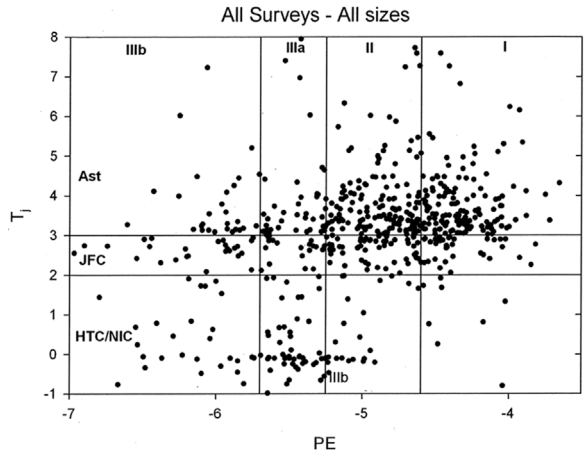

Fig. 30. Tisserand parameter with respect to Jupiter (T_J) versus the PE value for 600 fireballs from Halliday et al. (1996), Ceplecha and McCrosky (1976) , McCroskv et al. (1978), Ceplecha (1979a, 1979b), Ceplecha et al. (1976a, 1976b) , Ceplecha et al. (1980), Ceplecha et al. (1981), Ceplecha et al. (1983a, 1983b), Spurný (1994), Halliday et al. (1989), Ceplecha (1977), and Spurný and Porubčan (2002). PE values have been obtained using the mass scale conversion proposed in Ceplecha (1988) to normalize different scales to the original Ceplecha and McCrosky (1976) mass scale.

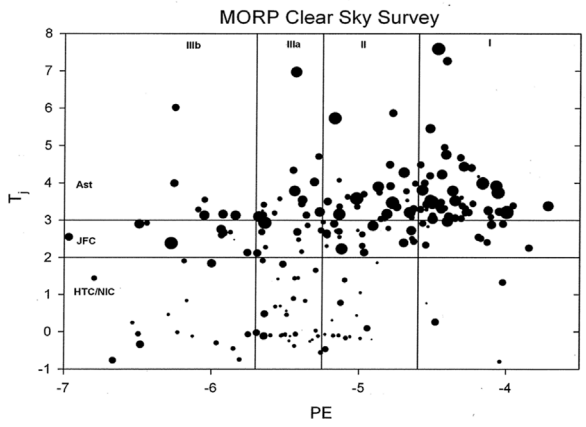

Fig. 31. The Tisserand parameter with respect to Jupiter (T_J) versus the PE value for the 213 fireballs in the unbiased deep sky survey of Halliday et al. (1996). Symbol size indicates relative meteor masses.

1. Most type I fireballs (associated with chondritic- type material having substantial strength) are indeed asteroidal in origin. A handful of fireballs in JFC-type orbits show evidence for strong material and a few examples exist of strong-type I fireballs in clearly comet-like orbits.
2. The general trend of increasing strength moving from comet to asteroid-type orbits is apparent, though exceptions exist.
3. There are a few instances of extremely weak fireballs in asteroidal orbits, though most are near the dividing line between asteroidal and JFC orbits.

With this caveat in mind, Fig. 31 shows the MORP clear-sky survey with each event plotted proportional to the log of its initial entry mass. Table 7 summarizes the results by overall percentage and percentage by apparent source region. The percentage distribution by fireball classes follows closely that given by Ceplecha (1988).

At smaller masses (few hundred grams and smaller), there are a few percent by number of fireballs which are very strong type I material, but in nearly isotropic comet (NIC)/Halley- type orbits. This has been noted previously (Borovička et al., 2005; Harvey, 1974). In particular, Borovička et al. (2002) noted that the Karlstein

Table 7
Percentage Distribution of 213 Fireballs Recorded in the Clear Sky Survey by Halliday et al. (1996) as a Function of PE Type and Tisserand Parameter.

Fireball Class	$T_J < 2$	$2 \leq T_J \leq 3$	$T_J > 3$	N_{total}*
IIIb	7%	5%	3%	15%
IIIa	16%	4%	7%	27%
II	8%	9%	12%	29%
I	2%	5%	22%	29%
Orbit Type*	33%	23%	44%	

*N_{total} is the sum of the Fireball class/rows and Orbit Type is the sum of each Tisserand orbit class.

fireball had a stony meteorite structure and composition based on spectra but retrograde NIC-type orbit. Together with the MORP results, this suggests the presence of high density, potentially compacted material in NIC type orbits. These objects may be pieces of irradiated cometary crusts (Borovicka et al., 2005) or they could represent asteroidal material originally implanted in the Oort cloud as suggested by Weissman and Levison (1997), who estimated ~1% of the Oort cloud population may be asteroidal in origin. Alternatively they may represent asteroidal material which is placed into retrograde orbits from the main- belt through the dynamical mechanism described by Greenstreet and Gladman (2013). They may also be unusually large, compact, refractory "inclusions" from Oort-cloud comets. There is no evidence in these surveys for larger (> kg-sized) material with these orbital/physical properties, a result noted by Gounelle et al. (2008), so the possibility of recoverable meteorites from objects in NIC/Halley-type orbits is low.

At the other extreme, there are a small number of asteroidal ($T_J > 3$) fireballs with very weak apparent structure (types IIIa and IIIb), again at the few percent level. Several of these are from the Taurid stream, which are known to have both large meteoroids and a wide range in strengths (Brown et al., 2013a) and are related to 2P/Encke. A number of other meteoroids with $T_J > 5$ are in very Earth-like orbits or are Atens. These evolved orbits have high collision probability with Earth (Morbidelli and Gladman, 1998), suggesting these may simply be the tail of a very small survivor population of cometary-like objects. One trend of particular note is that relatively few of the large (~10 kg or more) type III fireballs are associated with meteor showers; the major exception being the Taurids. This is not unexpected as conventional Whipple-type gas drag suggests an upper mass limit of this order for meteoroids in meteor streams being lofted from cometary nuclei (Whipple, 1951).

Although the statistics are small, based on the values in Table 7, it appears that fireballs from JFCs can range from type I to III, suggesting that meteorites from JFCs are possible, as has been noted previously (Campins and Swindle, 1998). Complicating this simple interpretation, however, are fireball measurement errors which may move T_J from the JFC to asteroidal range in the Halliday et al. (1996) data and dynamical pathways allowing JFCs to decouple from the effect of Jupiter and become asteroidal-like objects through close encounters with the terrestrial planets (Levison et al., 2006). The latter effect is enhanced among populations which are observed by impacting Earth.

For the population of fireball-producing meteoroids that are not represented in our meteorite collections (type IIIA/B), physical properties are inferred entirely from their flight behavior. This includes estimates of the ablation rate of the fireball [in the form of the magnitude of the ablation coefficient σ, discussed in detail in Ceplecha et al. (1998)] or from the height of flares or discrete fragmentation points identified in the model fits to data. Quantitative estimates of bulk density for type IIIA/B fireballs are difficult due to the lack of observable deceleration in most cases. However, Borovička and Spurný (1996) analyzed a meter-sized type IIIB fireball (Sumava) and were able to deduce with high confidence an overall bulk density near 0.10 g/cm^3 and a global strength, based on locations of flares in the light curve, between 0.025 – 0.14 MPa. They noted that the ablation coefficient was very large, and attributed this to a high degree of fragmentation. The strength values and low bulk density found for Sumava is consistent with the strengths and ablation behavior found for a few other multi-kilogram and larger type IIIA/B fireballs (Shrbený, 2009). These bodies appear to have high porosity and a structure similar to the canonical picture of cometary materials, with individual grains held together in a weak interconnected structure (Donn, 1990). The size of these grains can be estimated from the duration and intensity of meteor flares (Simonenko, 1968), who found the effective radii for constituent grains to range from of order a few tens to ~200 μm.

6.2.2. Fainter optical meteor population (mm – cm –sizes)

At mm to cm meteoroid sizes, narrow field optical instruments provide limits on compressive strength under a number of assumptions. On the basis of a number of common observational characteristics of faint meteors identified over the last half century (shorter than expected trail lengths, symmetrical light curves, abrupt beginning heights), together with more recent direct observations explicitly showing fragmentation or wake production (Borovička et al., 2007; Campbell-Brown et al., 2013), it is now clear that fragmentation is a ubiquitous process for smaller meteoroids during ablation, as first proposed by Jacchia (1955). As a consequence, a physical picture has developed of small meteoroids as dustball-like assemblages of refractory grains held together by a more volatile "glue" (Hawkes and Jones, 1975). In this model, the grains are released when the boiling point of the glue is reached at higher altitude where ablation occurs as a collective process on the suite of grains and the light produced is the sum of all the grains ablating. If this model describes a particular meteoroid, the concept of a compressive strength inferred from the maximum dynamic pressure along the trail has no physical meaning and bulk density can only be inferred based on a number of model assumptions.

Unlike brighter fireballs, smaller meteors rarely display flares during flight, thus not allowing unambiguous identification of discrete fragmentation points to estimate compressive strength reliably. In general the astrometric precision of data for small meteoroid ablation is not sufficient to isolate fragmentation points from dynamical (i.e., deceleration) data alone as can be done for larger, more deeply penetrating (and usually slower) fireballs (Ceplecha et al., 1993), so limits to the compressive strengths of small meteoroids, even assuming single body ablation applies, must be estimated based on the maximum ram pressure experienced by the meteoroid during flight.

With these limitations in mind, compressive strengths for smaller meteoroids associated with meteor showers have been estimated by Trigo-Rodriguez and Llorca (2006) and Shrbený (2009). They estimate bulk strengths to be 10^3 to 10^5 Pa, with the Geminids (associated with 3200 Phatheon) and Taurids (associated with 2P/Encke) having the highest bulk strengths and the Leonids (associated with 55P/Tempel- Tuttle) and October Draconids (21P/Giacobini-Zinner) showing the lowest. It is interesting to note that Shrbený (2009) also finds a positive correlation between meteoroid mass and bulk strength, particularly at larger masses (> 10 g), suggesting a fundamental change in ablation behavior.

Meteoroid properties have been estimated using various model approaches which include explicit allowance for fragmentation [quasi- continuous fragmentation – (Babadzhanov, 2002)], grain-release in the context of the dustball model triggered when the glue reaches its boiling point (Campbell-Brown and Koschny, 2004), grain release triggered by the energy flux received at the meteoroid surface (Borovička et al., 2007) or a single-body approach ignoring fragmentation (Rubio, 2002). A recent comparison of the last two versions of these models by Campbell-Brown et al. (2013) to obser-

Table 8
Meteoroid Strength Groups and Probable Material Associations.

Group	Strength Parameter	Probable Association
A:	$7.3 < K_B \leq 8$	Carbonaceous Chondrites/asteroidal/JFC
B:	$7.1 < K_B \leq 7.3$	Dense cometary material JFC/HTC
C:	$6.6 < K_B \leq 7.1$	Regular cometary material
D:	$6.6 > K_B$	Weak cometary material (JFC)

vations made with high resolution optical systems shows both to be somewhat deficient in simultaneously reproducing the light curves, deceleration and along the trail brightness profile of many small meteors, emphasizing the complexity of the fragmentation process.

As with larger meteoroids, an empirical one dimensional parameterization of the observed meteor characteristics has been proposed (Ceplecha, 1958) to assign relative strengths to smaller (mm to cm-sized) meteoroids. Unlike larger meteoroids, where atmospheric penetration ability and, hence, end height is the primary diagnostic, smaller meteoroids have been historically classified based on their beginning height, notionally representing relative differences in the bulk density, specific heat and thermal conductivity of the meteoroids (Ceplecha, 1967), with velocity and entry angle as normalizing variables.

This parameter, termed K_B, is defined as:

$$K_B = \log[\rho_B] + 2{\cdot}5\log[V_\infty] - 0.5\log[\cos Z] \quad (8)$$

where ρ_B is the air density at the start of the meteor (in g/cm^3), V_∞ is the initial speed (in cm/s^1) and Z is the local zenith angle of the radiant. Larger values of K_B indicate stronger/denser/less porous/higher specific heat/higher thermal conductivity of the meteoroid.

Examining beginning height as a function of speed shows at least four distinct meteor groups having common height versus velocity population profiles and hence similar values of K_B. Additional groupings are separable based on the a, e, and i orbital elements (Ceplecha et al., 1998). These strength groups and their probable material association at cm to mm sizes as given by Ceplecha et al. (1998) are shown in Table 8.

It is clear that there is a range of apparent strengths/densities of daughter meteoroids even among common parent populations, such as the JFCs. Some of these differences may be due to evolutionary processes, e.g., sintering of meteoroids at small perihelion distances, or reflect true underlying variations. It is likely that other than the A-type meteoroids, which are probably associated with carbonaceous chondrite-like material, the other smaller meteoroid classes are unrepresented in our meteorite collections, a consequence in part of their low bulk density.

However, the measured densities and porosities of the collected meteorites may not represent the bulk properties of their parent bodies. Under the same entry conditions, more porous meteorites of the same mass will have a larger cross-section and thus experience a greater force than less porous ones. Thus the Earth's atmosphere is likely to serve as a filter, with the more porous meteoroids preferentially fragmenting, resulting in lower probability of these meteorites surviving. Popova et al. (2011) discussed 13 meteorites recovered from instrumentally recorded fireballs and found that the bulk strengths on entry, inferred from breakup dynamics, were of order 1/10th to 1/100th the tensile strengths of meteorites very similar in type to those recovered from these 13 meteorite producing fireballs. These results are supported by the few measurements on the well-observed meteoroids that produced recovered meteorites whose compressive strength has been measured (Table 1), Almahata Sitta, and Chelyabinsk – each of which has a much higher compressive strength that inferred from the associated fireball. This indicates that the surviving meteorites are the strongest pieces of the incoming meteoroid, likely indicating that the measured densities of the surviving meteorites are significantly higher than the bulk density of the meteor that entered the atmosphere and the parent body of the meteorite. They further suggested that the weakness of some carbonaceous chondrite meteorites may result from very porous primordial accretional structures (Popova et al., 2011).

7. Impact cratering and resistance to disruption

Porous targets react significantly differently to impact cratering and disruption than non-porous targets of the same mass. Meteorite ejection from their parent bodies as well as subsequent impact fragmentation in space may be affected because of their porosity. In a series of hypervelocity cratering experiments in a vacuum, Love et al. (1993) determined that increased target porosity leads to deeper crater penetration, lower spall velocities, and greater localization of the impact damage. In addition, Michikami et al. (2007) reported that the average velocity of the crater ejecta decreases with decreasing material strength or increasing porosity of the target.

7.1. Hypervelocity disruption results

An alternative measure of the strength of a sample is provided by its resistance to fragmentation on impact. This "strength" or "threshold collisional specific energy," which is the energy required to disrupt a target such that the largest fragment has 50% of the mass of the target (a parameter called Q^*_D), is particularly important in modeling the collisional evolution of the asteroid belt. The value of Q^*_D is derived from the best fit to the power-law plot of the relative mass of the largest fragment (M_L/M_T) versus impactor specific energy (Fujiwara et al., 1989). Since no two natural targets have exactly the same shape and distribution of flaws, and no two projectiles ever hit the target in exactly the same spot, the results from several disruption experiments, conducted under similar conditions, must be averaged to provide a reliable result, especially for the determination of Q^*_D which relies critically on a single measurement, the mass of the largest fragment produced in each disruption.

Flynn and Durda (2004) disrupted nine ordinary chondrites and the CV3 carbonaceous chondrite Allende in hypervelocity impact experiments, using 1/8th inch and 1/4th inch Al projectiles shot at each target at between 4 and 6 km/s, comparable to the mean collision speed in the main belt, in an evacuated chamber at the NASA Ames Vertical Gun Range, and plotted the impact collisional specific energy versus the ratio of largest fragment mass to target mass (Fig. 32). The best fit line to these disruptions gives a value of Q^*_D of ~1400 J/kg for these stone meteorite disruptions, more than twice the literature value for compact terrestrial basalt. This result was confirmed by Cintala and Hörz (2008) , who compared successive disruptions of an L6 ordinary chondrite, ALH 85017, to that of terrestrial gabbro.

Because different meteorites have significantly different physical properties, Flynn et al. (2016b) conducted hypervelocity disruption experiments on ten samples of Northwest Africa 869, an L3-6 ordinary chondrite with weathering state W1 and shock state S3. They found a value of Q^*_D of ~1800 J/kg, and reported porosities ranging from 2.7 to 10.2%, with a mean of 6.4%.

These values of Q^*_D for ordinary chondrite meteorites are about twice the literature range of 700–800 J/kg for low porosity, terrestrial basalt, granodiorite, and glass targets (Fujiwara et al., 1989). This result indicates that ordinary chondrite meteorites are significantly more resistant to disruption than the terrestrial rocks whose parameters had been employed in many earlier models of

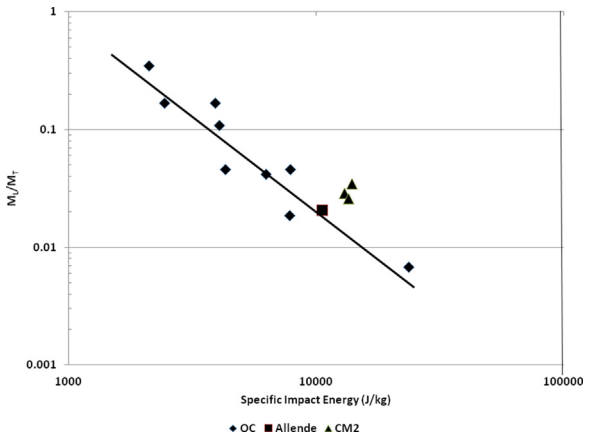

Fig. 32. Specific impact energy vs. the ratio of the mass of the largest fragment mass to the target mass for ten hypervelocity impact disruptions of anhydrous meteorites, nine ordinary chondrites, including the extremely friable meteorite, Saratov, and one carbonaceous chondrite, Allende. The least-squares fit to the ordinary chondrite data (line) gives a threshold collisional specific energy (Q^*_D) of 1419 J/kg (Flynn and Durda, 2004). The Allende dry carbonaceous chondrite point is consistent with the ordinary chondrite line. However, the three wet carbonaceous chondrite (CM2) data points all plot to the right of the ordinary chondrite data, suggesting these wet carbonaceous chondrites require even more specific impact energy for disruption than the ordinary chondrites.

asteroid disruption. Flynn and Durda (2004) attributed the greater "strength" of the ordinary chondrites to their ~10% porosity.

A disruption of the Allende CV3 meteorite plotted along the ordinary chondrite trend, suggesting it had disruption properties similar to the ordinary chondrites. However, three disruptions of CM2 wet carbonaceous chondrites all plotted to the right of the ordinary chondrite trend (Fig. 32), suggesting that the CM2 carbonaceous chondrites have an even larger Q^*_D value than the ordinary chondrites (Flynn et al., 2009; Flynn, 2014). Although the wet carbonaceous chondrites are among the weakest meteorites in the collection when characterized by their compressive strengths, laboratory hypervelocity impact experiments indicate that they are remarkably resistant to collisional disruption.

7.2. Hypervelocity cratering results

Hypervelocity impact cratering produces a significant mass of moderate speed ejecta, generally much more than the mass of the impactor. These crater ejecta, directed into the half- plane opposite the target, contribute to the momentum transfer to the target, characterized by the momentum multiplication factor β:

$$\beta = (m_p v_p + p_e)/m_p v_p = M_t Vt/m_p v_p \quad (9)$$

where p_e is the momentum of the ejecta, m_p and v_p are the mass and velocity of the impactor, and M_t and V_t are the mass and gain in velocity of the target. The $m_p v_p$ term is the direct momentum transfer and the p_e term is the momentum provided by the crater ejecta. A knowledge of the momentum transfer by crater ejecta is particularly important in designing space missions for the kinetic impactor deflection of asteroids (Holsapple, 2002). Modeling indicates that the momentum added by the crater ejecta can exceed that from direct momentum transfer by a factor of ten or more in non-porous targets (Holsapple, 2002), but β is modeled to decrease with increasing target porosity.

Flynn et al. (2016b) measured the momentum transferred to seven NWA 869 L3-6 ordinary chondrite targets, having a mean porosity of ~6%, impacted by 1/16" Al projectiles fired at 4.3–5.5 km/s, and found β values ranging from 1.8 to 3.8, about half the value found for compact river rocks by Housen and Holsapple (2012). This result indicates that, even for porous targets, crater ejecta contributes significantly to the momentum transfer in hypervelocity collisions. To date no β measurements have been reported on more porous meteorite targets, such as the carbonaceous chondrites.

7.3. Attenuation of shock

The attenuation of shock is important in determining the extent of damage to the rock surrounding the site of an impact. In compact terrestrial rocks the emplacement of one large impact crater causes sufficient damage to erase the evidence of nearby craters. However, multiple large impact craters were observed on the carbonaceous asteroid Mathilde, which has a bulk density of 1.3 ± 0.2 gm/cm^3 (Yeomans et al., 1997), indicating that Mathilde has a porosity >50% (Britt et al., 2002). Veverka et al. (1999) suggested that the poor transmission of shock in this highly-porous asteroid allowed the production of large, sometimes overlapping craters. However, shock attenuation measurements are lacking on meteorite samples.

8. Summary

Meteoroid orbit observations suggest that few, if any, cometary meteoroids survive atmospheric entry to produce meteorites. Thus, the meteorite collection is a biased sample of the small objects in space, with the strongest meteoroids and those which entered the Earth's atmosphere at the lowest speeds being overrepresented in the collection relative to weak meteoroids and those that enter the atmosphere at higher velocities. Even among the population of meteoroids with a Tisserand parameter >3, suggesting an asteroidal origin, Halliday et al. (1996) found a substantial fraction with inferred bulk densities lower than that of Orgueil, which has the lowest bulk density (1.61 g/cm^3) of any meteorite measured.

Two of the meteorites whose orbits were determined from the associated fireballs, Maribo and Sutter's Mill, both CM2 carbonaceous chondrites, have T_J values of ~2.91, consistent with JFCs. However, $T_J = 3$ is not a firm dynamical dividing line between asteroidal and JFC orbits, so the origin of Maribo and Sutter's Mill is not strictly constrained by these observations.

Although the meteorite collections sample a wide diversity of material, with porosities ranging from essentially zero to more than 40%, most of the range reported for the asteroids (Britt et al., 2002), meteor observations demonstrate the existence of a population of lower density, likely higher porosity, objects not represented in the meteorite collection.

Porosity has a significant effect on most of the other physical properties of the meteorites, reducing the speed of sound, thermal conductivity, compressive and tensile strengths of the porous meteorites, and increasing their resistance to hypervelocity impact disruption, compared to compact terrestrial rocks. To the extent that these meteorite properties represent those of their parent asteroids, models of asteroid thermal and orbital evolution, cratering and impact disruption, etc. that employed physical properties of compact terrestrial rocks may need to be reevaluated. Only the heat capacity, grain density and magnetic susceptability are unaffected by meteorite porosity.

The grain density and the magnetic susceptibility of unweathered ordinary chondrites can be used to non-invasively classify these meteorites, giving results consistent with traditional petrologic examination. This technique can rapidly screen whole stones from recent falls to identify interlopers in the strewn field or to identify misclassified meteorites in collections. The measurements indicate that terrestrial weathering is a relatively rapid process, with the mean porosity of ordinary chondrites being reduced by ~50% as the meteorites go from the W0 to the W1 weathering state.

Some meteorites preserve evidence of their pre-accretional porosity, typically in the form of interstitial pore spaces (Sasso et al., 1999). The observed correlation of decreasing porosity with increasing petrologic grade for H to L ordinary chondrites, a likely proxy for depth within the parent body, suggests that heat and gravitational pressure, which increase with depth, remove some, but generally not all, of the pre-accretional porosity from the samples from the greatest depths in their parent bodies.

The twenty-six well characterized meteors that produced recovered meteorites provide an opportunity to investigate and cross-correlate the physical properties inferred from meteor flight characteristics with measurements on the recovered samples. However, very few physical properties measurements have been reported on these meteorites (Table 1). Where measurements have been reported, the recovered meteorite is significantly stronger than the compressive strength derived from fragmentation of the parent meteor, indicating that only the strongest subunits of the meteoroid survive to reach the ground.

Because many of the physical properties, including the thermal conductivity, elastic moduli, sound speed, compressive strength, and response to hypervelocity impacts, depend on the porosity of the sample, it is highly desirable to have a variety of properties measured on the same sample of the meteorite. All of the physical properties of the meteorites, with the exception of the heat capacity, vary widely among the chondritic meteorites. However, in modeling a specific asteroid the dependence of an each physical property on the porosity can narrow the range of property values if both the bulk density and the asteroid type (or mineralogy) are determined, allowing a model porosity to be inferred.

Acknowledgements

This Invited Review was solicited and handled by Associate Editor Klaus Keil, and benefited from thoughtful comments by K. Keil, T. Kohout, and an anonyomous reviewer. This work was supported by NASA Solar System Workings grant NNX15AM22G to GJF. PGB was supported through funding provided by NASA co-operative agreement NNX15AC94A, the Canada Research Chairs program and the Natural Sciences and Engineering Research Council of Canada.

References

A'Hearn, M.F., Belton, M.J.S., Delamere, W.A., Feaga, L.M., Hampton, D., et al., 2011. EPOXI at comet Hartley 2. Science 332, 1396–1400.

Alexayeva, K., 1958. Physical properties of stony meteorites and their interpretation based on the hypothesis on the origin of meteorites. Meteoritika 16, 67–77.

Alexayeva, K., 1960. New data on the physical properties of stony meteorites. Meteoritika 18, 68–76.

Babadzhanov, P.B., 2002. Fragmentation and densities of meteoroids. Astron. Astrophys. 384 (1), 317–321, http://dx.doi.org/10.1051/0004-6361:20020010.

Baldwin, B., Sheaffer, Y., 1971. Ablation and breakup of large meteoroids during atmospheric entry. J. Geophys. Res. 76, 4653–4668.

Beech, M., Coulson, I.M., Nie, W., McCausland, P., 2009. The thermal and physical characteristics of the Gao-Guenie (H5) meteorite. Planet. Space Sci. 57, 764–770.

Biot, J.-B., 1803. Relation d'un Voyage Fait Dans Le département De l'Orne Pour Constater La réalité d'un météore Observé a l'Aigle Le 6 Floréal an 11. Ba udoin, Paris (47 pages).

Bischoff, A., Rubin, A.E., Keil, K., Stöffler, D., 1983. Lithification of gas-rich chondrite regolith breccias by grain boundary and localized shock melting. Earth Planet. Sci. Lett. 66, 1–10.

Bland, P.A., Sexton, A., Jull, A.J.T., Bevan, A.W.R., Berry, F.J., Thornley, D., Astin, T., Pillinger, C.T., 1998. Climate and rock weathering: a study of terrestrial age dated ordinary chondritic meteorites from hot desert regions. Geochim. Cosmochim. Acta 62, 3169–3184.

Bland, P.A., Towner, M.C., Sansom, E.K., Devillepoix, H., Howie, R.M., Paxman, J.P., Cupak, M., Benedix, G.K., Cox, M.A., Jansen-Sturgeon, T., Stuart, D., Strangway, D., 2016. Fall and recovery of the Murrili meteorite, and an update on the desert fireball network (abstract). 79th Meteoritical Society Meeting, LPI Contribution No. 1921, #6265.

Borovička, J., Kalenda, P., 2003. The Morávka meteorite fall: 4. Meteoroid dynamics and fragmentation in the atmosphere. Meteorit. Planet. Sci. 38, 1023–1043.

Borovička, J., Spurný, P., 1996. Radiation study of two very bright terrestrial bolides and an application to the Comet S–L 9 collision with Jupiter. Icarus 121, 484–510.

Borovička, J., Popova, O.P., Nemchinov, I.V., Spurný, P., Ceplecha, Z., 1998. Bolides produced by impacts of large meteoroids into the Earth's atmosphere: comparison of theory with observations I. Benesov bolide dynamics and fragmentation. Astron. Astrophys. 334, 713–728.

Borovička, J., Spurný, P., Koten, P., 2002. Evidences for the existence of non-chondritic compact material on cometary orbits. In: Warmbein, B. (Ed.), Asteroids, Comets, and Meteors: ACM 2002, ESA SP-500. , pp. 265–268.

Borovička, J., Spurný, P., Kalenda, P., Tagliaferri, E., 2003. The Morávka meteorite fall: 1. Description of the events and determination of the fireball trajectory and orbit from video records. Meteorit. Planet Sci. 38, 975–987.

Borovička, J., Spurný, P., Koten, P., 2007. Atmospheric deceleration and light curves of Draconid meteors and implications for the structure of cometary dust. Astronomy 473 (2), 661–672, http://dx.doi.org/10.1051/0004-6361.

Borovicka, J., Koten, P., Spurny, P., Bocek, J., Stork, R., 2005. A survey of meteor spectra and orbits: evidence for three populations of Na-free meteoroids. Icarus 174, 15–30.

Borovička, J., Toth, J., Igaz, A., Spurny, P., Kalenda, P., Haloda, J., Svourea, J., Kornos, L., Silber, E., Brown, P., HusáRik, M., 2013a. The Kosice meteorite fall: atmospheric trajectory, fragmentation, and orbit. Meteorit. Planet. Sci. 48, 1757–1779.

Borovička, J., Spurny, P., Brown, P., Wiegert, P., Kalenda, P., Clark, D., Shrbený, L., 2013b. The trajectory, structure and origin of the Chelyabinsk asteroidal impactor. Nature 503, 235–237.

Borovička, J., Spurný, P., Šegon, D., Andreić, Ž., Kac, J., Korlević, K., et al., 2015. The instrumentally recorded fall of the Križevci meteorite, Croatia, february 4, 2011. Meteoritics Planet. Sci. 50 (7), 1244–1259, http://dx.doi.org/10.1111/maps.12469.

Borovička, J., 2006. Physical and chemical properties of meteoroids as deduced from observations. In: Lazzaro, D., Ferraz-Mello, S., Fernandez, J. (Eds.), Proceed. Inter. Astron. Union, Vol. 1. Cambridge University Press, Cambridge, pp. 249–271 http://dx.doi.org/10.1017/S17439213 05006782.

Bottke Jr., W.F., Vokrouhlický, D., Rubincam, D.P., Nesvorný, D., 2006. The Yarkovsky and YORP effects: implications for asteroid dynamics. Ann. Rev. Earth Planet. Sci. 34, 157–191.

Britt, D.T., Consolmagno, G.J., 2003. Stony meteorite porosities and densities: A review of the data through 2001. Meteorit. Planet. Sci. 38, 1161–1180.

Britt, D.T., Yeomans, D., Housen, K., Consolmagno, G., 2002. Asteroid density, porosity, and structure. In: Bottke, W.F., Cellino, A., Paolicchi, P., Binzel, R.P. (Eds.), Asteroids III. Univ. of Arizona Press, Tucson, pp. 485–500.

Brown, P.G., Ceplecha, Z., Hawkes, R.L., Wetherill, G.W., Beech, M., Mossman, K., 1994. The orbit and atmospheric trajectory of the Peekskill meteorite from video records. Nature 367, 624–626.

Brown, P.G., ReVelle, D.O., Hildebrand, A.R., 2001. The Tagish lake meteorite fall: interpretation of fireball physical characteristics. In: warmbein B. (Ed.) proc. meteoroids 2001 conf. ESA SP 495, 497–505.

Brown, P.G., Revelle, D.O., Tagliaferri, E., Hildebrand, A.R., 2002. An entry model for the Tagish Lake fireball using seismic, satellite and infrasound records. Meteorit. Planet. Sci. 37, 661–676.

Brown, P.G., Pack, D., Edwards, W.N., Revelle, D.O., Yoo, B.B., Spalding, R.E., Tagliaferri, E., 2004. The orbit, atmospheric dynamics, and initial mass of the Park Forest meteorite. Meteorit. Planet. Sci. 39, 1781–1796.

Brown, P.G., McCausland, P.J.A., Fries, M., Silber, E., Edwards, W.N., Wong, D.K., Weryk, R.J., Fries, J., Krzeminski, Z., 2011. The fall of the Grimsby meteorite-I: Fireball dynamics and orbit from radar, video, and infrasound records. Meteorit. Planet. Sci. 46 (3), 339–363.

Brown, P.G., Marchenko, V., Moser, D.E., Weryk, R.J., Cooke, W., 2013a. Meteorites from meteor showers: a case study of the Taurids. Meteorit. Planet. Sci. 19, 270–288, http://dx.doi.org/10.1111/maps.12055.

Brown, P.G., Assink, J.D., Astiz, L., Blaauw, R., Boslough, et al., 2013b. A 500-kiloton airburst over Chelyabinsk and an enhanced hazard from small impactors. Nature 503, 238–241.

Brownlee, D.E., 1985. Cosmic dust collection and research. Ann. Rev. Earth Planet. Sci. 13, 147–173.

Buddhue, J.D., 1942. The compressive strength of meteorites. Contrib. Soc. Res. on Meteorites 3, 39–40.

Campbell-Brown, M.D., Koschny, D., 2004. Model of the ablation of faint meteors. Astron. Astrophys. 418, 751–775, http://dx.doi.org/10.1051/0004-6361:20041001-1.

Campbell-Brown, M.D., Borovička, J., Brown, P.G., Stokan, E., 2013. High-resolution modelling of meteoroid ablation. Astron. Astrophys. 557 (41), 1–13.

Campins, H., Swindle, D., 1998. Expected characteristics of cometary meteorites. Meteorit. Planet. Sci. 33, 1201–1211.

Cartwright, J.A., Hermann, S., McCausland, P.J.A., Brown, P.G., Ott, U., 2010. Noble gas analysis of the Grimsby H chondrite (abstract). Meteorit. Planet. Sci.

Ceplecha, Z., McCrosky, R.E., 1976. Fireball end heights: a diagnostic for the structure of meteoric material. J. Geophys. Res. 81 (35), 6257–6275.

Ceplecha, Z., ReVelle, D.O., 2005. Fragmentation model of meteoroid motion, mass loss, and radiation in the atmosphere. Meteorit. Planet. Sci. 40, 35–54.

Ceplecha, Z., Bocek, J., Jezkova, M., 1976a. Photographic data on the Arrach Fireball/En 290875, Aug 29, 1975. Bull. Astron. Instit Czechoslovakia 27 (4), 242–244.

Ceplecha, Z., Jezkova, M., Bocek, J., Kirsten, T., 1976b. Photographic data on the Leutkirch Fireball/EN 300874/, Aug. 30, 1974. Bull. Astron. Instit Czechoslovakia 27 (1), 18–23.
Ceplecha, Z., Boček, J., Ježková, M., Porubčan, V., Polnitzky, G., 1980. Photographic data on the Zvolen fireball (EN 270 579, May 27, 1979) and suspected meteorite fall. Bull. Astron. Inst. Czechosl. 31, 176–182.
Ceplecha, Z., Boček, J., Nováková- Ježková, M., Porubčan, V., Kirsten, T., Kiko, J., 1983a. European network fireballs photographed in 1977. Bull. Astron. Inst. Czehoslovakia 34, 195-212 No. 4.
Ceplecha, Z., Boček, J., Nováková, M., Ježková Polnitzky, G., 1983b. Photographic data on the Traunstein fireball (EN290181, Jan 29, 1981) and suspected meteorite fall. Bull. Astron. Inst. Czechosl. 34, 162–167, No.3.
Ceplecha, Z., Spurný, P., Borovička, J., Keclikova, J., 1993. Atmospheric fragmentation of meteoroids. Astron. Astrophys. 279, 615–626.
Ceplecha, Z., Brown, P.G., Hawkes, R.L., Wetherill, G.W., Beech, M., Mossman, K., 1996. Video observations, atmospheric path, orbit and fragmentation record of the fall of the Peekskill meteorite. Earth. Moon Planets 72, 395–404.
Ceplecha, Z., Borovička, J., Elford, W.G., Revelle, D.O., Hawkes, R.L., Porubčan, V., Šimek, M., 1998. Meteor phenomena and bodies. Space Sci. Rev. 84, 327–471.
Ceplecha, Z., 1958. On the composition of meteors. Bull. Astron. Inst. Czechoslovakia 9, 154–159.
Ceplecha, Z., 1961. Multiple fall of Pribram meteorites photographed. 1. Double-station photographs of the fireball and their relations to the found meteorites. Bull. Astron. Inst. Czechoslovakia 12, 21–47.
Ceplecha, Z., 1967. Classification of meteor orbits. Smithsonian Contr. Astrophys. 11, 35–60.
Ceplecha, Z., 1977. Fireballs photographed in central Europe. Bull. Astron. Instit. Czechoslovakia, 328–340.
Ceplecha, Z., 1979a. Earth-grazing fireballs/the daylight fireball of aug. 10, 1972. Bull. Astron. Instit Czechoslovakia 30 (6), 349–356.
Ceplecha, Z., 1979b. Photographic data on the Brno fireball/EN 140 977, Sep. 14, 1977. Bull. Astron. Instit Czechoslovakia 30 (4), 220–225.
Ceplecha, Z., 1988. Earth's influx of different populations of sporadic meteoroids from photographic and television data. Bull. Astron. Instit Czechoslovakia 39 (4), 221–236.
Ceplecha, Z., 1996. Luminous efficiency based on photographic observations of the Lost City fireball and implications for the influx of interplanetary bodies onto Earth. Astron. Astrophys. 311, 329–332.
Chen, M., Wopenka, B., El Goresy, A., Sharp, T.G., 1996. High-pressure assemblages in shock melt veins in the Peace River (L6) chondrite (abstract). Meteorit. Planet. Sci. 31, A27.
Cintala, M.J., Hörz, F., 2008. Experimental impacts into chondritic targets, part 1: Disruption of an L6 chondrite by multiple impacts. Meteorit. Planet. Sci. 43 (4), 771–803.
Consolmagno, G.J., Britt, D.T., 1998. The density and porosity of meteorites from the Vatican collection. Meteorit. Planet. Sci. 33, 1231–1241.
Consolmagno, G.J., Bland, P.A., Strait, M.M., 1999. Weathering and porosity: a preliminary SEM study of weathered meteorites. 30th Annual Lunar and Planetary Science Conference, abstract no. 1158.
Consolmagno, G.J., Macke, R.J., Rochette, P., Britt, D.T., Gattacceca, J., 2006. Density, magnetic susceptibility, and the characterization of ordinary chondrite falls and showers. Meteorit. Planet. Sci. 41, 331–342.
Consolmagno, G.J., Wignarajah, D.P., Britt, D.T., 2007. Bulk densities of assorted CK chondrites, primitive achondrites, and Bencubbin (abstract). Meteorit. Planet. Sci, 5118.
Consolmagno, G.J., Britt, D.T., Macke, R.J., 2008a. The density and porosity of carbonaceous chondrites: a new look (abstract). Meteorit. Planet. Sci., 5038.
Consolmagno, G.J., Britt, D.T., Macke, R.J., 2008b. What density and porosity tell us about meteorites. Lunar Planet. Sci., 1582 (XXXIX, LPI Contribution No. 1391, Abstract).
Consolmagno, G.J., Britt, D.T., Macke, R.J., 2008c. The significance of meteorite density and porosity. Chemie der Erde-Geochemistry 68, 1–30.
Consolmagno, G., Opeil, C., Britt, D.T., 2011. Uniaxial Stress/strain of Meteorites. EPSC Abstracts 6, abstract EPSC-DPS2011 574–1.
Consolmagno, G.J., Schaefer, M.W., Schaefer, B.E., Britt, D.T., Macke, R.J., Nolan, M.C., Howell, E.S., 2013. The measurement of meteorite heat capacity at low temperatures using liquid nitrogen vaporization. Planet. Space Sci. 87, 146–156, http://dx.doi.org/10.1016/j.pss.2013.07.009.
Corrigan, C.M., Zolensky, M.E., Dahl, J., Long, M., Weir, J., Sapp, C., Burkett, P.J., 1997. The porosity and permeability of chondritic meteorites and interplanetary dust particles. Meteoritics 32, 509–515.
Cotto-Figueroa, D., Asphaug, E., Garvie, L.A., Rai, A., Johnston, J., Borkowski, L., Datta, S., Chattopadhyay, A., Morris, M.A., 2016. Scale-dependent measurements of meteorite strength: implications for asteroid fragmentation. Icarus 277, 73–77.
Davidsson, B.J.R., Gutiérrez, P.J., 2004. Estimating the nucleus density of comet 19P/Borrelly. Icarus 168, 392–408.
Davidsson, B.J.R., Gutiérrez, P.J., 2006. Non-gravitational force modeling of Comet 81P/Wild 2: I. A nucleus bulk density estimate. Icarus 180 (1), 224–242, http://dx.doi.org/10.1016/j.icarus.2005.07.023.
Debye, P., 1912. Zur theorie der spezifischen Wärmen. Ann. Phys. 344, 789–839.
DeMeo, F., Binzel, R.P., 2008. Comets in the near-Earth object population. Icarus 194, 436–449.
Donn, B., 1990. The formation and structure of fluffy cometary nuclei from random accumulation of grains. Astron. Astrophys. 235, 441–446.
Dyl, K.A., Benedix, G.K., Bland, P.A., Friedrich, J.M., Spurný, P., Towner, M.C., O'Keefe, M.C., Howard, K., Greenwood, R., Macke, R.J., Britt, D.T., Halfpenny, A., Thostenson, J.O., Rudolph, R.A., Rivers, M.L., Bevan, A.W.R., 2016. Characterization of Mason Gully (H5): the second recovered fall from the desert fireball network. Meteorit. Planet. Sci. 51 (3), 596–613.
Fernández, J.A., 2005. Comets: Nature, Dynamics, Origin and Their Cosmogonical Relevance. Springer, Dordrecht Berlin Heidelberg, pp. 283.
Flesch, L.M., Li, B., Liebermann, R.C., 1998. Sound velocities of polycrystalline MgSiO3-orthopyroxene to 10 GPa at room temperature. Amer. Mineral. 83, 444–450.
Flynn, G.J., 2005. Physical properties of meteorites and interplanetary dust particles: clues to the properties of the meteors and their parent bodies. Earth Moon Planets 95, 361–374.
Flynn, G.J., Durda, D.D., 2004. Chemical and mineralogical size segregation in the impact disruption of inhomogeneous, anhydrous meteorites. Planet. Space Sci. 52, 1129–1140.
Flynn, G.J., Sutton, S.R., 1991. Cosmic dust particle densities – Evidence for two populations of stony micrometeorites (abstract). Lunar Planet. Sci. Conf. 21, 541–547.
Flynn, G.J., Moore, L.B., Klöck, W., 1999. Density and porosity of stone meteorites: implications for the density, porosity, cratering, and collisional disruption of asteroids. Icarus 142, 97–105.
Flynn, G.J., Rivers, M., Sutton, S.R., Eng, P., Klock, W., 2000. X-Ray computed microtomography (CMT): A non-invasive screening tool for characterization of returned rock cores from Mars and other Solar System bodies (abstract). Lunar Planet. Sci Conf. 31, 1893.
Flynn, G.J., Durda, D.D., Sandel, L.E., Kreft, J.W., Strait, M.M., 2009. Dust production from the hypervelocity impact disruption of the Murchison hydrous CM2 meteorite: implications for the disruption of hydrous asteroids and the production of interplanetary dust. Planet. Space Sci. 57, 119–126.
Flynn, G.J., Nittler, L.R., Engrand, C., 2016a. Composition of cosmic dust: sources and implications for the early solar system. Elements 12 (3), 177–183.
Flynn, G.J., Durda, D.D., Patmore, E.B., Jack, S.J., Molesky, M.J., Strait, M.M., 2016b. Hypervelocity impact disruption and cratering measurements on the Northwest Africa 869 ordinary chondrite (abstract). Lunar Planet. Sci Conf. 47, 1081.
Flynn, G.J., 2004. Physical properties of meteorites and interplanetary dust particles: clues to the properties of the meteors and their parent bodies. Earth, Moon and Planets 95, 361–374.
Flynn, G.J., 2014. Porosity as a significant factor in asteroid survival (abstract). Asteroids, Comets and Meteors, Helsinki, Finland (Abstract Volume, http://www.helsinki.fi/acm2014/pdf- material/Day-4/Session-2/Room-2/FLYNN-84D9.pdf).
Friedrich, J.M., Macke, R.J., Wignarajah, D.P., Rivers, M.L., Britt, D.T., Ebel, D.S., 2008. Pore size distribution in an uncompacted equilibrated ordinary chondrite. Planet. Space Sci. 56, 895–900.
Fry, C., Melanson, D., Samson, C., McCausland, P.J.A., Herd, R.K., Ernst, R.E., Umoh, J., Holdsworth, D.W., 2013. Physical characterization of a suite of Buzzard Coulee H4 chondrite fragments, Meteorit. Planet. Sci 48 (6), 1060–1073.
Fujiwara, A., Cerroni, P., Davis, D., Ryan, E., di Martino, M., 1989. Experiments and scaling laws for catastrophic collisions. In: Asteroids II. University of Arizona Press, pp. 240–265.
Gillett, J.A. Ph Barrat, Heulin Th Achouak, W., Lesourd, M., Guyot, F., Benzerara, K., 2000. Bacteria in the Tatahouine meteorite: nanometric-scale life in rocks. Earth Planet. Sci. Lett. 175, 161–167.
Gorshkov, E.S., 1973. Elastic properties of meteorites. Meteoritika 32, 126–135.
Gounelle, M., Zolensky, M.E., 2001. A terrestrial origin for sulfate veins in CI1 chondrites. Meteorit. Planet. Sci. 36, 1321–1329.
Gounelle, M., Morbidelli, A., Bland, P.A., Spurný, P., Young, E.D., Sephton, M., 2008. Meteorites from the outer solar system? In: Barucci, M.A., Boehnhardt, H., Cruikshank, D.P., Morbidelli, A. (Eds.), The Solar System Beyond Neptune. University of Arizona Press, pp. 525–541.
Grady, M.M., 2000. Catalog of Meteorites, 5th edition. Cambridge University Press, Cambridge UK (700 pages).
Greenstreet, S., Gladman, B., 2013. High-inclination Atens are indeed rare. Ap. J. 767 (1), L18, http://dx.doi.org/10.1088/2041-8205/767/1/L18.
Grokhovsky, V.I., Gladkovsky, S.V., Ryzhkov, M.A., Ishchenko, A.V., 2013. Mechanical and thermal properties of the Chelyabinsk meteorite (abstract). Meteorit. Planet. Sci.
Haak, H.W., Michelsen, R., Stober, G., Keuer, D., Singer, W., 2010. The Maribo CM2 fall: radar based orbit determination of an unusually fast fireball (abstract). Meteorit. Planet. Sci. Suppl., 5085.
Haak, H.W., Michelsen, R., Stober, G., Keuer, D., Singer, W., Williams, I.P., Encke, C., 2011. CM chondrites from comets? – New constraints from the orbit of the Maribo CM chondrite fall (abstract). In: Formation of the First Solids in the Solar System (Abstract 9100).
Haak, H.W., Grau, T., Bischoff, A., Horstmann, M., Wasson, J., Sørensen, A., et al., 2012. Maribo-A new CM fall from Denmark. Meteoritics Planet. Sci. 47 (1), 30–50, http://dx.doi.org/10.1111/j.1945- 5100.2011.01311.
Halliday, I., Blackwell, A.T., Griffin, A., 1978. The Innisfree meteorite and the Canadian camera network. Royal Astron. Soc. Canada J. 72, 15–39.
Halliday, I., Griffin, A., Blackwell, A.T., 1981. The Innisfree meteorite fall – A photographic analysis of fragmentation, dynamics and luminosity. Meteoritics 16, 153–170.
Halliday, I., Blackwell, A.T., Griffin, A.A., 1989. The typical meteorite event, based on photographic records of 44 fireballs. Meteoritics 24, 65–72.

Halliday, I., Griffin, A., Blackwell, A.T., 1996. Detailed data for 259 fireballs from the Canadian camera network and inferences concerning the influx of large meteoroids. Meteorit. Planet. Sci. 31 (2), 185–217.
Halliday, I., 1973. Photographic fireball networks. In: Hemenway, C.L., Millman, P.M., Cook, A.F. (Eds.), Evolutionary and Physical Properties of Meteoroids. , Proc. IAU Colloq., 13 (NASA SP 319) pp. 1-8.
Hanna, R.D., Ketcham, R.A., Zolensky, M., Behr, W.M., 2015. Impact-induced brittle deformation, porosity loss, and aqueous alteration in the Murchison CM chondrite. Geochim. Cosmochim. Acta 171, 256–282, http://dx.doi.org/10.1016/j.gca.2015.09.005.
Harvey, G., 1974. Strongly differentiated material in high-inclination and retrograde orbits. Astronom. J. 79 (2), 333–347.
Hawkes, R.L., Jones, J., 1975. A quantitative model for the ablation of dustball meteors. Month. Not. Royal Astron. Soc. 173, 339–356.
Hemingway, B.S., Robie, R.A., Evans Jr., H.T., Kerrick, D.M., 1991. Heat capacities and entropies of sillimanite fibrolite, andalusite, kyanite, and quartz and the Al2SiO5 phase diagram. Am. Mineral 76, 1597–1613.
Hildebrand, A.R., McCausland, P.J., Brown, P.G., Longstaffe, F.J., Russell, S.D.J., Tagliaferri, E., Wacker, J.F., Mazur, M.J., 2006. The fall and recovery of the Tagish Lake meteorite. Meteorit. Planet. Sci. 41, 407–431.
Hogan, J.D., Kimberley, J., Hazeli, K., Plescia, J., Ramesh, K.T., 2015. On the role of defects in the dynamic failure of an ordinary chondrite. 46th Lunar and Planetary Science Conference (abstract), LPI Contribution No. 1832, #1481.
Holsapple, K., 2002. Speed limits of rubble pile asteroids: Even fast rotators can be rubble piles. In: NASA Workshop on Scientific Requirements for Mitigation of Hazardous Comets and Asteroids, pp. 47–52. https:/noao.edu/meetings/mitigation/eav.html.
Hons, M., 2004. Compressional and Shear Wave Velocity in Meteorites B.Sc. Thesis. University of Calgary, Calgary, Alberta, Canada.
Housen, K.R., Holsapple, K.A., 2012. Deflecting asteroids by impacts: what is beta? (abstract). Lunar Planet Sci Conf. 43, 2539.
Ibrahim, E.-M.I., 2012. The Elastic Properties of Carbonaceous Chondrites M.Sc. Thesis. University of Calgary, Alberta, Canada.
Jacchia, L., 1955. The physical theory of meteors. VIII. Fragmentation as cause of the faint-meteor anomaly. Ap. J. 121, 521.
Jacchia, L., 1958. On two parameters used in the physical theory of meteors. Smithson. Contrib. Astrophys. 2, 181–187.
Jenniskins, P., Shaddad, M.H., Numan, D., Elsir, S., Kudoda, A.M., et al., 2009. The impact and recovery of asteroid TC(3). Nature 458, 485–488.
Jenniskens, P., Fries, M.D., Zolensky, M., Krot, A.N., Sandford, S.A., co-authors, 66, 2012. Radar-Enabled recovery of the Sutter's Mill meteorite, a carbonaceous chondrite regolith breccia. Science 338, 1583–1587.
Jenniskens, P., Rubin, A.E., Yin, Q.-Z., Sears, D.W.G., Sandford, S., co-authors, 43, 2014. Fall, recovery, and characterization of the Novato L6 chondrite breccia. Meteorit. Planet. Sci. 49, 1388–1425, http://dx.doi.org/10.1111/maps.12323.
Johanson, O., 1975. Thermal Conductivity of Soils Ph.D Thesis, Trondheim, Norway (CRREL Draft Translation 637, 1977) ADA 044002.
Johnson, R.B., DeGraff, J.V., 1988. Principles of Engineering Geology J. Wiley and Sons, New York.
Jones, S.F., 202 pages 2009. Elastic Wave Velocity, Porosity, and Pore Geometry of Ordinary Chondrites and Artifically Shocked Samples. M.Sc. Thesis. University of Calgary7, Canada.
Keil, K., 1962. Quantitav-erzmikroskopische integrationsanalyse der chondrite. Chemie der Erde 22, 281–348.
Keuer, D., Singer, W., Stober, G., 2009. Signatures of the ionization trail of a fireball observed in the HF, and VHF range above middle-Europe on Jan 17, 2009. In: Swarnalingham, N., Hocking, W.K. (Eds.), Proc. 12th Workshop Technical Scientific Aspects of MST radar, 154–158.
J.B., Kikwaya Eluo 293 pages. The Bulk Density of Small Meteoroids. Ph.D. Thesis. University of Western Ontario, London, Ontario, Canada 2011; (Thesis&).
Kikwaya, J.-B., Campbell-Brown, M., Brown, P.G., Hawkes, R.L., Weryk, R.J., 2009. Physical characteristics of very small meteoroids. Astron. Astrophys. 497, 851–867.
Kikwaya, J.-B., Campbell-Brown, M.D., Brown, P.G., 2011. Bulk density of small meteoroids. Astron. Astrophys. 113, 1–17, http://dx.doi.org/10.1051/0004-6361/201116431.
Kimberley, J., Ramesh, K.T., Barnouin, O.S., Ernst, C.M., 2010. Dynamic strength measurements of L5 chondrite Macalpine hills 88118 (abstract). Lunar Planet. Sci Conf. 41, 2588.
Kimberley, J., Ramesh, K.T., 2011. The dynamic strength of an ordinary chondrite. Meteorit. Planet. Sci. 46, 1653–1669.
Kohout, T., Kletetschka, G., Elbra, T., Adachi, T., Mikula, V., 2008. Physical properties of meteorites—Applications in space missions to asteroids. Meteorit.Planet Sci. 43 (6), 1009–1020.
Kohout, T., Kiuru, R., Montonen, M., Scheirich, P., Britt, D., Macke, R., Consolmagno, G., 2011. Internal structure and physical properties of the Asteroid 2008 TC3 inferred from a study of the Almahata Sitta meteorites. Icarus 212 (2), 697–700, http://dx.doi.org/10.1016/j.icarus.2011.01.037.
Kohout, T., Gritsevich, M., Grokhovsky, V.I., Yakovlev, G.A., Haloda, J., Halodova, P., Michallik, R.M., Penttilä, A., Muinonen, K., 2014a. Mineralogy, reflectance spectra, and physical properties of the Chelyabinsk LL5 chondrite – Insight into shock-induced changes in asteroid regoliths. Icarus 228, 78–85.
Kohout, T., Havrila, K., Tóth, J., Husárik, M., Gritsevich, M., co-authors, 19, 2014b. Density, porosity and magnetic susceptibility of the Košice meteorite shower and homogeneity of its parent meteoroid. Planet. Space Sci. 93, 96–100.
Kohout, T., Gritsevich, M., Lyytinen, E., Moilainen, J., Trigo-Rodríguez, J.M., Kruglikov, N., Ishchenko, A., Yakovlev, G., Grokhovsky, V., Haloda, J., 5 coauthors, 2015. Annama H5 meteorite fall: orbit, trajectory, recovery, petrology, noble gases, and cosmogenic radionuclides. 78th Meteorit. Soc. Meet., LPI Contribution No. 1856, 5209, http://dx.doi.org/10.1098/rsta.2013.0259.
Kohout, T., Haloda, J., Halodova, P., Meier, M.M.M., Maden, C., Busemann, H., Laubenstein, M., Caffee, M.W., Welten, K.C., Hopp, J., coauthors, 20, 2017. Annama H chondrite –mineralogy, physical properties, cosmic ray exposure, and parent body history. Meteorit Planet. Sci., http://dx.doi.org/10.1111/maps.12871 (in press).
Krot, A.N., Keil, K., Goodrich, C.A., Scott, E.R.D., Weisberg, M.K., 2014. Classification of meteorites and their genetic relationships. In: Davis, A.M., Holland, H.D., Turekian, K.K. (Eds.), Meteorites and Cosmochemical Processes: Treatise on Geochemistry, vol. 1, second edition. Elsevier, pp. 1–63.
Krupka, K.M., Robie, R.A., Hemingway, B.S., Kerrick, D.M., Ito, J., 1985. Low temperature heat capacities and derived thermodynamic properties of anthophyllite diopside, enstatite, bronzite, and wollastonite. Amer. Mineral. 70, 249–260.
Kumazawa, M., Anderson, O.L., 1969. Elastic moduli, pressure derivatives, and temperature derivatives of single-crystal olivine and single-crystal forsterite. J. Geophys. Res. 74, 5961–5972.
Levison, H.F., Terrell, D., Wiegert, P., Dones, L., Duncan, M.J., 2006. On the origin of the unusual orbit of Comet 2P/Encke. Icarus 182 (1), 161–168, http://dx.doi.org/10.1016/j.icarus.2005.12.016.
Levison, H.F., 1996. Comet taxonomy. In: Rettig, T.W., Hahn, J.M. (Eds.), Completing the Inventory of the Solar System, ASP Conference Series, Vol. 107. Astronomical Society of the Pacific, San Francisco, CA, pp. 173–191.
Llorca, J., Trigo-Rodríguez, J.M., Ortiz, J.L., Docobo, J.A., García-Guinea, J., Castro-Tirado, A.J., Rubin, A.E., Eugster, O., Edwards, W., Laubenstein, M., Casanova, I., 2005. The Villalbeto de la Peña meteorite fall: I Fireball energy, meteorite recovery, strewn field, and petrography. Meteorit. Planet. Sci. 40, 795–804.
Love, S.G., Hörz, F., Brownlee, D.E., 1993. Target porosity effects in impact cratering and collisional disruption. Icarus 105, 216–224.
Macke, R., 2007. Bulk and grain denstities of Allende and other carbonaceous chondrites (abstract). Bulletin Amer. Astron. Soc. 39, 448 (DPS meeting 39, id. 20.05).
Macke, R.J., 2010. Survey of Meteorite Physical Properties: Densitiy, Porosity and Magnetic Susceptibility Ph D. Dissertation. University of Central Florida, Orlando, FL (332 pp).
Macke, R.J., Consolmagno, G.J., 2014. Porosity and pore geometry influence on meteorite thermal conductivities. 77th Annual Meeting of the Meteoritical Society, 5045 (LPI Contribution No. 1800).
Macke, R.J., Britt, D.T., Consolmagno, G.J., 2010a. Analysis of systematic error in bead method measurements of meteorite bulk volume and density. Planet. Space Sci. 58, 421–426.
Macke, R.J., Consolmagno, G.J., Britt, D.T., Hutson, M.L., 2010b. Enstatite chondrite density, magnetic susceptibility, and porosity. Meteorit. Planet. Sci. 45, 1513–1526.
Macke, R.J., Consolmagno, G.J., Britt, D.T., 2011a. Density, porosity, and magnetic susceptibility of carbonaceous chondrites. Meteorit. Planet. Sci. 46, 1842–1862.
Macke, R.J., Britt, D.T., Consolmagno, G.J., 2011b. Density, porosity, and magnetic susceptibility of achondritic meteorites. Meteorit. Planet. Sci. 46, 311–326.
Macke, R.J., Wiggins, S., Britt, D.T., Benedix, G.K., Bland, P.A., Desert Fireball Network Team, 2016. Density, porosity and magnetic susceptiblity of the Murrili meteorite recovered by the desert fireball network. 79th Meteorit. Soc. Meet., 6147, http://dx.doi.org/10.1098/rsta.2013.0259 (LPI Contribution No. 1921).
Matsui, T., Osako, M., 1979. Thermal property measurement of Yamato meteorites. Mem. National Instit. Polar Res. 15, 243–252 (Special Issue).
Maurette, M., Jehano, C., Robin, E., Hammer, C., 1987. Characteristics and mass distribution of extraterrestrial dust from the Greenland ice cap. Nature 301, 473–477.
McCrosky, R.E., Posen, A., Schwartz, G., Shao, C.-Y., 1971. Lost City meteorite – its recovery and a comparison with other fireballs. J. Geophys. Res. 76, 4090–4108.
McCroskv, R.E., Shao, C.-Y., Posen, A., 1978. Prairie Network fireball data. I. Summary and orbits. Meteoritika 37, 44–59.
McPherson, G.J., Krot, A.N., 2002. Distribution of Ca-Fe-silicates in CV3 chondrites: possible controls by parent body compaction (abstract). Meteorit. Planet. Sci. 37, A91.
McSween, H.Y., Gosh, A., Grimm, R.E., Wilson, L., Young, E.D., 2002. Thermal evolution models of asteroids. In: Bottke, W.F., Cellino, A., Paolicchi, P., Binzel, R.P. (Eds.), Asteroids III. Univ. of Arizona Press, Tucson, pp. 559–571.
Medvedev, R.V., Gorbatsevich, F.I., Zotkin, I.T., 1985. Determination of the physical properties of stone meteorites with application to the study of processes of their destruction. Meteoritika 44, 105–110.
Michikami, T., Moriguchi, K., Hasegawa Fujiwara, A., 2007. Ejecta velocity distribution for impact cratering experiments on porous and low strength targets. Planet. Space Sci. 55, 70–88.
Milley, E.P., Hildebrand, A.R., Brown, P.G., Noble, M., Sarty, G., Ling, A., Mailler, L.A., 2010. Pre-fall orbit of the Buzzard Coulee meteoroid. Geocanada 2010–Working with the Earth, 4.
Milley, E.P., 2010. Physical Properties of Fireball- producing Earth-impacting Meteoroids and Orbit Determination Through Shadow Calibration of the

Buzzard Coulee Meteorite Fall MSc Thesis. University of Calgary, Alberta, Canada (166p).
Miura, Y.N., Noguchi, T., Tsuchiyama, A., Yano, H., Yoshida, S., Nagata, K., 2008. Compressive strength measurements of meteorites and terrestrial rocks: implications for physical properties of asteroidal surfaces. Proc. Japan Geoscience Union Meeting (abstract) (P168-P002).
Molesky, M.J., Patmore, E.B., Strait, M.M., 2015. Measurement of the density and compression strength in meteorites (abstract). 78th Meeting Meteoritical Society, 5300 (LPI Contribution No. 1856).
Morbidelli, A., Gladman, B., 1998. Orbital and temporal distributions of meteorites originating in the asteroid belt. Meteorit. Planet. Sci. 33, 999–1016.
Murray, C.D., Dermot, S.F., 2000. Solar System Dynamics. Cambridge University Press, Cambridge, UK (608 pages).
Nakamura, T., Noguchi, T., Zolensky, M.E., Takaoka, N., 2001. Noble gas isotopic signatures and x- ray and electron diffraction characteristics of Tagish Lake carbonaceous chondrite (abstract). Lunar Planet. Sci. Conf. XXXII, 1621.
Nesvorný, D., Janches, D., Vokrouhlický, D., Pokorný, P., Bottke, W.F., Jenniskens, P., 2011. Dynamical model for the zodiacal cloud and sporadic meteors. Astrophy. J. 743 (2), 129, http://dx.doi.org/10.1088/0004-637X/743/2/129.
Nishiizumi, K., Caffee, M.W., Hamajima, Y., Reedy, R.C., Welten, K.C., 2014. Exposure history of the Sutter's Mill carbonaceous chondrite. Meteorit. Planet. Sci. 49, 2056–2063, http://dx.doi.org/10.1111/maps.12297.
O'Rourke, L., Müller, T., Valtchanov, I., Altieri, B., González-Garcia, B.M., Bhattacharya, B., et al., 2012. Thermal and shape properties of asteroid (21) Lutetia from Herschel observations around the Rosetta flyby. Planet. Space Sci. 66 (1), 192–199, http://dx.doi.org/10.1016/j.pss.2012.01.004.
Opeil, C.P., Consolmagno, G.J., Britt, D.T., 2010. The thermal conductivity of meteorites: new measurements and analysis. Icarus 208, 449–454.
Opeil, C.P., Consolmagno, G.J., Safarik, D.J., Britt, D.T., 2012. Stony meteorite thermal properties and their relationship to meteorite chemical and physical states. Meteorit. Planet. Sci. 47, 319–329.
Pesonen, L.J., Teheo, M., Kukkonen, I.T., 1993. Physical properties of 368 meteorites: implications for meteorite magnetism and planetary geophysics. In: Yanai, K., Kojima, H., Misawa, K., Takaoka, K., Yoshida, Y. (Eds.), Seventeenth Symp. Antarctic Meteorites. Proc. NIPR Symp. Natl. Institute Polar Res Tokyo, pp. 401–416.
Petrovic, J.J., 2001. Review, mechanical properties of meteorites and their constituents. J. Mater. Sci. 36, 1579–1583.
Popova, O.P., Borovička, J., Hartmann, W.K., Spurný, P., Gnos, E., Nemtchinov, I.V., Trigo-Rodriguez, J.M., 2011. Very low strengths of interplanetary meteoroids and small asteroids. Meteorit. Planet. Sci. 46 (10), 1525–1550, http://dx.doi.org/10.1111/j.1945- 5100.2011.01247.
Richardson, J.E., Melosh, H.J., Lisse, C.M., Carcich, B., 2007. A ballistics analysis of the Deep Impact ejecta plume: determining Comet Tempel 1's gravity, mass, and density. Icarus 191 (2), 176–209.
Rochette, P., Sagnotti, L., Bourot-Denise, M., Consolmagno, G., Folco, L., Gattacceca, J., Osete, J.M.L., Pesonen, L., 2003. Magnetic classification of stony meteorites: 1: Ordinary chondrites. Meteorit. Planet. Sci. 38, 251–268.
Rochette, P., Gattacceca, J., Sagnotti, L., Folco, L., Consolmagno, G., Denise, M., 2006. Magnetic classification of C, E, K, R and ungrouped chondrites (abstract). Meteorit. Planet. Sci.
Rochette, P., Garttacceca, J., Bonal, L., Bourat-Denise, M.L., Chevrier, V., Clerc, J.-P., Consolmagno, G., Folco, L., Gounelle, M., Kohout, T., Pesonen, L., Quirico, E., Sagnotti, L., Skripnik, A., 2008. Magnetic classification of stony meteorites: 2. Non-ordinary chondrites. Meteorit. Planet. Sci. 43, 959–980.
Rochette, P., Gattacceca, J., Bezaeva, N.S., Obolonskaya, E.V., Polyarnaya, J.A., Skripnik, A., Nazarov, M.A., 2009. Scanning meteorite collections for misclassified/misidentified samples: examples from Saint Petersburg and Moscow (abstract). Meteorit. Planet. Sci., 5029.
Rubin, A.E., Scott, E.R.D., Keil, K., 1997. Shock metamorphoism of enstatite chondrites. Geochim. Cosmochim. Acta 61, 847–858.
Rubio, L.B., 2002. Modeling the photometric and dynamical behavior of Super-Schmidt meteors in the Earth's atmosphere. Astron. Astrophys. 691, 680–691, http://dx.doi.org/10.1051/0004-6361.
Sasso, M.R., Macke, R.J., Boesenberg, J.S., Britt, D.T., Rivers, M.L., Ebel, D.S., Friedrich, J.M., 2009. Incompletely compacted equilibrated ordinary chondrites. Meteorit. Planet. Sci. 44, 1743–1753.
Schultz, R.A., 1995. Limits on the strength and properties of basaltic rock masses. Rock Mech. Rock Eng. 28, 1–15.
Scott, E.R.D., Keil, K., Stoeffler, D., 1992. Shock metamorphism of carbonaceous chondrites. Geochim. Cosmochim. Acta 56, 4281–4293.
Shrbený, L., 2009. Meteor Shower Fireballs PhD Thesis. Astronomical Institute of the Czech Republic. Ondrejov Observatory (122 pp).
Sierks, H., Barbieri, C., Philippe, L., Rodrigo, R., 2015. On the nucleus structure and activity of comet 67P/Churyumov-Gerasimenko. Science, 347, http://dx.doi.org/10.1126/science.aaa1044.
Simonenko, A.N., 1968. The separation of small particles from meteor bodies, and its influence on some parameters of meteors. In: Kresak, L., Millman, P.M. (Eds.), Physics and Dynamics of Meteors, Proceedings of the I.A.U. Symposium, No. 33. Tatransks, Lomnica, Czechoslovakia, 1967. D. Reidel, Dordrecht, pp. 207–216.
Simon, S., Grossman, L., Clayton, R.N., Mayeda, T., Schwade, J., Sipiera, P., Wacker, J.F., Wadhwa, M., 2004. The fall, recovery, and classification of the Park Forest meteorite. Meteorit. Planet. Sci. 39, 625–634.
Slyuta, E.N., Nikitin, S.M., Korochantsev, A.V., Lorents, C.A., 2007. Preliminary data on the physical and mechanical properties of the Sayh al Uhaymir 001 meteorite (abstract). 46th Vernadsky-Brown Microsymposium, m46–m68.
Slyuta, E.N., Nikitin, S.M., Korochantsev, A.V., Lorents, C.A., 2008. Physical and mechanical properties of Sayh al Uhaymir 001 and Ghubara meteorites (abstract). Lunar Planet. Sci Conf. 39, 1056.
Slyuta, E.N., Nikitin, S.M., Korochantsev, A.V., Lorents, C.A., Skripnik, A., 2009. Strong physical and mechanical anisotropy of ordinary chondrites (abstract). Lunar Planet. Sci Conf. 40, 1051.
Slyuta, E.N., 2013. There's no creep in small solar system bodies (abstract). Lunar Planet. Sci Conf. 44, 1117.
Smith, D.L., Samson, C., Herd, R., Deslauriers, A., Sink, J.-E., Christie, I., Ernst, R.E., 2006a. Measuring the bulk density of meteorites nondestructively using three-dimensional laser imaging. J. Geophys. Res. 111 (E10) (CiteID E10002).
Smith, D.L., Ernst, R.E., Samson, C., Herd, R., 2006b. Stony meteorite characterization by non-destructive measurement of magnetic properties. Meteorit. Planet Sci. 41 (3), 355–373.
Spurný, P., 1994. Recent fireballs photographed in central Europe. Planet. Space Sci. 42, 157–162.
Spurný, P., 2015. Instrumentally documented meteorite falls: two recent cases and statistics from all falls. Proc. Int. Astron. Union 10, 69–79, http://dx.doi.org/10.1017/S1743921315009746.
Spurný, P., Porubčan, V., 2002. The EN171101 bolide-The deepest ever photographed fireball, In: Proceedings of Asteroids, Comets, Meteors – ACM 2002. International Conference, 29 July – 2 August 2002, Berlin, Germany. Ed. Barbara Warmbein. ESA SP-500. Noordwijk, p. 269–272.
Spurný, P., Heinlein, D., Oberst, J., 2002. The atmospheric trajectory and heliocentric orbit of the Neuschwanstein meteorite fall on April 6, 2002. In: Warmbein, B. (Ed.), Asteroids, Comets, and Meteors: ACM 2002. , pp. 137–140.
Spurný, P., Oberst, J., Heinlein, D., 2003. Photographic observations of Neuschwanstein, a second meteorite from the orbit of the Pribram chondrite. Nature 423, 151–153.
Spurný, P., Borovička, J., Kac, J., Kalenda, P., Atanackov, J., Kladnik, G., Heinlein, D., Grau, T., 2010. Analysis of instrumental observations of the Jesenice meteorite fall on April 9, 2009. Meteorit. Planet. Sci. 45, 1392–1407.
Spurný, P., Bland, P.A., Shrbený, L., Borovička, J., Ceplecha, Z., 7 co-authors, 2012a. The Bunburra Rockhole meteorite fall in SW Australia: fireball trajectory, luminosity, dynamics, orbit, and impact position from photographic and photoelectric records. Meteorit. Planet Sci. 47, 163–185.
Spurný, P., Bland, P.A., Borovička, J., Towner, M.C., Shrbeny, L., Bevan, A., Vaughan, D., 2012b. The Mason Gully meteorite fall in SW Australia: fireball trajectory, luminosity, dynamics, orbit and impact position from photographic records (abstract). In: Asteroids, Comets, Meteors. Lunar & Planetary Institute, Houston, pp. 6369 (LPI Contribution No. 1667).
Spurný, P., Borovicka, J., Haack, H., Singer, W., Keuer, D., Jobse, K., 2013. Trajectory and orbit of the Maribo CM2 meteorite from optical, photoelectric and radar records. Meteoroids 2013 Conference, Poster Presentation.
Spurný, P., Borovička, J., Haloda, J., Shrbený, L., Heinlein, D., 2016. Two very precisely instrumentally documented meteorite falls: Zdar nad Sazavou and Stubenberg? Prediction and Reality. 79th Meteoritical Soc. Meet., 6221 (LPI Contribution No. 1921).
Stöffler, D., Keil, K., Scott, E.R.D., 1991. Shock metamorphoism of ordinary chondrites, Geochim. Cosmochim. Acta 55, 3845–3867.
Strait, M.M., Consolmagno, G.J., 2002. The nature and origin of meteorite porosity: evidence from thin section analysis (abstract). Meteorit. Planet Sci. 37, A137.
Strait, M.M., Consolmagno, G.J., 2005. Validation of methods used to determine microcrack porosity in meteorites (abstract). 36th Lunar Planet. Sci Conf., 2073.
Sugiura, N., 1977. Magnetic properties and remanent magnetization of stony meteorites. J. Geomagn. Geoelectr. 29, 519–539.
Svetsov, V.V., Nemtchinov, I.V., Teterev, A.V., 1995. Disintegration of large meteoroids in Earth's atmosphere: theoretical models. Icarus 116, 131–153.
Szurgot, M., 2011. On the specific heat capacity and thermal capacity of meteorites (abstract). Lunar Planet Sci. Conf. 42, 1150.
Szurgot, M., Wach, R., Przylibski, T.A., 2012. Thermophysical properties of the Sołtmany meteorite. Meteorites 2, 53–65 http://www.meteorites.pwr.wroc.pl/i ssues/2/e-meteorites_1-2-2012.pdf.
Tancredi, G., 2014. A criterion to classify asteroids and comets based on the orbital parameters. Icarus 234, 66–80.
Taylor, S., Lever, J.H., Harvey, R.P., 1998. Accretion rate of cosmic spherules measured at the South Pole. Nature 392, 899–903.
Trieloff, M., Jessberger, E.K., Herrwerth, I., Hopp, J., Fiéni, C., Ghélis, M., Bourot-Denise, M., Pellas, P., 2003. Structure and thermal history of the H-chondrite parent asteroid revealed by thermochronometry. Nature 422, 502–506.
Trigo-Rodriguez, J.M., Llorca, J., 2006. The strength of cometary meteoroids: clues to the structure and evolution of comets. Monthly Not. Royal Astronom. Soc. 372 (2), 655–660, http://dx.doi.org/10.1111/j.1365- 2966.2006.10843.
Trigo-Rodriguez, J.M., Borovička, J., Spurný, P., Ortiz, J.L., Docobo, J.A., Castro-Tirado, A.J., Llorca, J., 2006. The Villalbeto de la Peña meteorite fall: II: Determination of atmospheric trajectory and orbit. Meteorit. Planet. Sci. 41, 505–517.
Trigo-Rodriguez, J.M., Lyytinen, E., Gritsevich, M., Bottke, W.F., Williams, I.P., Lupovka, V., et al., 2015. Orbit and dynamic origin of the recently recovered Annama's H5 chondrite. Mon. Not. R. Astron. Soc. 449, 2119–2127, http://dx.doi.org/10.1093/mnras/stv378.

Tsuchiyama, A., Mashio, E., Imai, Y., Noguchi, T., Miura, Y., Yano, H., Nakamura, T., 2009. Strength measurement of carbonaceous chondrites and micrometeorites using micro compression testing machine (abstract). Meteorit. Planet. Sci.
Tsvetkov, V.I., Skripnik, A.Y., 1991. Atmospheric fragmentation of meteorites according to the strength theory. Solar Syst. Res. 25, 273–279.
Van Schmus, W.R., Wood, J.A., 1967. A chemical-petrologic classification for the chondritic meteorites. Geochim. Cosmochim Acta 31 (5), 747–765.
Veverka, J., Thomas, P., Harch, A., Clark, B., Bell, J.F., Carcich, B., co-authors, 8, 1999. NEAR encounter with asteroid 253 Mathilde: overview. Icarus 140, 3–16.
Wach, R.A., Adamus, A., Szurgot, M., 2013. Specific heat capacity of Sołtmany and NWA 4560 meteorites (abstract). Meteorit. Planet Sci. 48, 5017.
Walsh, J.B., 1965. The effect of cracks on the uniaxial elastic compression of rocks. J. Geophys. Res. 70, 399–411.
Weissman, P.R., Levison, H.F., 1997. Origin and evolution of the unusual object 1996 PW: Asteroids from the Oort Cloud? Astrophy. J. 488 (2), L133–L136, http://dx.doi.org/10.1086/310940.
Welten, K.C., Meier, M.M.M., Caffee, M.W., Nishiizumi, K., Wieler, R., Jenniskens, P., Shaddad, M.H., 2010. Cosmogenic nuclides in Almahata Sitta ureilites: cosmic-ray exposure age, preatmospheric mass, and bulk density of asteroid 2008 TC3. Meteorit. Planet. Sci. 45 (10- 11), 1728–1742, http://dx.doi.org/10.1111/j.1945- 5100.2010.01106.
Whipple, F., 1951. A comet model. II. Physical relations for comets and meteors. Astrophys. J. 113, 464.
Wlotzka, F., Scherer, P., Schultz, L., Otto, J., Stepniewski, M., 1997. Petrography and nobel gases in the unusual L5 chondrites Baszkówka and Mt. Tazerzait (abstract). Meteorit. Planet Sci. 32, A140–A141.
Wlotzka, F., 1993. A weathering scale for the ordinary hondrites (abstract). Meteoritics 28, 460.
Yeomans, D.K., Barriot, J.P., Dunham, D.W., Farquhar, R.W., Giorgini, J.D., co-authors, 8, 1997. Estimating the mass of asteroid 253 Mathilde from tracking data during the NEAR Flyby. Science 278, 2106–2109.
Yomogida, K., Matsui, T., 1981. Physical properties of some antarctic meteorites,) the sixth symposium on antarctic meteorites. In: Nagata, T. (Ed.), Proc. 1981 Conf. Memoirs Natl. Institute Polar Research, 384–394 (Spec. Issue No. 20.).
Yomogida, K., Matsui, T., 1983. Physical properties of ordinary chondrites. J Geophys. Res. 88, 9513–9533.
Zotkin, I.T., Medvedev, P.V., Gorbatsevich, F.F., 1987. Strength properties of the Tsarev meteorite. Meteoritika 46, 86–93.